UNIVERSITY OF CYPRUS

DEPARTMENT OF CHEMISTRY

PhD DISSERTATION

RESONANCE RAMAN STUDIES ON NITRYL CHLORIDE DISSOLVED IN METHANOL

Marilena N. Trimithioti

JULY 2013

UNIVERSITY OF CYPRUS

DEPARTMENT OF CHEMISTRY

RESONANCE RAMAN STUDIES ON NITRYL CHLORIDE DISSOLVED IN METHANOL

MARLENA N. TRIMITHIOTI

Dissertation submitted for fulfillment of the requirements for a Doctoral Degree at the University of Cyprus

JULY 2013

ΣΕΛΙΔΑ ΕΓΚΥΡΟΤΗΤΑΣ

Υποψήφιος Διδάκτορας: Μαριλένα Ν. Τριμιθιώτη

Τίτλος Διατριβής: Resonance Raman Studies on Nitryl Chloride dissolved in Methanol

Η παρούσα Διδακτορική Διατριβή εκπονήθηκε στο πλαίσιο των σπουδών για απόκτηση Διδακτορικού Διπλώματος στο Τμήμα Χημείας του Πανεπιστημίου Κύπρου και εγκρίθηκε στις 05 Ιουλίου 2013 από τα μέλη της Εξεταστικής Επιτροπής.

Εξεταστική Επιτροπή:

- **Ερευνητική Σύμβουλος: Δρ. Σοφία Χ. Hayes, Επίκουρη Καθηγήτρια, Τμήμα Χημείας, Πανεπιστήμιο Κύπρου.**
- **Πρόεδρος Επιτροπής: Δρ. Επαμεινώνδας Λεοντίδης, Καθηγητής, Τμήμα Χημείας, Πανεπιστήμιο Κύπρου.**
- **Δρ. Αναστάσιος Κεραμιδάς, Αναπληρωτής Καθηγητής, Τμήμα Χημείας, Πανεπιστήμιο Κύπρου.**
- **Δρ. Ανδρέας Όθωνος, Καθηγητής, Τμήμα Φυσικής, Πανεπιστήμιο Κύπρου.**
- **Dr. Tony Parker, Professor Rutherford Appleton Laboratory, UK**

DECLARATION

All the experiments presented in this study took place in the Molecular Spectroscopy Laboratory at the Department of Chemistry of the University of Cyprus by the undersigned under the supervision of Assistant Professor Dr. Sophia C. Hayes. The *ab initio* calculations described in *Chapter 4* were performed at the CNRS Laboratoire de Photophysique Moleculaire (Paris, France) by Dr. Christophe Jouvet. I have analyzed the results derived from these calculations and related them to my experimental work. The Molecular Dynamics computations presented in *Chapter 6* were performed by Dr. Alexey Akimov, which comes from the Prezhdo Research group of the Department of Chemistry, University of Rochester.

DATE: 05/07/2013

SIGNATURE:

Στους γονείς μου

Acknowledgements

The success of any project depends largely on the encouragement and guidelines of many people in so many ways. I take this opportunity to express my gratitude to the people who have been instrumental in the successful completion of this Dissertation.

I would like to express my deepest appreciation to my supervisor, Assistant Professor Dr. Sophia C. Hayes for her excellent guidance, caring, patience, and providing me with an excellent atmosphere for doing research. She helped me realize the power of critical reasoning. She also demonstrated what a brilliant and hard-working scientist can accomplish. Without her guidance and persistent help this dissertation would not have been possible.

I would like to thank my committee members: Professor Epameinondas Leontidis Associate Professor Anastasios Keramidas from Department of Chemistry of University of Cyprus Professor Andreas Othonos from the Department of Physics of University of Cyprus and Professor Tony Parker from the Rutherford Appleton Laboratory, UK.

In addition, a thank you to Professor Christophe Jouvet from the CNRS Laboratoire de Photophysique Moleculaire (Paris, France) who performed the *ab initio* calculatios and to Dr. Alexey Akimov (Prezhdo Research group of the Department of Chemistry, University of Rochester) who performed the Molecular Dynamics Simulations.

Furthermore, I would also like to acknowledge with much appreciation the members of the Molecular Spectroscopy Lab, Galateia, Nicos, Varvara, Eleni, Souliana and Christiana for the excellent cooperation and the friendly relationship we have developed over these years.

I deeply thank my parents which have been a constant source of support – emotional, moral and of course financial – during my postgraduate years, and this thesis would certainly not have existed without them. I also would like to thank my brother and my sister in law, who helped me get through this agonizing period in the most positive way.

My husband was always there for supporting me and stood by me through the good times and the bad and I thank him.

ABSTRACT

Understanding the fundamental aspects of phase-dependent reactivity is a significant challenge in atmospheric chemistry. This area of environmental chemistry is closely related to current research in chemical physics on the role of solvent in photophysical and photochemical processes. The atmosphere is a heterogeneous mixture of a variety of environments (gases, droplets, aerosols, etc.) where photochemistry can occur, thus the study of atmospheric species in well-defined environments is the first step in the understanding of the role of phase in atmospheric chemistry. The study we present here constitutes our initial efforts to understand the phase-dependent reactivity of nitryl chloride, concentrating on methanol as a solvent.

Methanol was chosen as a suitable environment after preliminary experimental and theoretical studies examining the chemical behavior of $ClNO_2$ in solution. Resonance Raman (RR) spectroscopy was the method of choice for the investigation of $ClNO_2$ in methanol after excitation within the D absorption band in the region 200-240 nm. RR intensity along the NO symmetric stretch coordinate (v_1) at 1291 cm^{-1} is observed at all excitation wavelengths, while limited intensity corresponding to the N-Cl symmetric stretch (v_3) was observed only with excitation at the peak of the absorption band. Intensity corresponding to the O-N-O symmetric bend (v_2) was not observed. Depolarization ratios (DPR's) and absolute RR cross sections for v_1 were obtained at several excitation wavelengths spanning the D band. The depolarization ratios were found to deviate significantly from 1/3, consistent with more than a single dipole-allowed electronic transition contributing to the scattering. RR intensity analysis (RRIA) revealed that two closely-spaced excited electronic states contribute to the scattering, which are dissociative along the Cl-N coordinate.

This study was extended by analyzing in more detail the RR depolarization dispersion curve for v_1 at excitation wavelengths spanning the D absorption band. The DPR's were modeled using the time-dependent formalism for Raman scattering with the excited state model mentioned above. The analysis focused on the interplay between different types of broadening revealing the importance of inhomogeneous broadening in determining the relative contributions of the two electronic transitions. We find that the transition dipole moment (M) for 2^1A_1 is greater than for transition to 3^1B_1, in agreement with gas phase calculations in the literature (Lesar et al). However, we find that the polarity of the solvent influences the excited state energetics, leading to a reversal in the ordering of these two states with 3^1B_1 shifting to lower energies. The experimental findings were complemented and supported through preliminary classical Molecular Dynamic (MD) simulations along with *ab initio* and linear

response calculations. Specifically, these calculations provided insights on the excited state dephasing rate and revealed the nature of solvation effects in methanol, supporting our findings for a considerable contribution in the spectral broadening from inhomogeneous effects.

ΠΕΡΙΛΗΨΗ

Η κατανόηση των βασικών πτυχών της εξάρτησης της δραστικότητας ενός συστήματος απο τη φάση στην οποία βρίσκεται αποτελεί σημαντική πρόκληση για την ατμοσφαιρική Χημεία. Αυτή η περιοχή της περιβαλλοντικής χημείας είναι στενά συνδεδεμένη με συγχρονη ερευνητική δραστηριότητα στον τομέα της φυσικοχημείας που συνδέεται με τη διελεύκανση του ρόλου του διαλύτη σε διάφορες φωτοφυσικές και φωτοχημικές διαδικασίες. Η ατμόσφαιρα αποτελεί είναι ένα ετερογενές μείγμα με ποικιλία μικροπεριβάλλοντων (αέρια, σταγονίδια, αερολύματα, κ.τλ.) όπου λαμβάνουν χώρα πολλές φωτοχημικές αντιδράσεις. Γι αυτό το λόγο η μελέτη ατμοσφαιρικών χημικών ενώσεων σε ένα καλά-καθορισμένο περιβάλλον συνιστά το πρώτο βήμα για την κατανόηση του ρόλου της φάσης στην ατμοσφαιρική Χημεία. Η μελέτη που παρουσιάζουμε στα πλαίσια αυτής της διατριβής αποτελεί τις πρώτες μας προσπάθειες για την κατανόηση της φωτοχημείας του νιτριλίου του χλωρίου στο διάλυμα.

Μετά απο μια σειρά προκαταρκτικών θεωρητικών και πειραματικών μελετών επιλέχτηκε η μεθανόλη ως ο καταλληλότερος διαλύτης για τη μελέτη της χημικής συμπεριφοράς του $ClNO_2$ στο διάλυμα. Χρησιμοποιήσαμε τη φασματοσκοπία Raman συντονισμού (RR) για να μελετήσουμε το $ClNO_2$ στη μεθανόλη μετά απο διέγερση στην περιοχή της ζώνης απορρόφησης D στα 200 -240 nm.

Στο φάσμα RR παρατηρήθηκε σε όλα τα μήκη κύματος διέγερσης μία κορυφή στους 1291 cm^{-1}, που αντιστοιχεί στη συμμετρική έκταση NO (ν_1). . Μια κορυφή πολύ μικρής έντασης που αντιστοιχεί στη συμετρική έκταση N-Cl (ν_3) παρατηρήθηκε μόνο στα 200 nm, που αποτελεί την κορυφή της μετάπτωσης D στο φάσμα απορρόφησης. Δεν παρατηρήσαμε καμμία κορυφή που να αντιστοιχεί στη συμμετρική κάμψη O-N-O (ν_2). Οι λόγοι αποπόλωσης και οι απόλυτες διατομές σκεδασμού RR για τη ν_1 λήφθηκαν για διάφορα μήκη κύματος που εμπίπτουν στηζώνη απορρόφησης D. Οι λόγοι αποπόλωσης αποκλίνουν σημαντικά απο την τιμή 1/3 που αποτελεί την τιμή του λόγου αποπόλωσης όταν μόνο μια διεγερμένη ηλεκρονική κατάσταση συνεισφέρει στο σκεδασμό Raman. Διαμέσου της μελέτης των απόλυτων διατομών σκεδασμού Raman (RRIA) αποδείχθηκε ότι δύο ηλεκτρονικές καταστάσεις συμμετέχουν στο σκεδασμό και είναι μη δεσμικές κατα μήκος του δεσμού Cl-N.

Η εργασία αυτή επεκτάθηκε με μια αναλυτική και λεπτομερή μελέτη των λόγων αποπόλωσης στα μήκη κύματος διέγερσης που χρησιμοποιήσαμε. Η ανάλυση επικεντρώθηκε στη διερεύνηση της αλληλεπίδρασης μεταξύ των διαφόρων μορφών διαπλάτυνσης αποκαλύπτοντας τη σημασία της συνεισφοράς της ανομοιογενούς διαπλάτυνσης, για τον καθορισμό των σχετικών συνεισφορών των δύο ηλεκτρονικών καταστάσεων. Μέσω αυτής της μελέτης έχει βρεθεί ότι η πολικότητα του διαλύτη επηρεάζει τις ενέργειες των διεγερμένων καταστάσεων οδηγώντας σε μια αντιστροφή της σειράς των ενεργειακών τους επιπέδων στο διάλυμα σε σχέση με την αέρια φάση. Τα πειραματικά ευρήματα συμπληρώθηκαν με θεωρητικούς υπολογισμούς Μοριακής Δυναμικής, ab initio και υπολογισμούς γραμμικής απόκρισης, οι οποίοι βοήθησαν στην εξακρίβωση της φύσης των αλληλεπιδράσεων του $ClNO_2$ με το διαλύτη. Επίσης, οι υπολογισμοί αυτοί ανέδειξαν την απαραίτητη συνεισφορά της ανομοιογενούς διαπλάτυνσης, σε συμφωνία με τα πειραματικά αποτελέσματα.

CONTENTS

CHAPTER 3: EXPERIMENTAL AND COMPUTATIONAL METHODS

CHAPTER 4: PRELIMINARY STUDIES OF ClNO2 IN SOLUTION: THE CHOICE OF SOLVENT AND AB INITIO CALCULATIONS

CHAPTER 5: RESONANCE RAMAN INTENSITY ANALYSIS OF ClNO2 DISSOLVED IN METHANOL

CHAPTER 6: ANALYSIS OF DEPOLARIZATION RATIOS OF ClNO2 DISSOLVED IN METHANOL

CHAPTER 8: FUTURE WORK

LIST OF FIGURES

LIST OF TABLES

ABBREVIATIONS AND SYMBOLS

B3LYP	Becke, three-parameter, Lee-Yang-Parr
C,c	Concentration
c	Speed of the light
CFC's	Chlorofluorocarbon
CCSD	Couple cluster singles doubles
D	Magnitude of the energy correlation function
DFT	Density functional theory
DOS	Density of states
DPR	Depolarization ratios dispersion curve
$D(t)$	Dissipation function
E_{00}	Zero –zero energy
E_L	Incident energy
E_s	Scattered Energy
$\vert f\rangle$	final vibrational state
FC	Frank Condon orbital
GGA	Generalized Gradient approximation
$g(t)$	Dephasing function
HOMO	Higher occupied molecular orbital
$\vert i\rangle$	Initial vibrational state
I	Intensity
LUMO	Lower unoccupied molecular orbital
MD	Molecular Dynamics
M_{eg}	Transition moment length for the $e\rightarrow g$
MeOH	Methanol

MP2	Second order Møller–Plesset perturbation theory
MRD-CI	Multi-reference configuration interaction
n	Index of refraction
PBE	Perdew-Burke-Ernezehrof
PSCs	Polar Stratospheric clouds
P_u	Occupational probability of vibrational state u
REP	Raman excitation profile
RR	Resonance Raman
RRIA	Resonance Raman Intensities Analysis
T_1	Excited state lifetime
T_2	Pure dephasing time
T^*_2	Total dephasing time
V_e	Potential energy of the excited state
UFF	Universal Bond Field
UV	Ultraviolet
UV- VIS	Ultraviolet Visible
TRRR	Time resolved resonance Raman
α	Polarizabilty
β	Excited stated slope
Γ	Inhomogeneous broadening
Δ	The change of the equilibrium geometry upon electronic excitation
ε_i	The energy of the initial vibrational state
ε	Extinction coefficient
Θ	Inhomogeneous broadening
κ	Transition bond length
Λ^{-1}	Decay of the energy correlation function

λ	Wavelength
μ	Reduced mass
v_0	Incident frequency of the light
v_1	N-O symmetric stretch of $\mathrm{ClNO_2}$
v_2	O-N-O symmetric bend of $\mathrm{ClNO_2}$
v_3	Cl-N symmetric stretch of $\mathrm{ClNO_2}$
v_4	N-O asymmetric stretch of $\mathrm{ClNO_2}$
v_5	$\mathrm{NO_2}$ rock of $\mathrm{ClNO_2}$
v_6	Out-of-plane bend of $\mathrm{ClNO_2}$
ρ	Depolarization Ratio
σ_A	Absorption cross section
σ_R	Raman cross section
Σ^0	Isotropic part of the scattering tensor
Σ^1	Symmetric anisotropy
Σ^2	Antisymmetric part of the scattering tensor
ω_e	Excited -state harmonic frequency
ω_g	Ground-state harmonic frequency

CHAPTER 1

INTRODUCTION

Halogens such as chlorine are converted from halides, including $ClNO_2$, to reactive radicals by UV solar radiation. These radicals can affect ozone production and destruction in the stratosphere. Recently, it became clear that halogen radicals can also play a significant role in the chemistry of the troposphere. The atmosphere is a heterogeneous mixture of gases surfaces, aerosols, droplets. The examination of the reactivity of various atmospheric species over a range of well defined environments is the first step in understanding the role of phase in atmospheric photochemistry.

The UV- absorption spectrum of gaseous nitryl chloride is reported in several studies and it is characterized by four absorption bands referred to as A, B, C, and D. The D band, which appears below 200 nm, is the strongest transition. Previous photochemical studies on nitryl chloride ($ClNO_2$) focusing on the gas and solid state on resonance with the A and B absorption bands demonstrated a clear phase-dependent reactivity. However, no studies of this molecule have been reported in solution other than the reaction of $ClNO_2$ on wet aerosols and the Raman spectrum of liquid $ClNO_2$. Moreover, no work on $ClNO_2$ has provided information about the photodissociation dynamics on resonance with the strong D absorption band. In the condensed phase, an intermediate behavior would be expected between those in the gas and solid phases, where both dissociation and isomerization may occur, depending on the rigidity of the solvent cage around the molecule, resulting in more accessible product channels.

This doctoral dissertation aims to understand the solute-solvent interactions that favour certain reaction channels versus others and elucidate the chemical behaviour of nitryl chloride in a solution environment. Firstly, such investigations add to the knowledge of $ClNO_2$'sphase reactivity covering a gap in the literature. Moreover, the polar stratospheric clouds that promote the conversion of inert chloride species to active compounds such as $ClNO_2$ are formed during the long polar night from small amounts of water vapor that condenses at temperatures as low as -78^0C K and nitric acid trihydride. These can promote chemistry that is significantly different from that which occurs in the gas phase but probably similar with that in the solid and liquid phases. Thus, the study of nitryl chloride in solution is of central importance for atmospheric chemistry. Moreover, from a physical chemistry point of view the determination of the extent to which a given reaction path changes as a function of environment and the clarification of the reasons that lead to such behaviour is fundamental.

The originality of the present doctoral dissertation rests on the investigation of the effect of the surrounding environment on nitryl chloride photoreactivity using Resonance Raman spectroscopy as a tool. This is the first Resonance Raman study of nitryl chloride in any kind of environment. In this work, we were able to obtain information about the ground state geometry and chemical structure of $ClNO_2$ *in solution via RR frequencies, while Resonance Raman Intensity Analysis provided valuable information about the symmetry, geometry and early-time dynamics on the resonantly excited electronic state/states of this system. In addition, the knowledge about* $ClNO_2$ *in solution was extended through measurement and analysis of RR depolarization ratios, revealing thus the number and nature of the excited states that contribute to the RR scattering.*

The thesis is organized as follows: In *Chapter 2* we briefly review the literature on halooxide photochemistry and the potential role of nitryl chloride as an atmospheric trace species, as well as report previous photochemical, spectroscopic and theoretical studies on $ClNO_2$. The main aspects and the theoretical background of Resonance Raman (RR) spectroscopy, which is the main experimental technique used in this work, are also discussed in this Chapter, including a brief description of the time-dependent formalism of Raman spectroscopy. Other themes underlying our work, such as solute-solvent interactions, and the contribution of nearby excited states, the homogeneous linewidth, and a dissociative potential to the observed scattering are reviewed. Finally, we include some of the theory on depolarization ratios and discuss the effect of resonance with more than one electronic excited state.

In *Chapter 3* we describe in detail the experimental and theoretical methods used in this work. Nitryl chloride has not been studied in solution prior to our work. Therefore, besides developing a method to introduce the gaseous molecule in solution, we also investigated a variety of solvents to determine the most suitable ones to study its phase dependent reactivity. *Chapter 4* describes these preliminary experiments complemented by theoretical calculations. Even though our goal was to examine solvents that range from non-interacting (gas-phase-like) to polar protic, we found that methanol was the only medium in the range of solvents screened that stabilized the molecule.

Our initial study of $ClNO_2$ in methanol was the first step towards understanding the phase-dependent reactivity of this molecule. This work is reported in *Chapter 5* where we present a Resonance Raman Intensity Analysis (RRIA) study of $ClNO_2$ in methanol, with excitation at wavelengths resonant with the D absorption band of the molecule. Here we investigate the effect of solvent on the ground state structure (via RR frequencies), the early-time excited-state dynamics along with the nature of the electronic transitions. *Chapter 6* deals with the analysis of depolarization ratios (DPR's) of $ClNO_2$ dissolved in methanol. The DPR's measured at excitation energies on resonance with an electronic absorption can be used to model the theoretical depolarization ratio dispersion curve simultaneously with the REP and absorption cross sections. DPR's along with RR intensities are a sensitive probe of excited state structure and early-time dynamics in the Franck-Condon (FC) region. Through a systematic approach we demonstrated the interplay between several parameters and their importance in the modeling of the experimental observables, focusing especially on the contributions of homogeneous and inhomogeneous broadening. Preliminary molecular dynamics (MD) simulations complement the experimental work presented here, by providing insights on solute-solvent interactions operating in this molecular system.

The conclusions derived from this dissertation are discussed in *Chapter 7*.

We believe that various issues are still open and for that reason we propose specific future work in *Chapter 8*.

CHAPTER 2

EXISTING KNOWLEDGE AND THEORY

This chapter is organized in three parts. The first part is a brief description of the atmospheric chemistry of halogenated species. Their influence on stratospheric ozone depletion and their potential role in the tropospheric and stratospheric chemistry are discussed. The second part is a literature review of previous photochemical, spectroscopic and theoretical studies on nitryl chloride. In the last part of this section we deal with the theoretical background of Resonance Raman (RR) which is the main experimental technique used in this dissertation.

2.1 Atmospheric chemistry and nitryl chloride

2.1.1 Reactive halogen species in the stratosphere - The chlorine chemistry

Halogen-containing gases present in the stratosphere can be divided into two groups: *halogen source gases* and *reactive halogen gases*.

In recent decades various human activities have released halogenated source gases into the atmosphere. Of particular importance are chlorine and bromine containing species. Chemicals released into the atmosphere by industrial practices include chlorocarbon compounds (CCl_4 and $CHCl_3$), chlorofluorocarbon compounds, CFSs ($CFCl_3$, CF_2Cl_2) and halons especially CF_3Br and CF_2ClBr. Chlorocarbons are used as industrial solvents, degreasing compounds and CFC precursors. The chlorofluorocarbons have been used in many applications, including refrigeration, air conditioning, and foam blowing and through the 1970s as aerosol propellants. Halons are developed to extinguish fires and are widely used to protect large computers, military hardware and commercial aircraft engines. Human emissions of the halogen-containing gases have increased since the middle of the 20th century and resulted in global ozone destruction with the largest losses occurring in Polar Regions. The production and consumption of these halogen sources are regulated under the Montreal Protocol, as CFCs and halons have long lifetimes in the troposphere, and can thus pass through the tropopause into the stratosphere where they are converted to more reactive gases by solar ultraviolet radiation.

The chemical conversion of halogen source gases involves ultraviolet sunlight and other chemical reactions to produce a number of reactive halogen gases. These reactive gases contain all of the chlorine and bromine atoms originally present in the source gases. The most important reactive chlorine- and bromine containing gases are shown in Figure 2.1

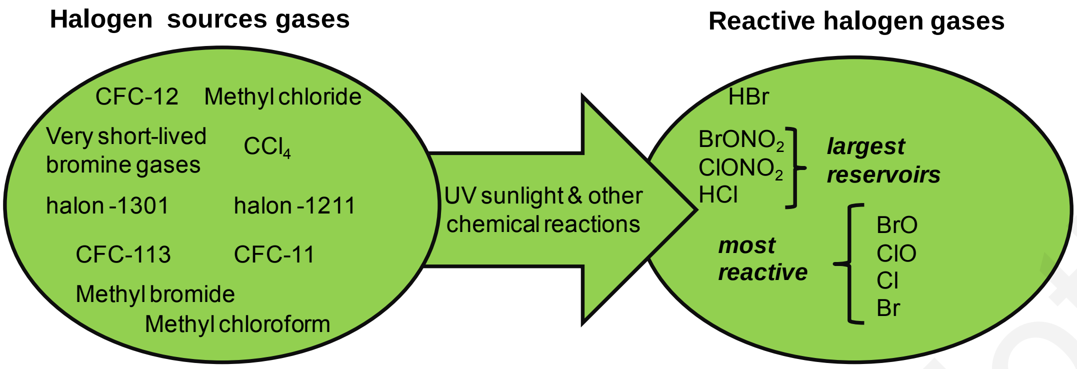

Figure 2.1 Chemical conversion of halogen source gases to reactive halogen gases in the stratosphere. The conversion requires sunlight and a few other chemical reactions. The reactive halogen gases contain all the bromine and chlorine originally present in the source gases. The reactive gases are separated into reservoir gases, which do not destroy ozone and reactive gases that participate in catalytic ozone destruction cycles.

The catalytic reaction cycles that efficiently destroy ozone require the participation of reactive species (Scheme 1).[1,2]. Here, X represents any halogen-containing species (Cl, Br, BrO, ClO, $ClONO_2$, $BrONO_2$, etc.)

$$\begin{array}{c} X^{\bullet} + O_3 \rightarrow XO^{\bullet} + O_2 \\ O_3 + hv \rightarrow O + O_2 \\ O + XO^{\bullet} \rightarrow X^{\bullet} + O_2 \\ \hline 2O_3 + hv \rightarrow 3O_2 \end{array}$$

Scheme 1

Ozone depleting gases are transported great distances by air motions and in combination with their long lifetime they find their way into the stratosphere. The destruction of O_3 can be ‘short-circuited’ by removing either Cl or Br or alternatively ClO and BrO. For chlorine atoms, this occurs by the reaction with methane that has been transported from the troposphere [2,3]:

$$Cl + CH_4 \rightarrow HCl + CH_3 \qquad (2.1)$$

and for ClO by the reaction with NO_2:

$ClO + NO_2 \rightarrow ClONO_2$ (2.2)

Away from Polar Regions the most abundant speciesare HCl and $ClONO_2$ which are considered as reservoir gases because they do not react directly with ozone but can be converted to the most reactive forms that do chemically destroy ozone. Partitioning between reactive chlorine and reservoirs depends on temperature and altitude.[2-4]

The above catalytic cycle is dramatically enhanced in the presence of polar stratospheric clouds (PSCs). PSCs are formed during the long polar night from small amounts of water vapor that are condensed at temperatures as low as ~-78^{0}C and are formed either from ice or nitric acid trihydride (NAT). Liberation of active chlorine from the reservoirs species HCl and $ClONO_2$ is rather slow, but the PSCs promote their conversion to active chlorine species via the efficient adsorption of HCl on the surface of PSCs, where a heterogeneous reaction of gaseous $ClONO_2$ with stratospheric aerosol takes place:[5,6]

$HCl(s) + ClONO_2 \rightarrow Cl_2 + HNO_3(s)$ (2.3)

The reaction between $ClONO_2$ and water may also take place:

$ClONO_2 + H_2O(s) \rightarrow HOCl + HNO_3(s)$ (2.4)

with gaseous HOCl rapidly photolysing to yield a free chlorine radical. If N_2O_5 is present, a further heterogeneous reaction reconverts HCl into active chlorine[7-10] with $ClNO_2$ released in the gas phase rapidly photolyzing to yield active chlorine.

$N_2O_5(g) + HCl_{(ice)} \rightarrow ClNO_{2(ice)} + HNO_3(ice)$ (2.5)

In summary, the reservoir species $ClONO_2$ and N_2O_5 react heterogeneously on the surface of the polar stratospheric clouds, where HCl has been adsorbed, to produce gaseous Cl_2, HOCl and $ClNO_2$. Subsequent photolysis of these species by solar radiation during polar sunrise results in chlorine radicals that react catalytically with ozone to yield ClO. The latter accumulates with the catalytic reaction cycle leading to substantial ozone depletion. However, solely gas-phase chemistry in the ClO_x system does not produce the necessary concentrations to account for the ozone hole.

Shindell *et al.*[11] investigated the interplay between emissions of greenhouses gases and levels of ozone depleting halogen species using a global climate model that incorporates simplified ozone depletion chemistry. They concluded that despite reductions in emissions of O_3–depleting CFCs, levels of ozone will continue to fall with especially severe declines occurring in the years 2010 to 2019. This is due to the radiative CO_2 and other greenhouses gases that result in global warming. In that way, more of the heat radiated from Earth's surface is trapped in the troposphere and less heat reaches the stratosphere which cools enhancing the conversion of reservoir specious to active chlorine radicals.

2.1.2 Reactive halogen species in the troposphere - The chlorine chemistry

The mechanisms governing the release of reactive halogen species in the troposphere has received increasing attention in recent years. The clarification of the role halogens play in the troposphere and the process in which reactive halogens are liberated in the lower atmosphere has been the focus of many fields, model and laboratory studies. Although some unresolved details still remain, two major sources are considered as the main sources of halogens in the troposphere: liberation of aerosols from sea salt and degradation of partially halogenated compounds. Sea salt aerosols are a large and a rapidly recycling reservoir of liquid water in the marine boundary layer produced in the sea surface by the bursting of air bubbles.[12] Volatile chlorine-containing gases such as HCl, dihalogens[13,14] and $ClNO_2$[7,8,15] arise from the release of halogen from salt particles or droplets. Globally, sea spray is the dominant source of tropospheric chloride,[16] which is transported as sea spray particles or gaseous HCl following acid displacement by HNO_3 and H_2SO_4.[17] Specifically, hydrogen halides can be liberated from sea salt aerosols by the action of strong acids such as H_2SO_4 and HNO_3.[13,14]

$$H_2SO_4 + 2\ NaCl_{(aerosol)} \rightarrow 2\ HCl + Na_2SO_4 \qquad (2.6)$$

Moreover, under polluted conditions, the reactions of N_2O_5 and NO_2 with aqueous NaCl and salt surfaces give gaseous nitryl chloride ($ClNO_2$) and ClNO[7,8,15] via the following reactions:

$$N_2O_5 + H_2O \rightarrow 2\ HNO_3 \qquad (2.7)$$

$$N_2O_5(s) + NaCl(s) \rightarrow ClNO_2(g) + NaNO_3(s) \qquad (2.8)$$

$$2NO_2 + NaCl \rightarrow ClNO + NaNO_3 \qquad (2.9)$$

$ClNO_2$ and ClNO can be subsequent photodissociated by solar radiation releasing Cl atoms and NO_2. The efficient production of $ClNO_2$ from the heterogeneous reaction of nitrogen pentoxide has been shown only in laboratory studies. Osthof and colleagues have observed high concentrations of nitryl chloride in coastal regions and ship plumes – places where chloride from sea salt meets pollution using chemical ionization mass spectrometry.[18] $ClNO_2$ is found to accumulate at night[17,18] and be photolysed after sunrise to produce chlorine atoms. Elemental mercury (Hg^0) which has a lifetime in the atmosphere of up to a year is oxidized by chlorine atoms forming an oxidized form of mercury (Hg^{+2}) which has a lifetime of a few days or less as a result of the higher solubility of Hg^{+2} in atmospheric moisture.[19] Chlorine also reacts with methane (greenhouse gas) forming methyl chloride one of the most common halogen source gases[20](Figure 2.1). Chlorine atoms also influence the catalytic cycles for production of tropospheric ozone[2,21], a greenhouse gas which is toxic to plant and animal life. Other sources of chloride are industrial activities,[16] biomass burning,[16] and transport of windblown soil dust.[22]

2.2 Photochemistry of nitryl chloride

It has been shown that the photochemistry of $ClNO_2$ is markedly influenced by its environment. Various photo-dissociation pathways are energetically accessible to this molecule upon exposure to solar radiation and evidence exists to support a phase-dependent reactivity (Scheme 1).

$$\begin{aligned}
\mathrm{ClNO_2} &\xrightarrow{h\nu} \mathrm{Cl} + \mathrm{NO_2} && (i)\\
&\xrightarrow{h\nu} \mathrm{ClO} + \mathrm{NO} && (ii)\\
&\xrightarrow{h\nu} \mathrm{ClNO} + \mathrm{O} && (iii)\\
&\xrightarrow{h\nu} \mathrm{Cl} + \mathrm{O} + \mathrm{NO} && (iv)
\end{aligned}$$

Scheme 2

Work on $ClNO_2$ photochemistry so far has mainly focused on the gas and solid phase. In the gas phase, $ClNO_2$ dissociates to Cl and NO_2 (channel (*i*)) with a quantum yield of 0.93.[23-26] No evidence exists supporting the involvement of channels (*ii*) and (*iv*) in the gas phase, and channel (*iii*) was found to be of only minor importance with a quantum yield of 0.02.[23,26] However, the latter has been recently challenged, as the quantum yield for $O(^3P_2)$ production was found to be wavelength and temperature dependent, reaching possibly 0.67 at 193 nm and 0.15 at 248 nm.[27] This high $\varphi(O(^3P_2))$ at 193 nm could, however, include contributions from both channel (*iii*) and secondary photodissociation of NO_2. All the channels above refer to the products in their ground electronic state. However, resonance enhanced multiphoton ionization/time of flight spectroscopic studies (REMPI-TOF) showed evidence that most of the NO_2 fragments (channel (*i*)) are formed in the excited electronic state A^2B_2 (85%) versus the ground state X^2A_1 (15%).[26]. In the solid phase, work on this molecule has been done in argon and water clusters, argon matrixes, in ice, as well as on pure films of $ClNO_2$.[28,29] In clusters, only channel (*i*) was found to be active, where part of the Cl and NO_2 fragments were produced with low translational and internal energy, which consequently would be less likely to further react with other molecules compared to the monomer products.[28] In matrixes, photoisomerization of 60% of $ClNO_2$ to *cis* (18%) and *trans* (42%) ClONO was observed.[29-31]. This is most probably due to the cage effect, where recombination of the Cl and NO_2 fragments leads to either reformation of $ClNO_2$ or to the *cis* and *trans* isomers. Subsequent photodissociation of the *cis* and *trans* isomers then provides for two other dissociation channels; one is channel (*ii*) above, and the other is ClON + $O(^1D)$, ClON rapidly isomerizing to ClNO. [29] Finally, the photochemistry of pure films of $ClNO_2$ and of $ClNO_2$ dissolved in ice is very different from that observed in matrixes. In the case of pure, solid $ClNO_2$, rupture of the Cl-N bond still occurs as in the gas phase, generating N_2O_4 instead. In ice, irradiation of $ClNO_2$ leads to the production of nitric acid.[32] It is thus apparent that the photochemistry of $ClNO_2$ depends on the environment the molecule encounters. Prior to our studies, no work on this molecule has been reported in bulk solution other than the reaction of $ClNO_2$ on wet aerosols[15,33] and the Raman spectrum of liquid $ClNO_2$.[34]

2.3. Structural parameters of gaseous $ClNO_2$

Resonance Raman spectroscopy is a ground state vibrational technique where the frequency of a vibrational mode is given by the equation:

$$v = \frac{1}{2\pi c}\sqrt{\frac{k}{\mu}} \qquad (2.10)$$

where the c is the speed of the light, κ is the force constant in the atomic scale, and μ is the reduced mass. The force constant is a criterion for the strength of the chemical bond in the diatomic molecule A-B. Therefore, the stronger the chemical bond (electronic effect) and the smaller the reduced mass m (mass effect), the higher the wave number of the absorption band becomes. Moreover, for a non isolated molecule (in liquid or solid state) interactions with the surroundings result in a change in its ground state geometry and a consequent shift of the vibrational frequency along a specific normal mode. It is obvious that there is a direct relationship between a vibrational spectroscopy and the geometry of molecule. Thus the investigation of the equilibrium structure of a molecule is complementary to Raman experiments not only to support the spectral assignment but also to clarify the ground state structure by observing the changes of the vibrational frequencies.

The determination of equilibrium structures has been carried out at the TZ2 /CCSD [35], MP2[36,37], CCSD(T)/TZ2P[38] and at B3LYP[37] levels of theory. The results for the structural parameters of $ClNO_2$, derived from *ab initio* calculations, using different basis sets [35-38] are summarized in Table 2.1. The comparison shows a good overall agreement with a slight overestimation of the Cl-N bond distance ($r_{Cl\text{-}N}$) (not more than 4%) and a corresponding underestimation of the N-O bond length (<ONO) by ~1% in the study of Papayiannis *et al.* [37]

These theoretical studies about nitryl's chloride geometry parameters are limited only in the gas phase and nitryl chloride's isomers. Similar calculations in the condensed phase would facilitate understanding of structural change in the ground state along with solute-solvent interactions in condensed media. In addition, information regarding the displacement of the equilibrium position of a potential energy curve along these coordinates may be derived by applying vibrational spectroscopy in nitryl chloride dissolved in a solvent.

Table 2.1 Comparison of optimized geometries (Å, deg) of gaseous $ClNO_2$

Structural parameters	Lee[35] TZ2 /CCSD	Durig *et al.*[36] MP2	Lesar *et al*[38]. CCSD(T)/TZ2P	Papayiannis[37] MP2 & B3LYP	Exp.[36]
$r_{Cl\text{-}N}$	1.877	1.906	1.885	1.952^{i} 1.942^{ii}	1.837
$r_{N=O}$	1.198	1.206	1.200	1.189^{i} 1.184^{ii}	1.202
<ONO	132	133.2	131.9	134.4^{i} 133.5^{ii}	130.2
<ONCl	-	113.4	114.0	112.8^{i} 113.2^{ii}	114.9

^{i} from ab initio calculations using MP2 level of theory
^{ii} from ab initio calculations using B3LYP level of theory

2.4. Symmetry elements and vibrational spectrum of nitryl chloride

Nitryl chloride is a planar molecule in its ground state (X^1A_1) with C_{2v} symmetry. Figure 2.3 shows the symmetry elements of $ClNO_2$. Of the total degrees of freedom (3N=12), six are vibrational (3N-6). Thus, in the vibrational spectrum of nitryl chloride six vibrational modes are expected. Based on selection rules of vibrational spectroscopy all the modes are active both in IR and Raman. The six fundamental vibrational modes of $ClNO_2$ and the symmetry of each coordinate are shown in Table 2.2.

Vibrational spectroscopy has been used for characterization of nitryl chloride, but these studies have been limited to infrared measurements and analysis of the spectra.[29,32,36,39-41] Very few Raman studies of this molecule have been reported in the literature and those were limited to reporting the Raman spectrum and structural analysis,[36,41] while no Resonance Raman (RR) studies have been performed to our knowledge to date, especially of $ClNO_2$ in solution.

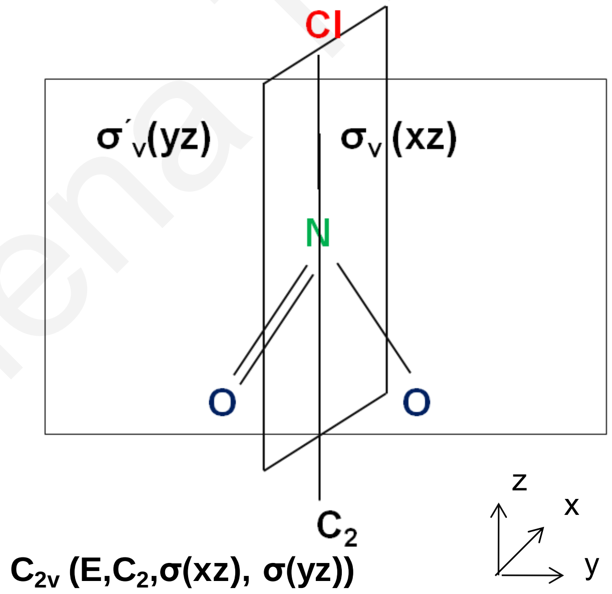

Figure 2.2 Symmetry and Symmetry elements of $ClNO_2$

Table 2.2 Fundamental modes of $ClNO_2$

Vibrational mode	Description of the motion	Symmetry
$v_1 = v_S^{NO}$	Symmetric stretch N-O	A_1
$v_2 = \delta_S$	Symmetric bend	A_1
$v_3 = v_S^{CLN}$	Symmetric stretch Cl-N	A_1
$v_4 = v_{AS}^{NO}$	Asymmetric stretch N-O	B_1
$v_5 = \delta_{AS}$	Asymmetric bend	B_1
v_6	Out of plane bend	B_2

In Table 2.3 the frequencies of the six fundamental vibrational modes of nitryl chloride (C_{2v}) derived from previous studies in different phases are summarized. It is obvious that moving from the gas phase to the liquid and solid states the frequencies for two of the three symmetric frequencies (ν_1, ν_2) are downshifted. A similar behavior is observed for the ν_4 asymmetric mode. The downshifting of the frequencies corresponding to motions along the N-O demonstrates a weakening of this bond in the ground state. In the previous section we mentioned the direct relationship between the vibrational frequency and the ground state molecular structure. On the other hand the ν_3 frequency corresponding to the N-Cl symmetric stretch is up shifted as the matter becomes more condensed denoting a strengthening of this bond. The same trend is also observed for the ν_5. The ν_6 frequency which corresponds to the out of plane bend does not significantly vary between the three states of matter.

Table 2.3 Vibrational modes of nitryl chloride

Modes	Gas phase[36]	Liquid State[34] cm^{-1}	Solid State [36] cm^{-1}
v_1	1267.3	1258.7	1259 1252
v_2	793.8	786.2	786.2
v_3	369.6	370	399 379
v_4	1684.6	1667	1664 1648
v_5	412	411	422 428
v_6	651.7	652	651.5

2.5 Theoretical description of resonance Raman intensities

2.5.1The definition of resonance Raman scattering

When a beam of monochromatic light having a frequency v_0 is directed to a sample, most of the light is transmitted, part of it might be absorbed and part is scattered. Most of the scattered light coming out of the sample has the same frequency as the incident light (*Rayleigh scattering*), while a small fraction of it is shifted to longer and shorter wavelengths because of its interaction with the molecules of the sample. Inelastic scattering was first observed in 1928 and owes its name to C.V. Raman who (with K.S. Krishnan) first reported this effect. The Raman scattering at wavelengths longer than the exciting wavelength is referred to as *anti-Stokes* scattering, while at shorter wavelengths it is called *Stokes* scattering.[42,43] In other words, Stokes scattering is the process where the energy is transferred from the electromagnetic field to the molecule while anti-Stokes scattering is the opposite process. Anti Stokes scattering is weak because for most of vibrations at or below room temperature the vibrational partition function places most of the thermal population in the ground state. Thus, most of the Raman experiments detect Stokes scattering. Resonance Raman (RR) scattering occurs when the incident radiation frequency falls within an allowed electronic absorption band of the molecule of interest, causing the vibrations of the absorbing species to be selectively enhanced by up to six orders of magnitude compared to the non resonant spontaneous Raman scattering. [43] This results in the high sensitivity of RR spectroscopy, where concentrations as low as 10^{-6} $\mathrm{molL^{-1}}$ may be detected.

In RR only modes that are coupled to electronic transitions display large enhancements of their intensities relative to the off-resonance case. These are the Franck-Condon-active modes, which facilitate structural change in the excited state. RR spectroscopy probes the dynamics in the FC region. Therefore, RR frequencies report ground state vibrational frequencies, which provide detailed information about the geometry and electronic structure of the molecule in its ground state, while the intensities of each vibrational line provides information about the symmetry and dynamics of the resonant excited electronic state along that particular normal coordinate [44-47]. Thus, RR spectroscopy is a useful tool for elucidating excited state structure, especially in the case of molecules that exhibit diffuse absorption spectra.

2.5.2 Resonance Raman Intensities Analysis (RRIA): Time-dependent formalism

RR intensities are sensitive to the difference between the ground state and excited state potential energy surfaces minima along a normal mode.[44] Thus, by performing a Resonance Raman Intensities Analysis (RRIA) we may predict the excited state structure at a harmonic minimum of a normal mode and the initial excited state dynamics in the Franck-Condon region. In this section we provide a short review of one of the most commonly employed approaches to provide RRIA; the time-dependent formalism. This process was originally developed by Lee and Heller in 1979 [48] and is based on molecular wavepacket dynamics on the excited state potential energy surface.

The intensity resulting from a Raman transition from an initial vibrational state $|i\rangle$ to a final vibrational state $|f\rangle$ at incident energy E_L is determined by the Raman cross section $\sigma_{i\to f}$ (in units of area per molecule):

$$P_{i\to f} = I\sigma_{i\to f}(E_L) \tag{2.11}$$

where $P_{i\to f}$ is the total power of the scattered photon, I is the incident photon flux in photons area^{-1} sec^{-1}. The expression for the Raman cross section, derived from second-order perturbation theory is given below:

$$\sigma_{i\to f}(E_L) = \frac{8\pi e^4 E_S^3 E_L}{9\hbar^4 c^4}\left|a_{i\to f}(E_L)\right|^2 \qquad (2.12)$$

$\alpha_{i\to f}(E_L)$ is the molecular polarizabilty tensor, E_L and E_S are the incident and scattered photon energies. In the time-dependent picture the Raman polarizabilty can be written as a half Fourier transform of the time-dependent overlap between the final vibrational state $|f\rangle$ and the initial vibrational wavepacket propagated under the influence of the excited-state Hamiltonian $|i(t)\rangle$:

$$\alpha_{i\to f}(E_L) = \frac{iM_{eg}^2}{\hbar}\int_0^\infty \langle f\,|\,i(t)\rangle \exp\left[\frac{i(E_L+\varepsilon_\iota)}{\hbar}\right] e^{-\Gamma t/\hbar}\,dt \qquad (2.13)$$

M_{eg} is the electronic dipole moment evaluated at the equilibrium nuclear geometry, ε_i is the energy of the initial vibrational state, Γ is the homogeneous linewidth. The complete expression for the RR cross section is: [48-50]

$$\sigma_{i\to f}(E_L) = \frac{8\pi\, \mathrm{e}^4 E_S^3\, E_L\, M_{eg}^4}{9\hbar^6 \mathrm{c}^4}\int_{-\infty}^{\infty} dE_{00}\, H(E_{00})\left|\int_0^\infty \langle \mathrm{f}\,|\,\mathrm{i(t)}\rangle \exp\left[\frac{i(E_L+\varepsilon_{\mathrm{i}})t}{\hbar}\right] e^{-\Gamma t/\hbar}\,dt\right|^2 \qquad (2.14)$$

$H(E_{00})$ is the contribution of inhomogeneous broadening, which corresponds to the presence of different solvent sites that are static on the timescale of Raman scattering. E_{00} is the energy difference between the ground and excited electronic states and the $D(t) = e^{-\Gamma t/\hbar}$ is the damping function.

The integrated area under each vibrational peak in a RR spectrum is proportional to the Raman cross section for the corresponding $|i\rangle$ to $|f\rangle$ transition. The plot of the cross sections for a $|i\rangle$ to $|f\rangle$ Raman transition as a function of excitation frequency is the Raman excitation profile (REP).

A similar time-dependent expression for the optical absorption cross section is derived from the full Fourier transform of the overlap between the initial vibrational state $|i\rangle$ and the initial vibrational wavepacket propagated under the influence of the excited-state Hamiltonian $|i(t)\rangle$:

$$\sigma_A(E_L) = \frac{4\pi\, \mathrm{e}^2 E_L {M_{eg}}^2}{6\hbar^2 \mathrm{cn}} \int_{-\infty}^{\infty} dE_{00} H(E_{00}) \int_{-\infty}^{\infty} \langle \mathrm{i} | \mathrm{i(t)} \rangle \exp\left[\frac{i(E_L + \varepsilon_{\mathrm{i}})t}{\hbar}\right] D(t)dt \qquad (2.15)$$

where *n* is the solution index of refraction. The above Equations (2.14 and 2.15) demonstrate that the absorption cross section depends on the same excited-state parameters as the RR cross section. Although the absorption spectrum of a molecule is often too diffuse to provide mode-specific information of the excited state potential energy surface, it can be measured very accurately and the excited state parameters used to model the Raman intensities can always be required to fit the absorption spectrum as well. Therefore, simultaneous modeling of the experimental absorption and Raman cross sections is imperative in order to obtain an accurate picture of the potential energy surfaces of the molecule of interest. In addition, since the absorption and Raman cross sections depend differently on homogeneous linewidth, simultaneous modeling of the two cross sections helps to distinguish the role of homogeneous and inhomogeneous broadening, thus providing an accurate measure of the excited state lifetime. Below, we discuss in more detail the sources of the two types of broadening and their effect in the REP and absorption spectra (see below).

A one-dimensional example of the wavepacket propagation is presented in Figure 2.3. The incident field E_L creates a copy of the ground state wavepacket on the excited state potential energy surface $|i(0)\rangle$. Because, this initial state is not an eigenstate of the excited state Hamiltonian, the wavepacket propagates on the excited state potential energy surface $|i(t)\rangle = e^{-iHt/\hbar}\,|i\rangle$. This evolution results in the displacement (Δ) of the excited minimum relative to the ground state. The time-dependent overlap with the initial state $\langle i | i(t) \rangle$, determines the absorption spectrum whereas the overlap with the final state $\langle f | i(t) \rangle$ generates the Raman excitation profiles. If the ground and excited state minima are weakly displaced, the wavepacket never propagates enough to gain a good overlap with the final state such that a low resonance Raman intensity is predicted. The Frank Condon (FC) overlaps are responsible for the selective enhancement of only specific vibrational modes: from symmetry arguments it is known that FC factors are non-zero only for totally symmetric modes whose equilibrium positions are displaced in the excited state, assuming that the molecular symmetry is not altered. This selectivity in enhancement of certain vibrational modes is a very important aspect in RR spectroscopy, since it leads to a considerable simplification of the observed spectra. It is important to stress that a RR experiment is not a time resolved experiment but the RR intensities may be interpreted in terms of a time-dependent vibrational wave packet similar to the one obtained from a femtosecond laser pulse.[50] In analogous fashion, absorption intensity is related to $\langle i | i(t) \rangle$ and corresponds to the time-dependent overlap of the initial ground state with the propagating state.

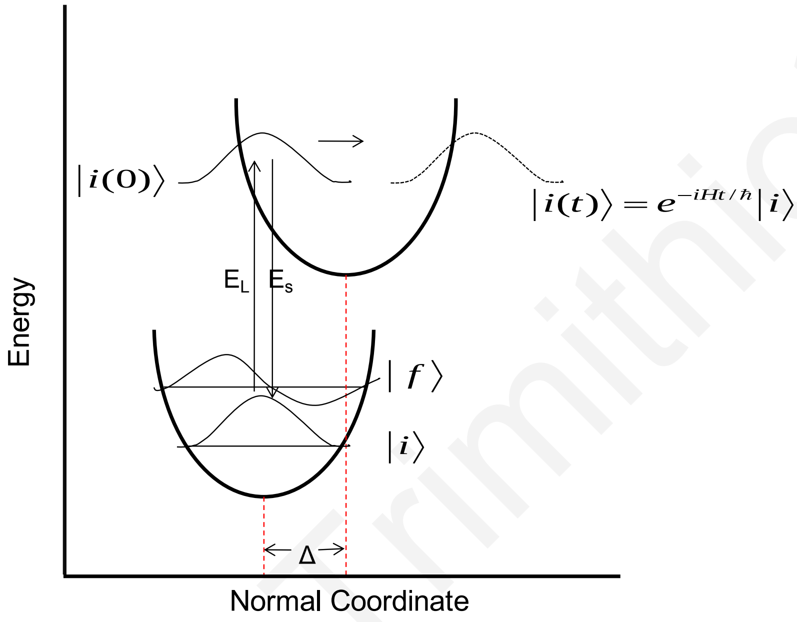

Figure 2.3 The time-dependent picture of RR scattering for a bound harmonic excited state surface. The change of the equilibrium geometry upon electronic excitation is denoted by Δ.

2.5.3 Solvent – solute interactions: Solvent induced spectral broadening

The role the environment plays in the spectral line broadening is a recurring question in the area of condensed matter molecular spectroscopy. The very breadth and featurelessness of the condensed phase spectra (electronic spectra and REP) are environmentally-induced and can be attributed to homogeneous and inhomogeneous broadening. Numerous spectroscopic studies were applied in order to separate the two types of broadening or to determine the total dephasing time which is the inverse of the homogeneous linewidth. The two fundamental ways in which dissolved molecules change their behavior compared to isolated molecules are the *vibrational relaxation* and/or pure dephasing. In the first event the dissolved molecule gets rid of any excess vibrational energy through energy exchange with the surrounding liquid with time scale T_1 while the second process derives from the fluctuation of the energetics of the solvent due to the solute-solvent interactions with a time scale T_2^*.[51-53] Homogeneous broadening (Γ) contains contributions from both processes taking place in condensed matter.

$$\Gamma = \frac{1}{T_2} = \frac{1}{2T_1} + \frac{1}{T_2^*} \qquad (2.16)$$

In the above equation T_2 is the total dephasing time.

In this section we make an attempt to look at the two processes in more detail based on existing literature. Firstly, our analysis will focus on vibrational relaxation. A vibrationally excited molecule dissolved in a liquid can relax via dissipation of the excess energy directly to the solvent or through dispensing of this energy between different intramolecular modes, with the solvent absorbing a sufficient quantity of energy to drive the process.[54,55] The rate constant for energy relaxation $1/T_1$ is proportional to the vibrational friction the solvent exerts on the surrounding medium and to the fluctuating force acting on the solute.[54-56] Determination of how a solvent influences relaxation dynamics is central to the understanding of chemical reactivity in condensed matter.[57] Since, the theory covering the vibrational relaxation is not a subject of this thesis we content ourselves with this short theoretical information.

The pure dephasing process is considered to arise mainly from solute-solvent interactions. However, the redistribution of internal energy among intramolecular vibrational degrees of freedom of the soluteis treated as a possible mechanism of dephasing, which is not associated with the environment. Here, we deal only with the intermolecular contribution to the total dephasing time and the spectral broadening. In order to treat this problem correctly one must realize that the expressions for Resonance Raman and absorption cross sections (Eq. 2.14 and Eq. 2.15) are valid for an isolated molecule. In that ideal case it is assumed that the system which interacts with light can be described by a wavefunction (or a state vector) that spans all of the degrees of freedom. The only relaxation times that enter into the expressions are the lifetimes of the excited states.[51,58] However, RR was proven a useful technique in the study of condensed matter, where the surrounding molecules have no resonant interaction with the light but perturb the chromophores that do.[44,59] When a molecule is dissolved, its behavior differs from that in the gas phase, and the situation becomes much less clear. In non-isolated molecules, these expressions (Equation 2.14 and 2.15) can be used if only the degrees of freedom of the bath are taken into account. [50,59,60] Since it is impractical to make the Hamiltonian used in these formalisms span the entire system, the dilute solutions are handled by considering a weak interaction between the resonant molecule and the environment. Thus, a density matrix formulation[61] is required in order to treat correctly the interactive system. The solvent creates a random perturbation resulting in the fluctuation of the energy levels of the solute. The interaction between the molecule and the solvent acts as a dephasing mechanism on the molecular density matrix, leading to the generation of a new population in the excited states.[50]

In order to analyze RR intensities in solution, Mukamel and co workers [61-63] presented an approach for fluctuating solute–solvent interactions, which was based on stochastic theory firstly developed by Kubo [64]. According to this approach, a molecule embedded in a solvent receives the influence of a stochastic force which results in the time-dependent fluctuation of the energy gap between the ground and excited state (zero-zero energy). The fluctuations of the solute’s electronic energy gap are expressed through an energy correlation function with magnitude Δ which decays with time Λ^{-1}:

$$\left\langle \delta E_0(0)\,\delta E_0(t)\right\rangle = D^2 \exp(-\Lambda t) \tag{2.17}$$

When the fluctuations in the zero - zero energy are fast compared to the ground state vibrational dephasing (rapid fluctuation limit) the resonance emission consists of two separated components: sharp lines that correspond to Raman and broad lines that correspond to fluorescence. In the general case these two events interfere and they are not separable.[44] Mukamel and co workers suggested that the rapid limit holds for the molecules dissolved in liquids. The Raman cross sections can be analyzed by the same approach as for isolated molecules (Eq. 2.14) with a minor difference: the damping function exp(-Γ t/h) is converted to exp[-g(t)]. The exp[-g(t)] is the dephasing function. $g(t)$ is the resulting form of the dephasing process in the solvent which is a sum over a number a vibrational modes each having its frequency, friction coefficient and excited state geometry change. Below, we show the simplest approach where only one effective mode lumps all the degrees of freedom of the solvent [58]:

$$g(t) = \left(D^2/\Lambda^2\right)\left[\exp(-\Lambda t) - 1 + \Lambda t\right] + t/\tau \tag{2.18}$$

where

$$\Lambda = \frac{\Omega^2}{f} \tag{2.19}$$

$$D = \left[\left(\lambda_s/\hbar\right)\Omega(2n+1)\right]^{1/2} \tag{2.20}$$

Ω is the frequency of the mode, f is the friction coefficient and n is the thermal average occupation number. τ represents the pure lifetime.[58] In this development the pure lifetime was assumed to be slow compared to the pure dephasing and was neglected. [60]

Here, we should point out that the true time scale for Raman is determined by the ground state vibrational dephasing since Raman scattering results in a change of vibrational quantum states.[50] Thus, a natural partition of the dephasing (broadening) mechanisms is derived according to whether the correlation time is long or short compared to the vibrational dephasing. In the rapid fluctuation limit of the solute solvent interactions ($\Lambda >> D$), the exp[-g(t)] decays exponentially with time (see Eq.2.18) and the line shape approaches a Lorentzian line shape considered as homogeneous. In the slow fluctuation limit ($\Lambda << D$), exp[-g(t)] decays approximately as a Gaussian (see Eq.2.18) resulting in a Gaussian line shape considered as inhomogeneous. As we mentioned previously in the fast limit the Raman cross sections may be analyzed in the same way as for non-interactive molecules.[44,50,58-60]. In the slow limit the inhomogeneous broadening must be factored in the expressions of the RR cross sections as an average of the different sites of the solvent. The bandshapes of the absorption and RR cross sections (REP) can be used together in order to partition the broadening in its homogeneous and inhomogeneous components, and to determine how much of the homogeneous broadening is due to Γ or due to dynamics derived from unseen low frequency vibrations or from a dissociative degree of freedom. The latest two damping parameters produce Gaussian line shapes. The Lorentzian broadening puts intensity in the low energy edge that is rarely seen in a real absorption spectrum. Thus, using very large values of Γ may cause errors on the low energy edge in the reproduction of the experimental absorption spectrum. An upper limit to the Lorentzian contribution to the bandwith is given by this low energy edge. On the other hand from the absorption spectrum it is not feasible to distinguish between homogenous and inhomogeneous broadening because they give similar line shapes (see Eq. 2.15). On the other hand, REP permits the quantitation of homogeneous and inhomogeneous broadening because they affect differently the REP (Eq. 2.14). Homogenous broadening damps the RR cross sections at the probability level, while inhomogeneous broadening acts by changing the distribution of the excited states. For example, by increasing homogeneous broadening(Γ) the REP intensity decreases, while increasing inhomogeneous broadening (Θ) broadens the absorption spectrum without affecting the integrated intensity of either the absorption spectrum or the REP.[44,49,75]

For a better understanding and a fuller investigation of the contributions of T_2, T_1, T_2^* to the value of Γ, time-resolved experiments and fluorescence cross sections measurements are required. These experiments can establish the excited state lifetime T_1. Given the values of T_1 and Γ (through RRIA studies), T_2^* can be calculated and the dominant contribution to the homogeneous linewidth can be clarified. Here, we take as an example the studies performed for the investigation of chlorine dioxide's (an atmospheric molecule) solvent response. Through a RRIA of this molecule in solution it was shown that Γ was essentially the same in a variety of different solvents (cyclohexane, chloroform, water) corresponding to a total dephasing time T_2 of about 60 *fs.*[65] The excited state lifetime was measured via fluorescence and pump-probe studies, which established that T_1 was 200 *fs.*[66,67]. From these studies it became clear that the contribution of pure dephasing was dominant to the homogeneous broadening. The solvent independence of Γ suggested that the solvent induced pure dephasing occurred in similar time scales and therefore its origin is common for three solvents; mechanical or non polar solvation (solvation dynamics are dominated by mechanical solvent – solute interactions and dipolar solvation is absent).[68] In order to test this hypothesis and determine the nature of the solute-solvent interactions, a Molecular Dynamics simulation study was performed using the viscoelastic continuum for non-polar solvation.[68] An excellent agreement was found between the theoretical and experimental linewidths [66] that suggested that mechanical solvation is dominant to the solvent response. Stratt *et al.* [52] stressed that computer simulations have played an important role in shaping the understanding of the mechanisms governing solvation dynamics (pure dephasing).[69,70] Another representative example for the investigation of the solvent-dependent photochemistry is nitrosyl chloride (another atmospheric molecule) in solution, which was investigated through RRIA[71] and time resolved studies[72,73]. The RRIA have shown that in this case the Γ is solvent dependent and is dramatically increased as the polarity increases. The lifetimes of the excited states (T_1) which were measured using Time Resolved IR studies, are also solvent dependent.[73] The increase in the linewidth was accompanied by a notable increase of the Cl-N bond. It was proposed that the enhancement of the vibrational relaxation rates in more polar solvents results in the increase of homogeneous broadening while the strengthening of the NO bond results in a larger inhomogeneous broadening.(It was assumed that the strengthening of the bond is due to the solvent)[73]

It became clear from the above description that the solvent has a great effect on the broadening mechanisms that arise from solvent–solute interactions. RRIA is a valuable tool for the separation of the broadening to its homogeneous and inhomogeneous components.

2.5.4 Linear Dissociative excited state potential

In this section we briefly discuss the effects of a dissociative excited state along a normal mode coordinate. An excited state surface is considered as linearly dissociative if it is repulsive along a normal mode coordinate or it has a very large displacement along a low frequency anharmonic coordinate.[44] Figure 2.4 shows the potential energy surface $V(q) = -\beta q$ along a specific vibrational mode. In the expression of the potential, β is the slope of the excited state surface and q is the dimensionless normal coordinate.

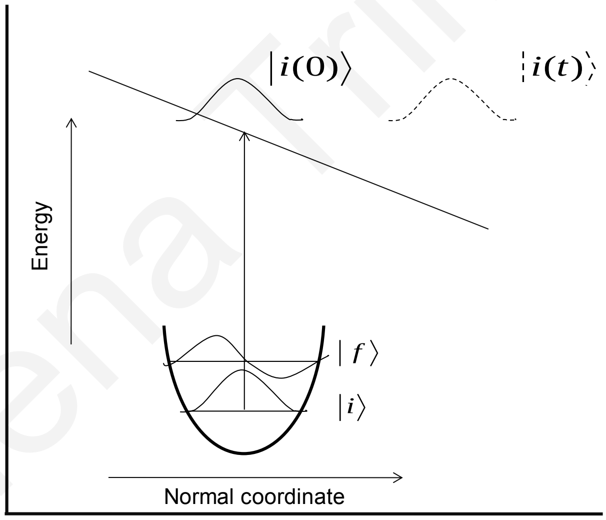

Figure 2.4 The excited state surface of a bound coordinate is linearly dissociative with slope β.The time dependent overlap decays irreversibly as the excited state moves away from the FC region.

When a surface is dissociative the wavepacket never returns to the Frank Condon region after leaving it, in contrast to what happens in a bound vibrational mode where the wavepacket returns periodically. The main effect of adding a dissociative vibrational mode to a system of one or more harmonic modes is the damping of absorption and RR overlaps, broadening of the absorption spectrum and Raman excitation profiles and the reduction of the Raman cross sections in the harmonic modes.[44,74,75] As mentioned above, the damping of overlaps caused by evolution along a dissociative mode resembles the damping due to $D(t) = e^{-\Gamma t/\hbar}$. The two processes have different time dependences and result in different lineshapes. A motion along a dissociative normal mode produces a damping more nearly to Gaussian, in time and a Fourier transform results in a Gaussian line shape compared to the Lorentzian lineshape derived from the damping factor $D(t)$. [44]

Moreover, it has been shown that solvent-solute interactions have a great impact in the dissociation dynamics along a specific normal coordinate. Nyhlom *et al.*[71] have shown in their RRIA study of ClNO in solution that excited state structural evolution following excitation is dominated by evolution along the dissociative N-Cl stretch whose slope is solvent dependent. Specifically, the excited state slope decreases in acetonitrile relative to cyclohexane, as a result of weakening of the N-Cl bond with a corresponding shift of the ground state potential energy surface along this coordinate, as the polarity of the solvent increases.

2.5.5 Depolarization ratios

In our RRIA study, depolarization ratios are of central significance in order to determine the number of excited states involved in the scattering, thus a brief overview of depolarization ratio theory is necessary here. Polarization is a property of a beam of radiation and describes the plane in which the radiation vibrates. Raman spectra are excited by plane-polarized radiation. The scattered radiation is found to be polarized to various degrees depending upon the type of vibration responsible for the scattering. Calculation of depolarization ratios for specific vibrations of the molecule at several excitation wavelengths is significant in RR spectroscopy. Firstly, this information facilitates the measurement of absolute RR cross sections (see experimental section), and secondly the value of ρ in RR spectroscopy is indicative of the number of excited states accessible on resonance.

The depolarization ratio is defined as the intensity ratio between the perpendicular component and the parallel component of the Raman scattered light with respect to the polarization of the incident beam:[42]

$$\rho = \frac{I_{\perp}}{I_{II}} = \frac{5\Sigma^1 + 3\Sigma^2}{10\Sigma^0 + 4\Sigma^2} \qquad (2.21)$$

In the above equation Σ^0, Σ^1, Σ^2, are the rotational invariants for randomly oriented molecules which are a linear combination of the matrix elements of the polarizability tensor, α_{mn}, which in general has nine elements.[42]. Σ^0 is the isotropic part of the scattering tensor, Σ^2 refers to symmetric anisotropy, while the Σ^1 is the antisymmetric part of the tensor.

$$\Sigma^0 = \frac{1}{3}\left|\alpha_{xx} + \alpha_{yy} + \alpha_{zz}\right|^2 \quad (2.22)$$

$$\Sigma^1 = \frac{1}{2}\{\left|\alpha_{xy} - \alpha_{yx}\right|^2 + \left|\alpha_{xz} - \alpha_{zx}\right|^2 + \left|\alpha_{yz} - \alpha_{zy}\right|^2\} \quad (2.23)$$

$$\Sigma^2 = \frac{1}{2}\{\left|\alpha_{xy} + \alpha_{yx}\right|^2 + \left|\alpha_{xz} + \alpha_{zx}\right|^2 + \left|\alpha_{yz} + \alpha_{zy}\right|^2\} + \frac{1}{3}\{\left|\alpha_{xx} - \alpha_{yy}\right|^2 + \left|\alpha_{xx} - \alpha_{zz}\right|^2 + \left|\alpha_{yy} - \alpha_{zz}\right|^2\} \quad (2.24)$$

The above equations relate the components of Raman polarizabilty α with what is measured in the laboratory, depending on the polarization and propagation directions of the incident and scattered light.

For ordinary Raman scattering (off resonance) the polarization properties are independent of excitation frequency and the intensity depends only on the wavenumber of the scattered light to the fourth power. Moreover, ordinary Raman scattering is characterized by a symmetric scattering tensor and Σ^1 is generally vanishing. The zero value of Σ^1 restricts the value of depolarization ratio to the range $0 \leq \rho \leq 3/4$.

On the other hand, in RR scattering, the polarizabilty tensor is not symmetric and no upper limit for depolarization ratio exists, while the scattering tensor may have up to nine non zero scattering terms. In RR scattering, measurement of depolarization ratios as a function of excitation frequencies spanning the absorption band (Depolarization Dispersion Curve) is fundamental in order to extract information about the excited states of the scattering molecule. Mortensen and Hassing separate the relation between the properties of the scattering molecule and Raman scattering into two parts: the contribution to the scattering tensor of a single electronic state and the interference from other excited states. In the first case the authors used the term *state tensor* to interpret the phenomena derived from single states' contributions to the Raman tensor. The *state tensor* is a convenient expression for each state in the summation over all the molecular states, which is contained in the expression for the Raman tensor. [42,76] The general form of the state tensors determined by symmetry has been derived for most point groups by Mortensen and Hassing [42] by using the method of non commuting generators.[77] In this method, the character tables are replaced by eigenvalue tables which allow straightforward calculation of matrix elements. [78] Here we quote an example: the state tensors belonging to the C_{2v} point group.

$$A_1 : \begin{bmatrix} B_1 & 0 & 0 \\ 0 & B_2 & 0 \\ 0 & 0 & A_1 \end{bmatrix} \qquad A_2 : \begin{bmatrix} 0 & B_2 & 0 \\ B_1 & 0 & 0 \\ 0 & 0 & 0 \end{bmatrix}$$

$$B_1 : \begin{bmatrix} 0 & 0 & A_1 \\ 0 & 0 & 0 \\ B_1 & 0 & 0 \end{bmatrix} \qquad B_2 : \begin{bmatrix} 0 & 0 & 0 \\ 0 & 0 & A_1 \\ 0 & B_2 & 0 \end{bmatrix}$$

In the above expressions the symmetry of the vibrational mode is indicated to the left of each tensor and the symmetries that are written in the state tensor are due to an intermediate state with that particular symmetry.

As mentioned above, the value of depolarization ratio on resonance provides information about the number of electronic states contributing to the observed scattering. Specifically, on resonance with a single electronic excited state e.g. α_{xx}, ρ is 1/3 because only this diagonal polarizabilty tensor element is taken to be non-vanishing. On resonance with two electronic excited states e.g. $\alpha_{xx} = \alpha_{yy}$ the depolarization ratio is 1/8.

2.5.6 Interference effects on Resonance Raman excitation profiles caused by nearby excited states

The time-dependent equations for absorption and Raman scattering (Eq. 2.14& 2.15) are based on the assumption that the observed scattering is governed by only one electronic excited state and is not influenced by other excited states. The calculation and interpretation of REP's is complicated by the presence of nearby excited states that contribute to the average RR intensities. The interference from one or more excited state depends on the magnitude of the dipole moment of the specific transitions, the energy difference between the excited state of interest and the nearby excited state, the damping factor Γ and from the displacements Δ of the minimum of the excited state potential energy surfaces. The most important physical parameter that must be taken into consideration in a RRIA study, where two or more excited states are involved, is the transition dipole moment (M) of each excited state. The general feature from the studies reported in the literature is that the excited state with the larger M will dominate the Raman excitation profile. This is supported from equation 2.14 where the Raman cross section is proportional to the forth power of M.

The time-dependent expression for the RR cross sections is in this case modified as follows in order to include the contribution from two excited states:

$$\sigma_{\iota\to f}(E_L)=\frac{8\pi e^4 E_s E_L}{9\hbar^6 c^4}\times\sum_u P_u\times\int_{-\infty}^{\infty}\partial E_{00}H(E_{00})\times\left|\begin{array}{l} M_1^2\int_0^{\infty}\langle f|i_1(t)\rangle\exp\left[\frac{i(E_L+\varepsilon_\iota)}{\hbar}\right]e^{-\Gamma_1 t/\hbar}\,dt+ \\ \qquad M_2^2\int_0^{\infty}\langle f|i_2(t)\rangle\exp\left[\frac{i(E_L+\varepsilon_\iota)}{\hbar}\right]e^{-\Gamma_2 t/\hbar}\,dt \end{array}\right|^2 \qquad (2.23)$$

Subscripts 1 and 2 refer to the first and the second excited state, respectively. Similar considerations are made for the absorption cross section. P_u refers to the occupational probability of vibrational state u in the ground state determined from Boltzmann statistics (see Chapter 3)

Various studies demonstrate the interference between excited states. Shin et *al.*[79] studied the interference effects on REP derived from two electronic excited states by applying the time-dependent formalism for two general cases. In the first case the excited state of interest is well separated in energy by the second electronic state, which has a larger transition dipole moment. The interference from the second excited state is stronger when the transition dipole moment of this state increases. The Raman intensities are greatly affected by the displacements of both the first and second excited states. The Raman intensity on resonance with the first excited state with smaller M is unaffected on Γ. The Raman intensity on resonance with the second excited state increases as the Γ of the second excited state decreases. In the second case the two electronic excited states are energetically close and their dipole moments are similar. As the M of the first excited state increases the Raman intensity from the corresponding excited state increases. In this case the effect of Δ does not obey general rules like in the first case. The Raman excitation profiles are strongly affected by the Γ of the second excited state, and as the Γ of the second excited state increases the interference from that state decreases.

2.6. RR studies on various atmospheric species

The atmosphere is a heterogeneous mixture of different environments such as surfaces, droplets, liquid aerosols. Thus, understanding the role of phase in the atmospheric photochemistry of atmospherically-relevant compounds over a range of well-defined environments is a central issue. The clarification of the role the environment plays in the photochemical behavior of various atmospheric species such as halooxides and nitryl halides is necessary. The environmental reactivity of such species has attracted significant attention due to their role as reservoir species for atmospheric atomic chlorine and NO.[5,80,81] The solution-phase photochemistry of various halooxides and particular OClO and ClNO has been extensively explored by the Reid group by performing RRIA and time-resolved experiments in various solvents ranging from polar to non-polar.[65,71,73,82-91] Given the diversity in behaviors of OClO and ClNO, understanding the environmental dependence is important in order to evaluate their contribution in chemical processes occurring in the atmosphere. These studies clearly demonstrated that the solvent plays a key role in the photochemistry of each compound.

In this section we briefly review these studies, because we find it useful to compare the results derived from them. Moreover, since the photochemistry of nitryl chloride (which is also a reservoir species of chloride in the stratosphere) has not been fully explored in solution, these studies provided the impetus to carry out similar experiments for this molecule.

To begin with, RRIA studies on ClNO revealed that photoexcitation in solution phase (cyclohexane, acetonitrile) results in substantial evolution of the N-Cl stretch compared to the gas phase, consistent with the dissociation of the N-Cl bond.[71] The frequency of the N-Cl stretch is solvent-dependent downshifting in more polar solvents. Many more transitions are observed in cyclohexane relative to acetonitrile due to a significant increase in the homogeneous line width in acetonitrile, resulting in the depression of the RR cross sections in this solvent. It is also shown that the transition frequencies and the curvature of the ground state potential energy surface are solvent-dependent. Moreover, Bixby *et al.* [73] showed through an FTIR absorption study that the N=O symmetric stretch is shifting to higher frequencies as the polarity increases. Femtosecond pump-probe experiments in acetonitrile and chloroform demonstrated that NO and Cl are generated in both solvents.[72] Additionally, it was shown that both product formation and geminate recombination are solvent-dependent.

In the case of OClO, RRIA studies showed that structural evolution in the gas phase[92] occurs along the symmetric stretch (v_1), the symmetric bend (v_2), and along the overtone of the asymmetric stretch. However, RR studies of OClO in various solvents (cyclohexane, water and chloroform) showed that structural evolution along the asymmetric stretch overtone is restricted in solution resulting in the preservation of the C_{2v} symmetry in the excited state,[65] which was suggested as the main reason for enhanced Cl production in the condensed phase. In contrast to the ClNO RRIA, in OClO Γ was not found to be solvent-dependent and had the same origin in all solvents. To support these results pump-probe studies were performed and found that the excited state lifetime was the same in all three solvents.

After numerous experimental studies of ClNO in different solvents its environmental impact in tropospheric chemistry was suggested for the first time in a recent work of Patterson *et al.*[91] As the photochemistry of ClNO is dependent on environment it is interesting to consider how this dependence

may alter the current climate models that describe the gas phase photochemistry of ClNO.The gas phase models may overestimate the production of NO and Cl from ClNO in condensed media. The photochemistry of ClNO in the air/water interface is relevant in the evaluation of the role of ClNO in catalytic cycles in the troposphere. Experiments aiming to evaluate the polarity of this interface have shown that this value is close to the polarity of cyclohexane.[93] Thus, they suggested that the ground state structure of ClNO in air/water mixtures and the excited state population is similar to that observed in cyclohexane.

It is obvious that understanding the various aspects governing the phase dependent photochemical reactivity is a great challenge in atmospheric chemistry. RRIA studies on atmospheric species, which may be supplemented with time-resolved studies, contribute significantly to the clarification of this phase-dependent photochemistry. However, a number of studies are required in a variety of solvent environments in order to obtain a clear picture for the environmental impact.

The RRIA studies on ClNO and OClO in various solvents were crucial for the elucidation of the photochemistry of these halooxides in solution. Therefore, we will initiate our investigation of the chemical behavior of $ClNO_2$ in the solvent environment utilizing the same toolboxes. We believe that the application of RR spectroscopy will provide a broader understanding of $ClNO_2$ photochemistry by answering crucial questions such as(1) how the solvent environment affects its photochemistry, (2) what processes are involved in the photochemistry of this molecule, (3) what is the structural evolution of the molecule following photoexcitation and (4) whether the excited states are harmonic or dissociative.

References

(1) Garcia, R. R.; Solomon, S. *J. Geophys. Res* **1994**, *99*,755.

(2) Wayne, R. P. *Chemistry of Atmospheres*; Second edition ed.; Oxford Science Publications University of Cambridge, UK, **1990**.

(3) Fish, D. J.; Burton, M. R. *J. Geophys. Res.* **1997**, *102*, 25537.

(4)Seinfeld, J. H.; Pandis, S. N. *Atmospheric Chemistry and Physics – from Air Pollution to Climate Change*; John Wiley and Sons: New York, Chichester, Weinheim, **1998**.

(5) Solomon, S.; Garcia, R. R.; Rowland, F. S.; Wuebbles, D. J. *Nature* **1986**, *321*, 755.

(6) Molina, M. J. *Atmos. Environ.* **1991**, *25A*, 2535.

(7) Tolbert, M. A.; Rossi, M. J.; Golden, D. A. *Science* **1988**, *240*, 1018.

(8) Finlayson-Pitts, B. J.; Ezzel, M. J.; Pitts Jr, J. N. *Nature* **1989**, *337*, 241.

(9) Livingston, F. E.; Finlayson-Pitts, B. J. *Geophys.Res. Lett.* **1991**, ***18***, 17.

(10) Hanson, D. R.; Ravishankara, A. R. *J. Geophys. Res* **1991**, *96*, 5081.

(11) Shindell, D. T.; Rind, D.; Lonergan, P. *Nature* **1998**, *392,* 589.

(12) Keene, W. C.; Khalil, M. A. K.; Erickson, D. J., III; McCulloch, A.; Graedel, T. E.; Lobert, J. M.; Aucott, M. L.; Gong, S. L.; Harper, D. B.; Kleiman, G.; Midgley, P.; Moore, R. M.; Seuzaret, C.; Sturges, W. T.; Benkovitz, C. M.; Koropalov, V.; Barrie, L. A.; Li, Y. F. *J. Geophys. Res.* **1999**, *104*, 8429.

(13) Vogt, R.; Crutzen, P. J.; Sander, R. *Nature* **1996**, *383*, 327.

(14) Sander, R.; Rudich, Y.; von Glasow, R.; Crutzen, P. J. *Geophys. Res. Lett.* **1999**, *26*, 2857.

(15) Behnke, W.; George, C.; Scheer, V.; Zetzsch, C. *J.Geoph.Res.* **1997**, *102,* 3795.

(16) Graedel, T. E.; Keene, W. C. *Global Biogeochemical Cycles* **1995**, *9*, 47.

(17) Thornton, J. A.; Kercher, J. P.; Riedel, T. P.; Wagner, N. L.; Cozic, J.; Holloway, J. S.; Dube, W. P.; Wolfe, G. M.; Quinn, P. K.; Middlebrook, A. M.; Alexander, B.; Brown, S. S. *Nature* **2010**, *464*, 271.

(18) Osthoff, H. D.; Roberts, J. M.; Ravishankara, A. R.; Williams, E. J.; Lerner, B. M.; Sommariva, R.; Bates, T. S.; Coffman, D.; Quinn, P. K.; Dibb, J. E.; Stark, H.; Burkholder, J.

B.; Talukdar, R. K.; Meagher, J.; Fehsenfeld, F. C.; Brown, S. S. *Nature Geoscience* **2008**, *1*, 324.

(19)Donohoue, D. L.; Bauer, D.; Hynes, A. J. *Journal of Physical Chemistry A* **2005**, *109*, 7732.

(20) Platt, U.; Allan, W.; Lowe, D. *Atmospheric Chemistry and Physics* **2004**, *4*, 2393.

(21) Knipping, E. M.; Dabdub, D. *Environmental Science & Technology* **2002**, *37*, 275.

(22) Abuduwailli, J.; Gabchenko, M. V.; Xu, J. R. *Journal of Arid Environments* **2008**, *72*, 1843.

(23) Nelson, H. H.; Johnston, H. S. *J.Phys.Chem.* **1981**, *85*, 3891.

(24) Plenge, J.; Flesch, R.; Schurmann, M. C.; Ruhl, E. *J.Phys.Chem.* **2001**, *105*, 4844.

(25) Carter, R. T.; Hallou, A.; Huber, J. R. *Chemical Physics Letters.* **1999**, *310*, 166.

(26) Furlan, A.; Haeberli, M. A.; Huber, J. R. *J.Phys.Chem.A* **2000**, *104*, 10392.

(27) Ghosh, B.; Papanastasiou, D. K.; Talukdar, R. K.; Roberts, J. M.; Burkholder, J. B. *Journal of Physical Chemistry A* **2011**, *116*, 5796.

(28) Li, Q.; Huber, J. R. *Chemical Physics Letters.* **2002**, *354*, 120.

(29) Coanga, J. M.; Schriver-Mazzuoli, L.; Schriver, A.; Dahoo, P. R. *Chem.Phys.Lett.* **2002**, *276*, 309.

(30) Tevault, D. E.; Smardzewski, R. R. *Journal of Chemical Physics* **1977**, *67*, 3777.

(31) Scheffler, D.; Grothe, H.; Willner, H.; Freznel, A.; C.Zetzsch *Inorg. Chem* **1997**, ***36***, 335.

(32) Schriver-Mazzuoli, L.; Coanga, J. M.; Schriver, A. *Journal of Physical Chemistry A* **2003**, *107*, 5181.

(33) Schweitzer, F.; Mirabel, P.; George, C. *Journal of Physical Chemistry A* **1998**, *102*, 3942.

(34) Christe, K. O.; Schack, C. J.; Wilson, R. D. *Inorganic Chemistry* **1974**, *13*, 2811.

(35) Lee, T. J. *Journal of Physical Chemistry* **1994**, *98*, 111.

(36) Durig, J. R.; Kim, Y. H.; Guirgis, G. A.; McDonald, J. K. *Spectrochim. Acta A* **1994**, *50*, 463.

(37) Papayiannis, D. K.; Kosmas, A. M. *Mol.Phys.* **2006**, *104*, 2561.

(38) Lesar, A.; Hdoscek, M.; Muhlhauser, M.; Peyerimhoff, S. D. *Chemical Physics Letters* **2004**, *383*, 84.

(39) Orphal, J.; Morillon-Chapey, M.; Guelachvili, G. *J.Mol.Spec.* **1994**, *165*, 315.

(40) Orphal, J.; Morillon-Chapey, M.; Guelachvili, G. *J.Mol.Spec.* **1994**, *166*, 280.

(41) Rayson, R.; Wilson, M. K. *Journal of Chemical Physics* **1954**, *22*, 2000.

(42) Mortensen, O. S.; Hassing, S. In *Advances In Infrared and Raman Spectroscopy*; Hester, R. J. H. C. a. R. E., Ed.; Wiley: London, 1980; Vol. 6.

(43) Ferraro,J.R; Nakamoto, K.; Brown, C. W. In *ntroductory Raman Spectroscopy (Second Edition)* Elsevier: 2002.

(44) Myers, A. B.; Mathies, R. A. In *Biological Applications of Raman Spectroscopy*; Spiro, T. G., Ed.; John WIley &Sons, Inc.: New York, **1987**; Vol. 2, p 1.

(45) Tannor, D. J. *Journal of Physical Chemistry* **1988**, *92*, 3341.

(46) Myers, A. B. *Chemical Reviews* **1996**, *96*, 911.

(47) Myers Kelley, A. *The Journal of Physical Chemistry A* **2008**, *112*, 11975.

(48) Lee, S.-Y.; Heller, E. J. *The Journal of Chemical Physics* **1979**, *71*, 4777.

(49) Myers, A. B.; Mathies, R. A.; Tannor, D. J.; Heller, E. J. *Journal of Chemical Physics* **1982**, *77*, 3857.

(50) Myers, A. B. *Journal of the Optical Society of America B-Optical Physics* **1990**, *7*, 1665.

(51) Myers, A. B.; Hochstrasser, R. M. *Journal of Chemical Physics* **1987**, *87*, 2116.

(52) Stratt, R. M.; Maroncelli, M. *Journal of Physical Chemistry* **1996**, *100*, 12981.

(53) Larsen, R. E.; Stratt, R. M. *Journal of Chemical Physics* **1999**, *110*, 1036.

(54) Deng, Y. Q.; Stratt, R. M. *Journal of Chemical Physics* **2002**, *117*, 1735.

(55) Goodyear, G.; Stratt, R. M. *Journal of Chemical Physics* **1997**, *107*, 3098.

(56) Tuckerman, M.; Berne, B. J. *Journal of Chemical Physics* **1993**, *98*, 7301.

(57) Oxtoby, D. W. *Annual Review of Physical Chemistry* **1981**, *32*, 77.

(58) Myers, A. B. *Chemical Physics* **1994**, *180*, 215.

(59) Myers, A. B. *Journal of Raman Spectroscopy* **1997**, *28*, 389.

(60) Myers, A. B.; Li, B. L. *Journal of Chemical Physics* **1990**, *92*, 3310.

(61) Mukamel, S. *Journal of Chemical Physics* **1985**, *82*, 5398.

(62) Sue, J.; Yan, Y. J.; Mukamel, S. *The Journal of Chemical Physics* **1986**, *85*, 462.

(63) Yan, Y. J.; Mukamel, S. *The Journal of Chemical Physics* **1987**, *86*, 6085.

(64) Takagahara, T.; Hanamura, E.; Kubo, R. *Journal of the Physical Society of Japan* **1977**, *43*, 802.

(65) Reid, P. J. *Journal of Physical Chemistry A* **2002**, *106*, 1473.

(66) Foster, C. E.; Barham, B. P.; Reid, P. J. *Journal of Chemical Physics* **2001**, *114*, 8492.

(67) Hayes, S. C.; Cooksey, C. C.; Wallace, P. M.; Reid, P. J. *Journal of Physical Chemistry A* **2001**, *105*, 9819.

(68) Brooksby, C.; Prezhdo, O. V.; Reid, P. J. *Journal of Chemical Physics* **2003**, *118*, 4563.

(69) Olender, R.; Nitzan, A. *Journal of Chemical Physics* **1995**, *102*, 7180.

(70) Brown, R. *Journal of Chemical Physics* **1995**, *102*, 9059.

(71) Nyholm, B. P.; Reid, P. J. *Journal of Physical Chemistry B* **2004**, *108*, 8716.

(72) Cooksey, C. C.; Johnson, K. J.; Reid, P. J. *Journal of Physical Chemistry A* **2006**, *110*, 8613.

(73) Bixby, T. J.; Patterson, J. D.; Reid, P. J. *Journal of Physical Chemistry A* **2009**, *113*, 3886.

(74) Myers, A. B.; Harris, R. A.; Mathies, R. A. *Journal of Chemical Physics* **1983**, *79*, 603.

(75) Myers, A. B.; Trulson, M. O.; Pardoen, J. A.; Heeremans, C.; Lugtenburg, J.; Mathies, R. A. *Journal of Chemical Physics* **1986**, *84*, 633.

(76) Jernshoj, K. D.; Hassing, S. *Journal of Raman Spectroscopy* **2010**, *41*, 727.

(77) Mortensen, O. S. *Structure and Bonding* **1987**, *68*, 1.

(78) Sonnich Mortensen, O. *Chemical Physics Letters* **1970**, *5*, 515.

(79) Shin, K. S. K.; Zink, J. I. *Journal of the American Chemical Society* **1990**, *112*, 7148.

(80) Rowland, F. S. *Annual Review of Physical Chemistry* **1991**, *42*, 731.

(81) Renard, J. B.; Pirre, M.; Robert, C.; Huguenin, D. *Journal of Geophysical Research-Atmospheres* **1998**, *103*, 25383.

(82) Cooksey, C. C.; Reid, P. J. *Photochemistry and Photobiology* **2004**, *80*, 386.

(83) Philpott, M. J.; Charalambous, S.; Reid, P. J. *Chemical Physics Letters* **1997**, *281*, 1.

(84) Hayes, S. C.; Philpott, M. J.; Reid, P. J. *Journal of Chemical Physics* **1998**, *109*, 2596.

(85) Hayes, S. C.; Philpott, M. P.; Mayer, S. G.; Reid, P. J. *Journal of Physical Chemistry A* **1999**, *103*, 5534.

(86) Thomsen, C. L.; Philpott, M. P.; Hayes, S. C.; Reid, P. J. *Journal of Chemical Physics* **2000**, *112*, 505.

(87) Philpott, M. P.; Hayes, S. C.; Thomsen, C. L.; Reid, P. J. *Chemical Physics* **2001**, *263*, 389.

(88) Esposito, A. P.; Reid, P. J.; Rousslang, K. W. *Journal of Photochemistry and Photobiology a-Chemistry* **1999**, *129*, 9.

(89) Cooksey, C. C.; Reid, P. J. *Journal of Physical Chemistry A* **2003**, *107*, 5508.

(90) Bolinger, J. C.; Bixby, T. J.; Reid, P. J. *Journal of Chemical Physics* **2005**, *123*.

(91) Patterson, J. D.; Reid, P. J. *Journal of Physical Chemistry B* **2012**, *116*, 10437.

(92) Esposito, A. P.; Stedl, T.; Jansson, H.; Reid, P. J.; Peterson, K. A. *The Journal of Physical Chemistry A* **1999**, *103*, 1748.

(93) Wang, H. F.; Borguet, E.; Eisenthal, K. B. *Journal of Physical Chemistry B* **1998**, *102*, 4927.

CHAPTER 3

EXPERIMENTAL AND COMPUTATIONAL METHODS

3.1 Experimental methods

3.1.1 Materials

The reaction of anhydrous nitric acid with chlorosulfonic acid [1,2] proved to be a convenient method to synthesize nitryl chloride in this study. A 100 mL three-necked round-bottom flask, equipped with a dropping funnel and a thermometer, was charged with 47 g anhydrous nitric acid (Merck, fuming, 0.75 mol), kept at 0°C in which 87 g of chlorosulfonic acid (Fluka, > 98%, 0.75 mol) was slowly added from the dropping funnel over a period of 3 hours while the content of the flask was stirred by a PTFE coated magnetic stirring bar. The gaseous products were frozen in a trap cooled with liquid nitrogen at –196°C. Subsequently the product mixture was separated by trap-to-trap condensation in vacuum in a series of traps kept at –100°C (diethylether/dry ice), –125°C (methylocyclohexane/liquid nitrogen), and –196°C (liquid nitrogen). The main fraction of pure $ClNO_2$ was collected at –125°C. The free-from-impurities $ClNO_2$ was left to evaporate and then bubbled in methanol (HPLC grade, Aldrich). An alternative and easier way to get the pure product in methanol was by freezing the solvent in the round bottom flask at 125^0C. The $ClNO_2$/methanol mixture cooled in the trap was then let to come to room temperature. Absorption spectroscopy was used in order to determine the sample purity. The $ClNO_2$ concentration of the solution used in the RR experiments was adjusted to 1.5-3.6 mM depending on the excitation wavelength employed, so that the absorption at the specific λ_{exc} was ~1. In order to assess the effect of the solvent environment on $ClNO_2$ photochemistry, the gas was introduced in a variety of solvents of different polarity such as sulfuric acid, dichloromethane, carbon tetrachloride and methanol. Initial experiments in the first three solvents showed that $ClNO_2$ was not stable in these environments as no signature of the molecule was observed in the Raman spectrum. Instead, we observed signatures from various photoproducts. Additionally, *ab initio* calculations of $ClNO_2$ in carbon tetrachloride and sulfuric acid clusters (not shown) confirmed that the molecule dissociates in these solvents. Therefore, the solution phase characterization of $ClNO_2$ focused on methanol due to its better stability in this solvent.

3.1.2 Calculation of extinction coefficient

Calculation of the extinction coefficient of $ClNO_2$ in methanol was necessary for an accurate knowledge of the concentration of $ClNO_2$ in the RR experiments. This was accomplished by weighing the amount of pure nitryl chloride gas introduced into specific amount of solvent and recording the absorption. The extinction coefficient, ε, was calculated through Beer–Lambert's law for all the λ_{exc} (199.8, 208, 217.9, 228.7 and 239.5 nm), using different dilutions of the $ClNO_2$/MeOH stock solution.

3.1.3 Resonance Raman studies

The absolute RR intensities of nitryl chloride dissolved in methanol were measured using the setup shown in Figure 3.1 at 199.8, 208.8, 217.9, 228.7 and 239.5 nm. The excitation wavelengths employed in the UVRR experiments were produced via Raman shifting the second and the fourth harmonic from a Q-switched Nd:YAG laser (PRO-230, 30 Hz, Spectra Physics), at 532 nm and 266 nm respectively in a 1 m stainless-steel cell tube containing H_2 gas at 1.5 bars. The diameter of the Raman cell was 1 inch and the plane-parallel windows used on each end were UV-grade fused silica. The excitation light was focused into a spinning cell consisting of an EPR quartz tube (diameter: 4 mm) attached to a rheostat-controlled motor for choice of rotation speed. The EPR tube is held in place by a perforated Teflon holder attached to the motor, which is tightened uniformly by screwing a plastic threaded ring. (Figure 3.2) Use of the spinning cell prolonged the lifetime of the samples and reduced the evaporation of both solute and solvent that would change $ClNO_2$ concentration during the experiment. Modest excitation energies (17 μJ per pulse) and soft focus of the beam were employed in order to avoid decomposition of the sample. Since our laboratory was not equipped by a beam profiler in order to measure the focal length we performed power dependence experiments to find the energy where the sample remained stable and free from impurities. The Raman scattered light was collected in a backscattering geometry and delivered to a 0.75 m focal-length Czerny-Turner spectrograph, equipped with a 2400-grooves/mm UV-enhanced holographic grating. The slit width was set to 100 μm providing for 10-13cm^{-1} spectral resolution at the wavelengths used in this work. The scattered light was detected by a LN_2-cooled 2048×512 pixel, back-illuminated UV-enhanced CCD detector (Spec10:2KBUV/LN, Princeton Instruments). The concentration of the sample was measured before and after each experiment to ensure that sample photodegradation was < 10%. The absence of characteristic electronic bands corresponding to possible photoproducts in the absorption spectrum after RR experiments also ensured that the sample remained free of impurities such as NOCl, NO, NO_2. Frequency calibration of the spectra was accomplished with the use of cyclohexane. MATLAB software was used for spectral treatment and analysis.

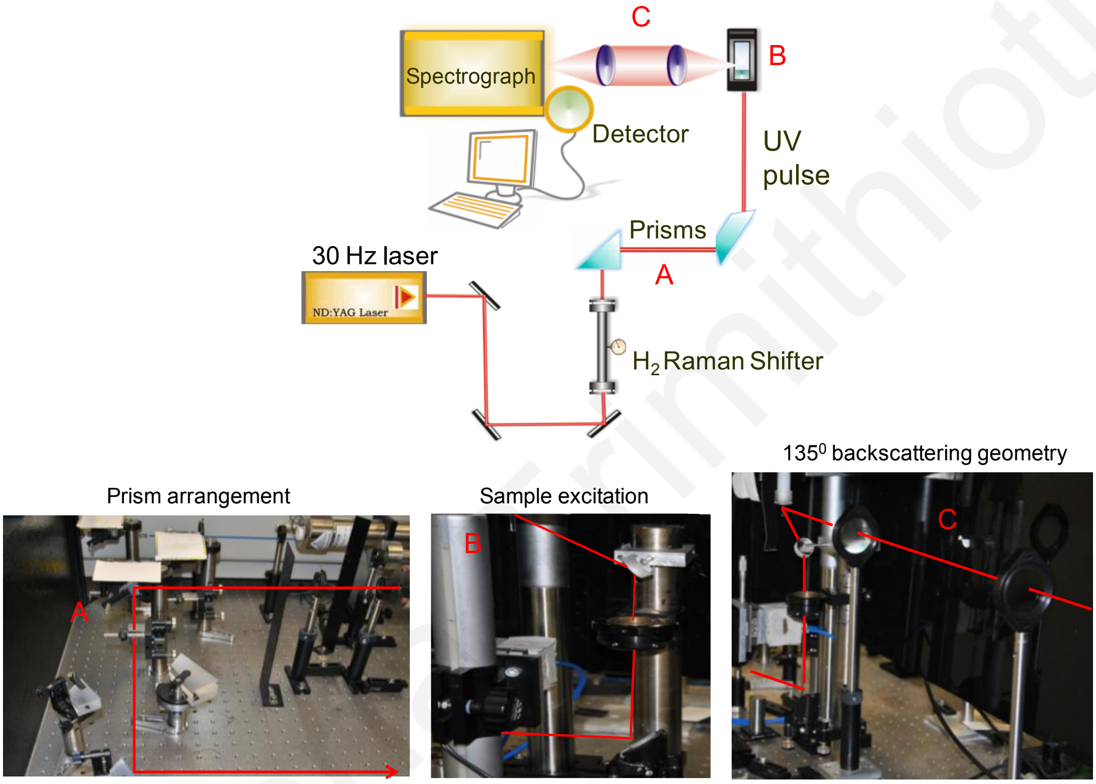

Figure 3.1 Experimental setup for UV Resonance Raman.[3]

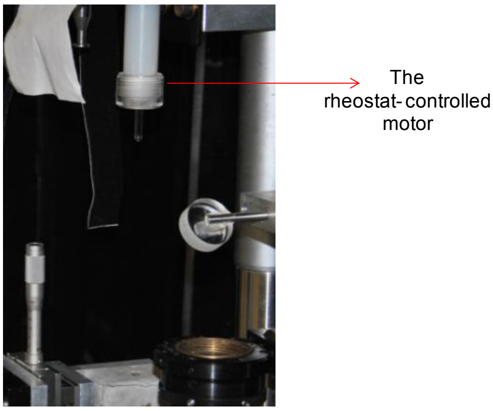

Figure 3.2 The EPR cell attached to the rheostat-controlled motor.

3.1.4 Depolarization ratios

The depolarization ratio for the N-O symmetric stretch (ν_1) was measured at all excitation wavelengths. This is defined as the intensity of the scattered light with polarization perpendicular to that of the incident radiation divided by the intensity of the detected scattered light with parallel polarization to that of the excitation light. To measure this ratio, the polarization of the incident light was defined by passing the excitation light through a stack of five air-spaced quartz microscope slides placed at Brewster's angle with respect to the beam path. The polarization of the scattered light was analyzed using an α-BBO polarizer (EKSMA) placed before the polarization scrambler. Measurement of the depolarization ratio of the 801 cm^{-1} line of cyclohexane at each wavelength was performed in order to correct for the non-ideal extinction of the polarizer via Eq.3.1:[4]

$$\frac{I_{per}^{measured}}{I_{par}^{measured}} = \frac{I_{per}^{ideal} + c\,I_{par}^{ideal}}{I_{par}^{ideal} + c\,I_{per}^{ideal}} \qquad (3.1)$$

Here, *c* is a constant that represents the amount of orthogonally polarized light that leaks through the polarizer. The measured values of depolarization ratios of the cyclohexane 801 cm^{-1} transition (0.14 ± 0.02, 0.09 ± 0.02, 0.12 ± 0.03, 0.10 ± 0.02 and 0.13 ± 0.008 at 199.75, 208.8, 217.85 228.8 and 239.5nm respectively) and its known value of 0.08 ± 0.01 were used to determine *c* at each excitation wavelength. The corresponding values of *c* were 0.05 ± 0.02, 0.04 ± 0.01, 0.01 ± 0.01, 0.03 ± 0.02 and 0.05 ± 0.01. This correction value was then used to calculate the depolarization ratios reported in this study. The cyclohexane and $ClNO_2$ intensities both in parallel and perpendicular spectra were determined by peak integration using the trapezoidal rule.

3.1.5 Determination of Absolute Resonance Raman Cross Sections

Calculation of the absolute RR cross sections necessitates the use of an intensity standard, which in this case was methanol. The depolarization ratios and absolute Raman cross sections of the vibrational bands of methanol in the spectral region between 1000 and 1800 cm^{-1} with excitation in the UV region investigated here have not been reported in the literature to our knowledge and were thus calculated herein. At a later stage we discovered that the differential cross sections for the CH stretches in methanol have been previously measured.[5] To confirm the accuracy of our results we used the ratio of intensities of the corresponding modes, which is proportional to the ratio of their absolute cross sections, and we found a good agreement between the two sets of measurements. Since the methanol bands are quite broad and in order to avoid errors due to deconvolution of peaks, we obtained the absolute RR cross section of the band spanning the region 888 to 1240 cm^{-1} via comparison to the intensity of the 932 cm^{-1} band of $NaClO_4$ (Eq. 3.2). This methanol band corresponds to the C-O stretch at 1033.5 cm^{-1}, the CH_3 in-plane rock at 1074 cm^{-1}, and the CH_3 out-of-plane rock at 1145.5 cm^{-1}.[6]

$$\sigma_R(v(x)) = \frac{I_{v(x)}.C_i.\left(\frac{1+2\rho}{1+\rho}\right)_{v(x)}}{I_i.C_{v(x)}\cdot\left(\frac{1+2\rho}{1+\rho}\right)_i}\cdot\sigma_i \qquad (3.2)$$

In Eq. 3.2, σ_R is the Raman scattering cross section of mode $v(x)$, ρ is the depolarization ratio, C is the concentration and $I_{v(x)}$ and I_i are the experimentally determined intensities for the mode of interest and the internal standard, respectively. The intensities of the Raman bands were corrected for the spectral response of the instrument using a calibrated D_2 lamp (Heraeous, Noblelight, Cathodeon Ltd) and were determined by peak integration using the trapezoidal rule. Eq. 3.2 was then used for the experimental determination of the cross section for the v_1 band of $ClNO_2$ as a function of excitation wavelength.

3.2 Computational Analysis

RRIA was employed in order to reproduce the electronic spectra and the excitation-energy-dependent absolute RR cross-sections (Raman excitation profile, REP). This analysis entails the simultaneous modeling of the absorption spectrum and the REP, using expressions from the time-dependent formalism for absorption and Resonance Raman scattering.[7] Due to the deviation of the depolarization ratios from 1/3 (the value obtained for a single dipole-allowed transition), modified versions of the expressions for the Raman and absorption scattering cross sections were employed, where transitions to two optically–accessible excited states were included (Eqs 3.3 & 3.5).[8]

$$\sigma_{\iota\to f}(E_L)=\frac{8\pi e^4 E_s E_L}{9\hbar^6 c^4}\times\sum_u P_u\times\int_{-\infty}^{\infty}\partial E_{00}H(E_{00})\times\left|\begin{array}{r} M_1^2\int_0^{\infty}\langle f\,|i_1(t)\rangle\exp\left[\frac{i(E_L+\varepsilon_\iota)}{\hbar}\right]e^{-\Gamma_1 t/\hbar}dt+ \\ M_2^2\int_0^{\infty}\langle f\,|i_2(t)\rangle\exp\left[\frac{i(E_L+\varepsilon_\iota)}{\hbar}\right]e^{-\Gamma_2 t/\hbar}dt \end{array}\right|^2 \quad (3.3)$$

In the above equations E_s and E_L are the scattered and incident frequencies, respectively. The transition dipole moments for the two electronic transitions are given by M_1 and M_2, c is the speed of light, ε_i is the energy of the initial vibrational state and Γ_1 and Γ_2 are the homogeneous linewidths of excited states 1 and 2, respectively. The expression $\langle \mathrm{f}\,|\mathrm{i_n(t)}\rangle$ represents the time-dependent overlap of the final state in the scattering process with the initial state propagating under the influence of the excited state Hamiltonian in the intermediate state n. Homogeneous broadening corresponding to each exited state is given by damping functions $D_1(t)$ = $e^{-\Gamma_1 t/\hbar}$ and $D_2(t)$ = $e^{-\Gamma_2 t/\hbar}$. In this analysis the homogeneous broadening was taken to be Lorentzian. P_u refers to the occupational probability of vibrational state u in the ground state determined from Boltzmann statistics:

$$P_u=\exp\left(\frac{-u\hbar\omega}{k\mathrm{T}}\right)\left(1-\exp\left(-\frac{\hbar\omega}{kT}\right)\right) \quad (3.4)$$

Inclusion of Boltzmann probabilities is necessary as the lowest vibrational frequency of $ClNO_2$ is 372 cm^{-1}, for which coordinate higher vibrational states are populated at room temperature.

The absorption cross section at the same level of approximation is given by Eq.3.5:

$$\sigma_A(E_L)=\frac{4\pi\,\mathrm{e}^2E_L}{6\hbar^2\mathrm{cn}}\times\sum_u P_u\times\int_{-\infty}^{\infty}dE_{00}H(E_{00})\times\left[\begin{array}{l}\int_{-\infty}^{\infty}M_1^2\langle\mathrm{i}|\mathrm{i}_1(\mathrm{t})\rangle\exp\left[\frac{i(E_L+\varepsilon_{\mathrm{i}})t}{\hbar}\right]D_1(t)dt \quad + \\ \int_{-\infty}^{\infty}M_2^2\langle\mathrm{i}|\mathrm{i}_2(\mathrm{t})\rangle\exp\left[\frac{i(E_L+\varepsilon_{\mathrm{i}})t}{\hbar}\right]D_2(t)dt\end{array}\right] \quad (3.5)$$

where $\langle\mathrm{i}|\mathrm{i_n(t)}\rangle$ is the time-dependent overlap of the initial ground vibrational state with the same state propagating on the excited state potential energy surface. *n* is the solvent index of refraction.

The excited state potential energy surface was initially taken to be harmonic along the six normal coordinates of $ClNO_2$, however this model did not reproduce well the absolute RR cross sections, especially in the high frequency region, predicting higher cross sections. The best fit to both the absorption spectrum and the REP was obtained by modeling the excited state surface along the Cl-N coordinate as linearly dissociative with slope *β* (Eq. 3.6).

$$
\begin{aligned}
V_e = {} & \frac{1}{2}\frac{\omega_{e1}^2}{\omega_{g1}^2}\left(q_1-\Delta_1\right)^2+\frac{1}{2}\frac{\omega_{e2}^2}{\omega_{g2}}\left(q_2\right)^2+\left(-\beta q_3\right) \\
& +\frac{1}{2}\frac{\omega_{e4}^2}{\omega_{g4}}\left(q_4\right)^2+\frac{1}{2}\frac{\omega_{e5}^2}{\omega_{g5}}\left(q_5\right)^2+\frac{1}{2}\frac{\omega_{e6}^2}{\omega_{g6}}\left(q_6\right)^2
\end{aligned}
\tag{3.6}
$$

The subscripts 1, 2, 3, 4, 5, 6 refer to the N-O symmetric stretch (v_1), O-N-O symmetric bend (v_2), Cl-N symmetric stretch (v_3), N-O asymmetric stretch (v_4), NO_2 rock (v_5) and NO_2 out-of-plane bend (v_6) vibrational modes respectively. ω_e and ω_g denote the excited- and ground-state harmonic frequencies. The potentials along v_2, v_4, v_5, and v_6 are described as harmonic with however no difference in equilibrium position between ground and excited state and no change in the excited state frequency relative to the ground state, while the potential along the Cl-N stretch (v_3) was described as linearly dissociative with slope *β.* The six vibrational degrees of freedom are considered separable such that the multidimensional, time-dependent overlaps in the absorption and Resonance Raman cross sections were decomposed into products involving one dimensional overlaps:

$$\langle i|i(t)\rangle=\prod_{k=1}^{6}\langle i_k|i_k(t)\rangle \tag{3.7}$$

$$\langle f|i(t)\rangle=\langle f_1|i_1(t)\rangle\prod_{k=2}^{6}\langle i_k|i_k(t)\rangle \tag{3.8}$$

In the above equations, subscript 1 refers to the Raman active coordinate (N-O symmetric stretch). Time-dependent overlaps along the N-O symmetric stretch, O-N-O symmetric bend, N-O asymmetric stretch, asymmetric bend and out-of-plane bend were calculated using analytical expressions by Mukamel.[9] Time-dependent overlaps along the dissociative N-Cl stretch coordinate were calculated using the split-time propagator algorithm by Feit and Fleck:[10-12]

$$\left|i(t)\right\rangle=\exp(i\Delta(t)\nabla^2/4M)\exp(-i\Delta(t)V_e)\times\exp(i\Delta(t)\nabla^2/4M\left|i(0)\right\rangle+\partial(\Delta(t^3)) \tag{3.9}$$

Equations (3.6) – (3.9) are valid for the two excited states included in the expressions of the absorption and Resonance Raman cross sections (Eqs. 3.3 and 3.5). In calculating the RR cross sections, the contribution from each excited state is added at the amplitude level such that interference can occur, leading to the reduction or enhancement of the scattering cross sections depending on the sign of displacement. Both excited states were taken as dissociative along Cl-N coordinate.

References

(1) Schweitzer, F.; Mirabel, P.; George, C. *Journal Physiscal Cheistry.A* **1998**, *102*, 3942.

(2) Rayson, R.; Wilson, M. K. *Journal of Chemical Physics* **1954**, *22*, 2000.

(3) Pieridou, G. K.; Hayes, S. C. *Physical Chemistry Chemical Physics* **2009**, *11*, 5302.

(4) Reid, P. J.; Esposito, A. P.; Foster, C. E.; Beckman, R. A. *Journal of Chemical Physics* **1997**, *107*, 8262.

(5) Waterland, M. R.; Kelley, A. M. *Journal of Chemical Physics* **2000**, *113*, 6760.

(6) Duan, Y. B.; Yuan, S. P.; Wang, R. B.; Mukhopadhyay, I. *Chemical Physics* **2006**, *330*, 9.

(7) Myers, A. B.; Mathies, R. A. In *Biological Applications of Raman Spectroscopy*; Spiro, T. G., Ed.; John WIley &Sons, Inc.: New York, **1987**; Vol. 2, p 1.

(8) Nyholm, B. P.; Reid, P. J. *Journal of Physical Chemistry B* **2004**, *108*, 8716.

(9) Mukamel, S. *Journal of Chemical Physics* **1985**, *82*, 5398.

(10) Feit, M. D. F., J.A. *Journal of Chemical Physics* **1983**, *78*,301.

(11) Feit, M. D. F., J.A.; Steiger, A. *Journal of Computational Physics* **1982**, *47*, 412.

(12) Foster, C. E.; Reid, P. J. *Journal of Physical Chemistry A* **1998**, *102*, 3514.

CHAPTER 4

PRELIMINARY STUDIES OF $ClNO_2$ IN SOLUTION: THE CHOICE OF SOLVENT AND AB INITIO CALCULATIONS

4.1 Introduction

Previous work on $ClNO_2$ photochemistry reported in the literature and outlined in the theoretical section exemplifies that the photochemistry of this halide is markedly influenced by its environment. Even though $ClNO_2$ has been extensively studied in the gas and solid phase, so far, its liquid phase photochemistry and reactivity has been essentially ignored. Our first goal was the synthesis of gaseous $ClNO_2$ in a range of solvents in order to investigate $ClNO_2$ photochemistry in a variety of environments, ranging from polar protic to non polar. We used sulfuric acid (H_2SO_4), methanol (MeOH), dichloromethane (CH_2Cl_2) and carbon tetrachloride (CCl_4). It was expected that less polar solvents such as CH_2Cl_2 and non-polar solvents such as CCl_4 would emulate the situation in the gas phase, while strong hydrogen bonding solvents such as H_2SO_4 and MeOH would provide a similar behavior as in the solid state or somewhere in between.

The characterization of solution-phase $ClNO_2$ was undertaken firstly via implementation of UV-Vis spectroscopy after the synthesis of nitryl chloride in these solvents. Then, UV Resonance Raman spectra in different environments were recorded in order to elucidate the phase-dependent photochemistry and early time dynamics of $ClNO_2$ through its exposure to different solvent environments. Both spectroscopic techniques have shown that nitryl chloride is stable only in methanol solvent with no evidence of impurities which would indicate a possible dissociation of the molecule.

Moreover, ab initio calculations of $ClNO_2$ in solvent clusters confirmed the dissociation of the molecule in CCl_4 and H_2SO_4, while a more stable configuration was achieved by immersing the molecule in a methanol cluster.

4.2 Results and discussion

4.2.1 Solution phase characterization by UV-Vis spectroscopy

The room temperature normalized absorption spectra of nitryl chloride bubbled in sulfuric acid (H_2SO_4) and methanol (MeOH), compared to that of gaseous nitryl chloride obtained from the literature[1] are displayed in Figure 4.1A, while the absorption spectra in dichloromethane (CH_2Cl_2) and carbon tetrachloride (CCl_4) are displayed in Figure 4.1B. These spectra were normalized at the wavelengths that correspond to the maximum of each absorption spectrum. We observe that the solvent produces a large effect on the absorption spectrum of nitryl chloride. Specifically, the absorption spectrum appears to red shift with an increase in solvent polarity, but also broadens. The gas phase spectrum displays a weak absorption between 300 – 400 nm (Band A), followed by an onset at 280 nm, a weak vibronic structure in the range 220-280 nm (Band B), a peak at 215 nm (Band C) and a strong absorption band below 200 nm (D band).[1]

The absorption spectrum of $ClNO_2$ in MeOH consists of three bands with D being the most dominant and appearing below 240 nm. The C band is observed at 269 nm, while the B band is placed between 310-390 nm with a vibronic series characteristic of nitryl chloride in methanol.[2] In Chapter 5 we discuss in more detail this absorption spectrum and we attempt to assign the observed electronic bands based on previous theoretical calculations in the gas phase.

The spectrum in H_2SO_4displays a broad peak at 276 nm, which may be assigned to the C band, and a strong D band below 220 nm. In carbon CCl_4 and CH_2Cl_2, the shape of the spectra on the high energy edge seems unusual and is most probably caused by a large absorption of the solvent and subtraction problems of the instrument. For these reasons the latter spectra are shown in different figure.

Table 4.1 summarizes the λ_{max} of the electronic transitions in the solvents employed in this study, as well as the corresponding positions of the transitions in gaseous nitryl chloride. It is obvious that in MeOH the absorption spectrum is most closely related to the one in the gas phase, with three distinct transitions and with band B displaying a characteristic vibronic structure.

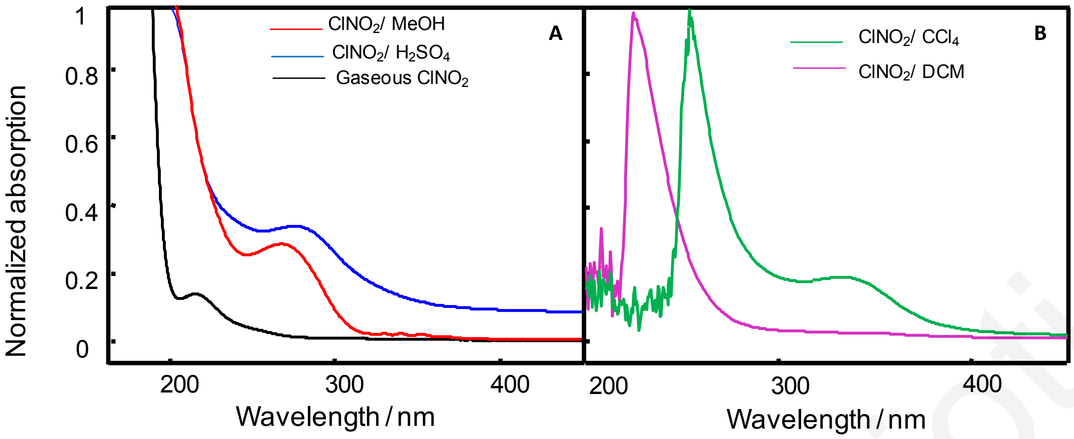

Figure 4.1 (A) Normalized absorption spectra of $ClNO_2$ recorded in methanol (red), sulphuric acid (blue) with λ_{max} at 200 nm. The absorption spectrum of gaseous nitryl chloride is normalized at 189nm(black). **(B)** Normalized absorption spectra of $ClNO_2$ recorded in CCl_4 (green) and DCM (purple). The spectra were normalized to the lowest wavelength absorption where solvent subtraction problems created an artificial λ_{max}.

Table 4.1 Absorption bands of $ClNO_2$ in the gas phase, H_2SO_4, MeOH, CCl_4 and CH_2Cl_2

Absorption Band	Gas Phase	CCl_4	CH_2Cl_2	H_2SO_4	MeOH
D	188 nm			201 nm	200 nm
C	215 nm	253	225	276 nm	269 nm
B	220-280 nm	335	320-385	-	310-390 nm
A	300-400 nm	-	-	-	-

4.2.2 Analysis of the vibronic structure in the B band in the UV-Vis spectrum of $ClNO_2$ in methanol

Although the wavelength range the vibronic structure appears (320-385 nm) is not within the range of interest in our investigations (the RRIA we will present in the next chapters focuses on the strong D band), the assignment of the weak B band of $ClNO_2$ in methanol is quite important, because this transition is characteristic for nitryl chloride and it is a confirmation that this molecule is formed and is stable in this environment.[2,3] Moreover, the assignment of the vibronic progression could provide information about the energetics, the structural evolution and geometry in the solution compared to the gas phase.

An enlarged view of the 310 – 390 nm spectral region is displayed in Figure 4.2.The vibronic progression has its origin (0-0 transition) around 370 nm, and five vibronic bands are identified. The spacing decreases as we move to higher energy, characteristic of anharmonicity in the system. The differences between bands in cm^{-1} are displayed in Table 4.2.

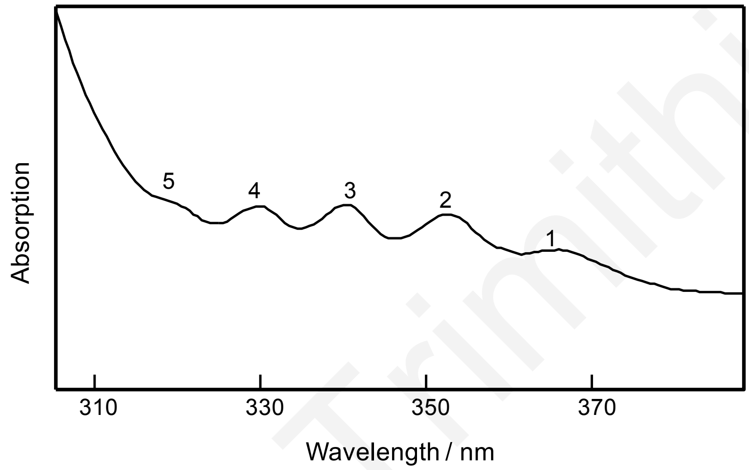

Figure 4.2. Enlarged view of the UV-Vis spectral region 310 – 385 nm for $ClNO_2$ in MeOH.

Using the anharmonic oscillator equation for the energy difference between adjacent energy levels,

$$\Delta \mathrm{E} = \varepsilon_{v+1} - \varepsilon_{v} = \varpi_{e}\left(1 - 2x_{e}\left(v+1\right)\right)\ cm^{-1} \qquad 4.1$$

we can extract the excited state anharmonicity parameter $x_e = 0,017 cm^{-1}$ and the harmonic vibrational frequency $\varpi_e = 1036{,}16\, cm^{-1}$. The corresponding spacing in gaseous nitryl chloride is an average 427 cm^{-1}, which was attributed to the O-N-O symmetric bend in the excited state.[1] Considering the vibrational mode frequencies of neat $ClNO_2$ presented in Table 2.2 (see Chapter 2), possible candidates for the vibronic progression are the N-O symmetric stretch of A_1 symmetry and the N–O asymmetric stretch of B_1 symmetry in the C_{2v} group. This result is not in accordance with the vibrational mode involved in the progression observed in the gas phase spectrum, indicating an alteration in the photochemical pathways in the condensed phase. In Chapter 5 we will discuss the observed vibronic progression in relation to the RRIA in methanol in an attempt to explore the role of solvent in excited state structural evolution.

Table 4.2 The maxima and the spacing of the vibronic progression within band B

Transition	λ (nm)	Spacing cm^{-1}
1 (0-0)	366.5	27285
2 (0-1)	353.4	28297
3(0-2)	341.1	29317
4 (0-3)	330.6	30248
5(0-4)	321	31153

4.2.3 Preliminary Resonance Raman spectra

The implementation of UV Resonance Raman spectroscopy for the elucidation of the phase-dependent photochemistry and early time dynamics of $ClNO_2$ through its exposure to different solvent environments was the initial goal of this dissertation. Thus, after the synthesis of gaseous nitryl chloride and its dissolution in various solvents we performed RR spectroscopy in these condensed systems. Resonance Raman spectra of $ClNO_2$ dissolved in MeOH, CH_2Cl_2 and H_2SO_4 were obtained with excitation at 239 nm. In Table 4.3 we summarize the frequencies of possible photoproducts observed after irradiation of nitryl chloride trapped in water ice [4] and after photolysis in Ar, O_2, and N_2 matrices.[5] This review is useful for the assignment of the peaks observed in RR spectra, which do not belong to totally symmetric modes of the molecule.

In the RR spectra of $ClNO_2$/MeOH a low intensity peak is clearly observed at 1290 cm^{-1} (Figure 4.3A). This peak was attributed to the N-O symmetric stretch. The considerations leading to that assignment are explained and discussed extensively in Chapter 5. Figure 4.3B presents the Resonance Raman spectrum of $ClNO_2$ dissolved in CH_2Cl_2, where a vibrational mode at 1718 cm^{-1} is observed. No totally-symmetric modes are expected at this frequency. The N-O asymmetric stretch possesses the closest frequency (1648 cm^{-1}), however this mode is of B_2 symmetry and not allowed in Resonance Raman scattering, unless through a B-term enhancement. No evidence of the N-O symmetric stretch is observed in this solvent; however this could be due to overlap with solvent peaks in the same region. It is highly probable, though, that nitryl chloride is not stable in this solvent and the band at 1718 cm^{-1} is due to a photoproduct, most probably due to HNO_3(Table 4.3).

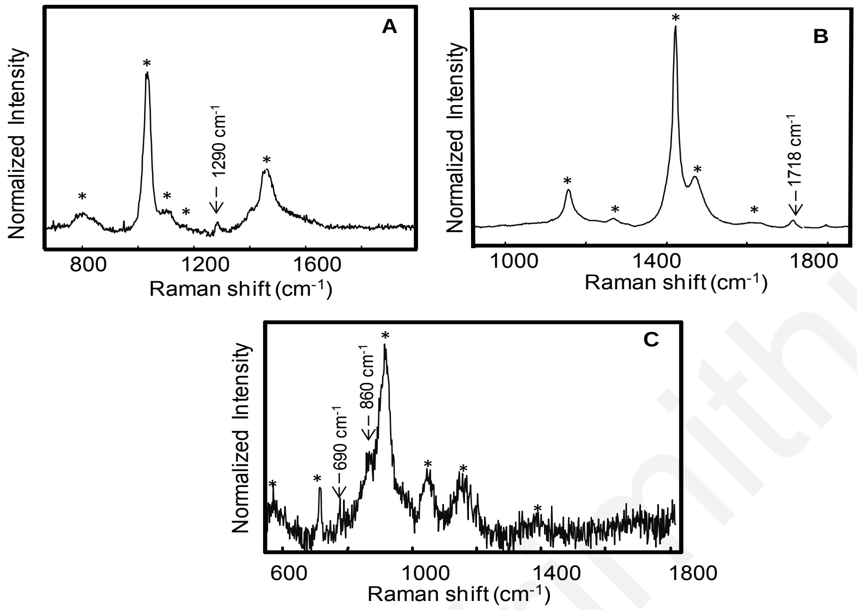

Figure 4.3 RR spectra of $ClNO_2$ (A) in MeOH (B) in CH_2Cl_2 and (C) in H_2SO_4 at 239.5 nm. The asterisks indicate the frequencies corresponding to the solvents.

The Resonance Raman spectrum of $ClNO_2$ in H_2SO_4 is shown in Figure 4.3C. Bands around 700 and 860 cm^{-1} are observed in this spectrum, which, however, do not correspond closely to any of the $ClNO_2$ totally-symmetric modes. It is very possible that $ClNO_2$ hydrolyzes in this solvent. According to Table 4.3, the band at 700 cm^{-1} may be assigned to nitric acid tri-hydrate (NAT) or HNO_3 while the 860 cm^{-1} band may be attributed to hydrated NO_3^- or to ClONO. Through this study, the stability of the molecule in MeOH was confirmed.

Table 4.3 Photoproduct frequencies observed after UV irradiation of $ClNO_2$ in ice surface and in matrices [4]

IR absorption (cm^{-1})	Assignment
1873[i]	NO[i]
1844[i]	NAT
1842[ii]	ClON
1804[ii]	ClNO
1745[i]	H_3O^+
1721[ii]	$ClONO_2$
1711[i]	HNO_3
1652[i]	NAT
1343[i]	Hydrated NO_3^-
986[i]	HNO_3
850[ii]	ClONO
834[i]	Hydrated NO_3^-
777[i]	HNO_3
729 – 701[i]	NAT
639[i]	H_3O^+

[i] photoproducts after UV irradiation of a mixed $ClNO_2$/water [4]

[ii] photoproducts formed on photolysis of matrices containing $ClNO_2$.[5]

4.2.4 Preliminary *ab initio* calculations

The development of new *ab initio* methods as well as the increase of computer power opens new possibilities for modeling excited state dynamics of many molecular systems. In particular, the resolution-of-the-identity (RI) approximation for the evaluation of the electronrepulsion integrals decreases the calculation time by one order of magnitude as compared to more conventional methods.

The implementation of gradient methods in the excited states allows studying the minimum energy path of many excited states either at the cc2 level or with the TD-DFT method. The latter method is faster but cannot be used if charge transfer states are involved in the excited states. It is therefore possible to study the solvent effect at the molecular level by immersing the molecule in small clusters containing tens of solvent molecules for the ground state. This will identify the most relevant neighbor to perform the *ab initio* minimum energy path, and the main effect of the nearby molecules on the fragmentation dynamics. Here, this study involved electronic excited state calculations.

4.2.4.1 *Ab initio* calculations for gaseous $ClNO_2$

Theoretical studies of the electronic absorption spectrum of $ClNO_2$ complement the existing experimental studies and support the spectral assignment. Moreover, examination of the potential energy curves may clarify the photodissociation process of nitryl chloride. Only one theoretical study of $ClNO_2$ excited states is reported in the literature.[6] Lesar *et al*, calculated the vertical excitation energies and oscillator strengths to singlet excited states of $ClNO_2$ and the potential energy curves along the Cl-N bond using MRD-CI methods with the cc–pVDTZ basis set. We extend this study by calculating more excited states using ricc2-aug-cc-pVTZ(2). Moreover, we calculated the potential energy curves along the N-O bond and O-N-O bend.

The ground state configuration of $ClNO_2$ is $(5a_1)^2$ $(2b_2)^2$ $(1a_2)^2(4b_1)^2$ when the 24 valence electrons are considered active. The lowest excitation of $ClNO_2$ populates the lowest unoccupied molecular orbital LUMO $6a_1$. As can be seen from Figure 4.4, the LUMO $6a_1$ is considered to be an antibonding σ^*(Cl-N) type molecular orbital, while in the $4b_1$ molecular orbital the charge density is located largely at the chlorine. The vertical excitation energies, the strength of the various transitions and the dipole moments for the free molecule were calculated with ricc2-aug-cc-pVTZ(2) and are summarized in **Table 4.4**. The experimental values obtained for the gaseous $ClNO_2$[1] are also included for comparison.

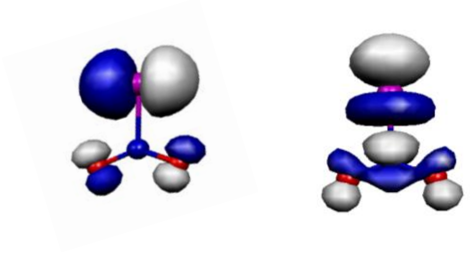

HOMO ($4b_1$) LUMO ($6a_1$)

Figure 4.4 Charge density surfaces of highest occupied molecular orbital (HOMO) and the lowest unoccupied molecular orbital (LUMO).

The results reported in the Table indicate the accuracy of the calculations since the experimental and theoretical values for the gas phase are in a reasonable agreement. The oscillator strengths indicate the most allowed optical transitions, which correspond very closely to the absorption bands observed in the experiment. It is important to stress here, that at energies greater than 6.2 eV (D absorption band) there are two nearby transitions.

Figures 4.5, 4.6 and 4.7 present the potential energy curves along the Cl-N, ONO and N-O coordinates respectively. A molecular potential energy curve is a graph that shows how the energy of the molecule varies as bond lengths and bond angles are changed. To examine the role of $ClNO_2$ as a possible source of Cl and NO_2 radicals we studied the excited states along the Cl-N coordinate. Figure 4.5 gives the potential energy surfaces for singlet excited states of $ClNO_2$ symmetric fragmentation pathway along Cl-N bond. It can be seen that the strongest transitions with symmetry $2A_1$, $1A_1$ and $1B_1$ are dissociative states. $2B_1$ and $2A_2$ are weakly bound states, but both of these transitions have very small oscillator strength.

Table 4.4 Calculated vertical excitation energies ΔE (eV) and oscillator strengths *f* to singlet excited states of free $ClNO_2$, along with their dipole moments at the ricc2-aug-cc-pVTZ(2) level of theory.

ricc2-aug-cc-pVTZ(2)					
State	**Excitation**	**ΔE(eV)**	***f***	**μ(D)**	**ΔE_{exp} (eV)**
X^1A_1	$(5a_1)^2(2b_2)^2$ $(1a_2)^2(4b_1)^2$	0	0	0.42	
1^1B_1	**$6b_1 \rightarrow 11a_1$**	**4.16**	**0.009384**	**1.624**	~4.1
1^1A_2	$6b_1 \rightarrow 4b_2$	4.79	0.000	0.603	
1^1B_2	$3b_2 \rightarrow 11a_1$	5.11	0.00010	1.634	
2^1B_2	$10a_1 \rightarrow 4b_2$	5.45	0.000020	1.205	
1^1A_1	**$10a_1 \rightarrow 11a_1$**	**5.66**	**0.1699**	**0.0055**	**~5.8**
2^1A_2	$1a_2 \rightarrow 11a_1$	5.86	0.000	4.44	
2^1B_1	$5b_1 \rightarrow 11a_1$	5.92	0.0092	0.8591	
2^1A_1	**$3b_2 \rightarrow 4b_2$**	**6.71**	**0.396**	**1.874**	**>6.2**
3^1A_2	$5b_1 \rightarrow 4b_2$	6.75	0.000	1.364	
3^1B_1	**$1a_2 \rightarrow 4b_2$**	**7.65**	**0.21**	**0.022**	**>6.2**
4^1B_1	$6b_1 \rightarrow 12a_1$	8.57	-0.00016	0.2353	
3^1A_1	$10a_1 \rightarrow 12a_1$	9.14	0.048	0.49	
3^1B_2	$3b_2 \rightarrow 12a_1$	9.60	0.093	0.41	
4^1A_2	$6b_1 \rightarrow 5b_2$	9.94	0.00	1.36	
4^1A_1	$6b_1 \rightarrow 7b_1$	10.011	0.048	0.49	
4^1B_2	$10a_1 \rightarrow 5b_2$	10.491	0.006	1.46	

The potential energy curves for the singlet states of $ClNO_2$ along the ONO bend coordinate are shown in Figure 4.6**.** The same trend is observed in this graph. The most probable transitions to states $2A_1$, $1A_1$ and $1B_1$ are dissociative because they exhibit a linear potential in the equilibrium position. $2B_2$ is weakly bound but this transition is very weak due to the very small oscillator strength. The calculated potential energy curves of the singlet states of $ClNO_2$ along the N-O stretch coordinate are depicted in Figure 4.7. The excited states along this coordinate all possess strongly bound potential wells. This graph also shows that there is a large displacement in the equilibrium position between ground and excited states, which corresponds to a large change in geometry, something we also observed in our theoretical simulations.

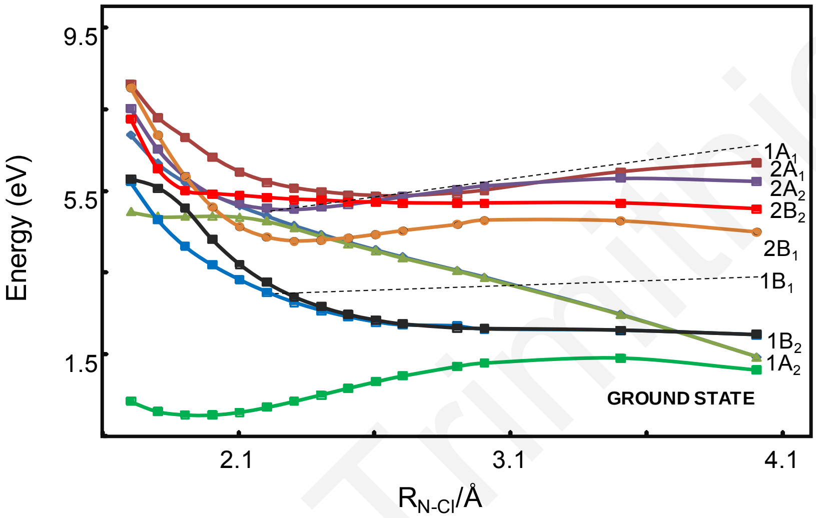

Figure 4.5 Calculated potential energy curves of the singlet states of $ClNO_2$ along a Cl-N bond.

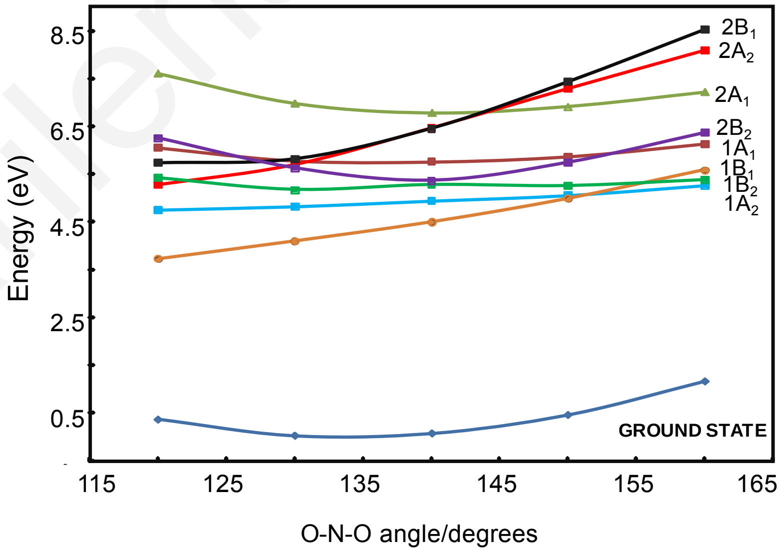

Figure 4.6 Calculated potential energy curves of the singlet states of $ClNO_2$ along ONO angle.

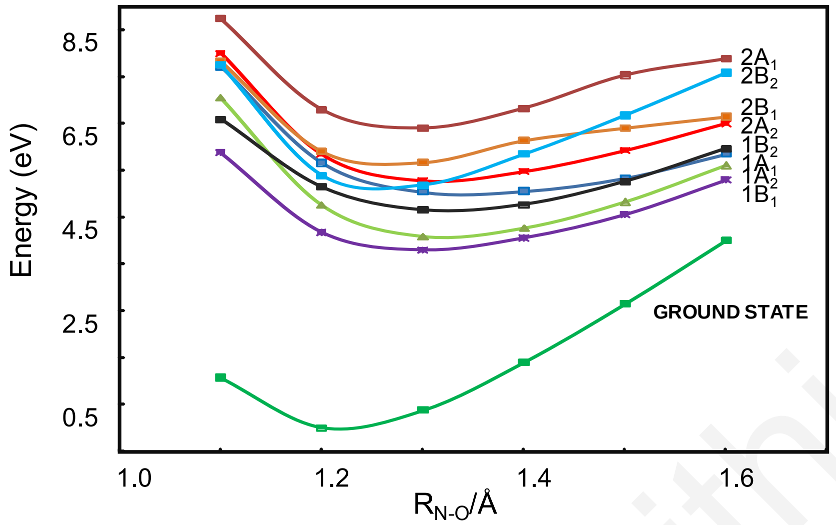

Figure 4.7 Calculated potential energy curves of the singlet states of $ClNO_2$ along a N-O bond.

4.2.4.2 *Ab initio* calculations of nitryl chloride immersed in methanol clusters

Ab initio calculations in CCl_4, H_2SO_4 and MeOH clusters were performed in order to investigate the stability of the molecule in these environments and assess the effect of solvent on excited state energetics and photodissociation. Initial calculations on $ClNO_2$ in carbon tetrachloride clusters showed that the Cl-N distance increased by 0.2 Å after complexation of the free molecule to the cluster, essentially causing dissociation of the molecule. In addition, our initial experiments in this solvent proved that this molecule was not stable, with no signature in the Raman spectrum due to nitryl chloride, but instead we observed signature from various photoproducts (see above). Calculations were also done for the molecule in H_2SO_4, but the same situation as in CCl_4 was observed with the Cl-N distance increasing, also in agreement with the experimental results mentioned above. Thus, the *ab initio* studies concentrated on the $ClNO_2$/MeOH system where the initial experimental studies had shown that methanol could be a suitable solvent.

Here, this study involved excited state calculations and calculations of the minimum energy path at the RI-cc2 and RI-TD-DFT level, followed by calculation of $ClNO_2$ immersed in a cluster of enough methanol molecules to make a cage (10 molecules).

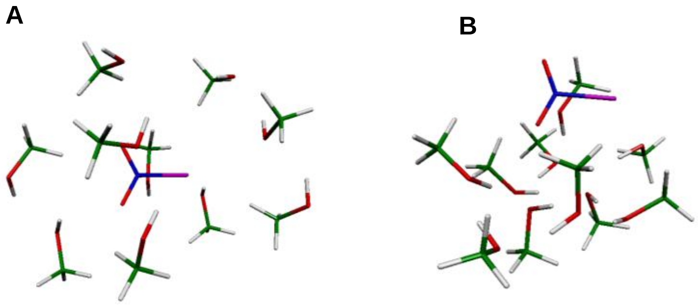

Figure 4.8 $ClNO_2$/MeOH (n) clusters before (A) and after (B) optimization of the cluster

The $ClNO_2$/MeOH (n) clusters have been calculated up to n = 10, using DFT (B3-LYP + dispersion) to optimize the ground state geometry. However, we observed that upon optimization of the cluster (Figure 4.8B) the $ClNO_2$ molecule initially embedded in the cluster (Figure 4.8A) is expelled. This is due to entropy as these calculations were run at 0^o K, where the most stable structure for the cluster involves strong H bonds between MeOH molecules. If the calculations could be run at 300^o K the entropy would overcome the formation of these bonds allowing $ClNO_2$ to stay inside the cluster. However, calculations at higher temperatures are very difficult for such large systems.

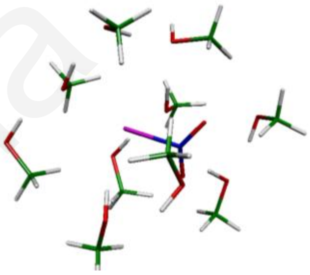

Figure 4.9 $ClNO_2$ immersed in a MeOH (10) cluster at equilibrium geometry.

Figure 4.9 depicts the molecule in an immersed geometry which is not a global minimum for the cluster but for which the Cl-NO_2 distance has reached an equilibrium. Table 4.5 presents the variation of excitation energy as a function of the position of ClNO2 with respect to the solvation shell. Here, the excitation energy has been calculated at the TD-DFT level. The third column of the table refers to the energies calculated a short time after the optimization of the cluster geometry has initiated, when $ClNO_2$ is still in the cluster with equilibrium $ClNO_2$ distances (as in Figure 4.5). The second column refers to the case where the geometry optimization has been completed and $ClNO_2$ is sitting on the outside surface of the cluster. These calculations show there is a strong variation of the excitation energy with the local structure, which explains the red-shift of the absorption spectrum with the polarity of the solvent.

Table 4.5 The variation of the excitation energy as function of the solvation shell.

	Free $ClNO_2$ (eV)	$ClNO_2$ outside (eV)	$ClNO_2$ inside (eV)
S1	3.73	2.84	2.52
S2	3.80	2.99	2.93
S3	4.17	3.31	3.15

Since we had to essentially trap $ClNO_2$ in the cluster at an optimized geometry, it was not possible to generate energy curves of the form presented in Figures 4.5-4.7 Such investigations in the cluster environment may provide useful information about nitryl chloride excited state structural evolution along the specific normal modes.

The initial experiments that are shown in this Chapter lead to the adoption of methanol as the most suitable environment for the investigation of the solution phase of nitryl chloride. Moreover, ab initio calculations on the low lying excited states of $ClNO_2$ demonstrated that the excited states that contribute to the D absorption band along N-Cl potential energy surfaces are not bound. In Chapter 5 we describe our RRIA study of nitryl chloride in methanol on resonance with the D band of the absorption spectrum. In Chapter 6, we describe partial density of state calculations of this chemical system, which also show clearly the influence of the solvent on state energetics providing additional information on the solute-solvent interactions.

References

(1) Furlan, A.; Haeberli, M. A.; Huber, J. R. *Journal of Physical Chemistry A* **2000**, *104*, 10392.

(2) Eiserich, J. P.; Cross, C. E.; Jones, A. D.; Halliwell, B.; vanderVliet, A. *Journal of Biological Chemistry* **1996**, *271*, 19199.

(3) Collis, M. J.; Gintz, F. P.; Goddard, D. R.; Hebdon, E. A.; Minkoff, G. J. *Journal of the Chemical Society* **1958**, 438.

(4) Schriver-Mazzuoli, L.; Coanga, J. M.; Schriver, A. *Journal of Physical Chemistry A* **2003**, *107*, 5181.

(5) Coanga, J. M.; Schriver-Mazzuoli, L.; Schriver, A.; Dahoo, P. R. *Chemical Phyiscs Letters* **2002**, *276*, 309.

(6) Lesar, A.; Hdoscek, M.; Muhlhauser, M.; Peyerimhoff, S. D. *Chemical Physics Letters* **2004**, *383*, 84.

CHAPTER 5

RESONANCE RAMAN INTENSITY ANALYSIS OF $ClNO_2$ DISSOLVED IN METHANOL

5.1 Introduction

In this chapter, we report our initial studies of nitryl chloride in solution as a first step towards understanding the phase-dependent reactivity of this molecule. We present a Resonance Raman Intensity Analysis (RRIA) study of $ClNO_2$ in methanol, with excitation at wavelengths resonant with the D absorption band. The absorption spectrum of nitryl chloride in the solvent environment is indicative of the changes in the electronic excited states in comparison to the corresponding spectrum in the gas phase. Resonance Raman (RR) spectroscopy was a useful tool for the clarification of the structural changes that occur under the influence of the solvent in the molecular ground state. By performing RRIA we got the first indications about the excited state structure, the initial excited state dynamics along with the nature of the electronic transitions in the Frank Condon region.

The experimental setup and the experimental and computational methods used are described in detail in Chapter 3.

5.2 Experimental results

5.2.1 Absorption spectrum

Nitryl chloride is a planar molecule in its ground state (X^1A_1) with C_{2v} symmetry. The room temperature UV/Vis absorption spectrum of gaseous $ClNO_2$ has been reported in several studies.[1-4] Figure 5.1 presents the room temperature absorption spectrum of nitryl chloride dissolved in methanol in comparison to the gas phase absorption spectrum obtained from the literature.[1] The gas phase spectrum is characterized by four absorption bands. It displays a weak absorption between 300 – 400 nm (Band A), followed by an onset at 280 nm, a weak vibronic structure in the range 220-280 nm (Band B), a peak at 215 nm (Band C) and a strong increase below 200 nm (Band D). The red shift observed in the spectrum in solution demonstrates the pronounced effect of the solvent on state energetics. Three out of the four characteristic absorption bands are evident in the solution phase absorption spectrum, with, however, a broader linewidth. The B band is placed between 310-390 nm and it consists of a vibronic series characteristic of nitryl chloride in methanol, [5] while the peak referred to as C band is observed at 269 nm. The D band which is the strongest transition appears below 240 nm. The absence of an absorption band at 460 nm proves that the sample is free of NOCl impurities.[6]

Previous gas phase studies have provided detailed understanding of the dissociation dynamics following excitation resonant mainly with the B band (220-280 nm) [1-4] and A band (300-400 nm).[2,4] Photodissociation of thin films of nitryl chloride and nitryl chloride in amorphous ice and in matrices were studied at 266 nm, while the dynamics following photodissociation in clusters were studied at 235nm. Only one recent study has provided information about the photodissociation process that occurs following photoexcitation at 193 nm, resonant with the D band.[7] This photolysis wavelength falls within the spectral region where solar photolysis in the stratosphere occurs unfiltered by O_3, O_2, and N_2.

Table 5.1 lists the calculated values for the $ClNO_2$ extinction coefficient in methanol at the excitation wavelengths used in this study.

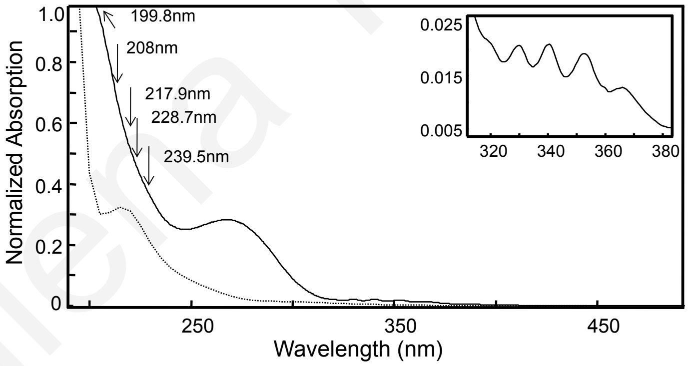

Figure 5.1 Absorption spectrum of $ClNO_2$ in methanol (24.65M) (solid line) and gaseous $ClNO_2$ (dotted line).[1] An enlarged view of the region 310 – 380 nm of the solution phase absorption spectrum is shown in the inset. Also indicated are the excitation wavelengths employed in the resonance studies.

Table 5.1 Experimentally determined values for the extinction coefficient of $ClNO_2$ in methanol

λ (nm)	**ε (M^{-1} cm^{-1})**
199.76	4700
208.8	3430
217.85	2290
228.7	630
239.5	430

5.2.2 Absolute Resonance Raman Cross Sections

The RR cross sections and depolarization ratios for methanol used in the calculation of the RR cross sections of $ClNO_2$ are reported in Table 5.2 along with the total differential Raman cross sections of perchlorate calculated for all the excitation wavelengths used in this study from the fit to the Albrecht A-term.[8] The methanol cross sections were calculated via Eq.3.2 (see experimental section) while the absolute resonance Raman cross sections (σ_i) of perchlorate were obtained via Eq. 5.1

$$\sigma_R = \frac{8\pi}{3}\left(\frac{1+2\rho}{1+\rho}\right)\left(\frac{d\sigma_R}{d\Omega}\right) \qquad (5.1)$$

σ_R is the absolute RR cross section, ρ is the depolarization ratio and $\left(\frac{d\sigma_R}{d\Omega}\right)$ is the differential cross section at all excitation wavelengths.

Table 5.2 Differential σ_R for the 932 cm^{-1} mode of ClO_4^{-1}, depolarization ratios and absolute RR cross sections for the 888 – 1240 cm^{-1} region of methanol**.**

λ (nm)	$\left(\frac{d\sigma_R}{d\Omega}\right)_{ClO_4^{-1}}$ ($\times 10^{12}$ Å^2)	ρ_{MeOH}	σ_{MeOH} ($\times 10^{12}$ Å^2)
199.76	13.30	0.22 ± 0.05	12.27 ± 0.10
208.8	12.1	0.19 ± 0.02	10.99 ±0.50
217.85	8.04	0.23 ± 0.01	8.78 ± 0.90
228.7	6.11	0.20 ± 0.03	6.56 ± 0.30
239.5	4.75	0.29 ± 0.01	5.36 ± 0.08

5.2.3 Resonance Raman Intensity Analysis

Representative RR spectra of $ClNO_2$ in methanol obtained with excitation at 199.8, 208.8, 217.9, 228.7, and 239.5 nm are shown in Fig. 5.2. A portion of the RR spectrum at 199.8 nm in the low frequency region is also presented. By symmetry, fundamental intensity corresponding to the N-O symmetric stretch (v_1), O-N-O symmetric bend (v_2), and N-Cl symmetric stretch (v_3) is expected since these coordinates are totally-symmetric in the C_{2v} point group for the ground state of $ClNO_2$. Fundamental intensity involving the N-O asymmetric stretch, NO_2 rock, and NO_2 out-of-plane bend is not predicted on resonance. Fundamental transitions reported for the gas, liquid and solid state of $ClNO_2$ observed in IR and Raman experiments are listed in Table 5.5.

N-O symmetric stretch. Inspection of Fig. 5.2 demonstrates that the spectrum is dominated by intensity corresponding to methanol vibrational modes. The band observed at 1291 cm^{-1} is assigned to the N-O symmetric stretch (v_1) after comparison to the solvent spectrum and the mode frequencies observed in the gas and liquid phase for this molecule (Table 5.3). A comparison of the spectra presented in Fig.5.2 demonstrates that the intensity corresponding to the N-O symmetric stretch (v_1) decreases with respect to the solvent bands as we move away from the peak of D band as expected, resulting in the depression of the RR cross sections, σ_R (Eq.3.3). Even though this assignment seems straightforward, this transition can also be assigned to the overtone of the out-of-plane bend (ν_6). This mode is of B_1 symmetry and can only appear either through B-term enhancement or through a change in the frequency of this mode in the excited state. B-term enhancement occurs when two excited electronic states are closely spaced. This can be investigated through the measurement of depolarization ratios, and our measurements demonstrate such a possibility (see below). However, observation of this overtone vs. a fundamental with allowed symmetry would be very unlikely. Therefore, it is logical to assume that the band appearing in the RR spectrum of $ClNO_2$ must belong to the N-O symmetric stretch.

Table 5.3 reveals that the ν_1 frequency in methanol is ~24 and ~33 cm^{-1} up-shifted relative to the gas and solid phase, respectively. A similarly large shift is also observed with respect to the liquid phase (neat $ClNO_2$). This shift reflects strengthening of the N-O bond in this polar solvent, probably due to preferential solvation of the electronegative Cl (see below).

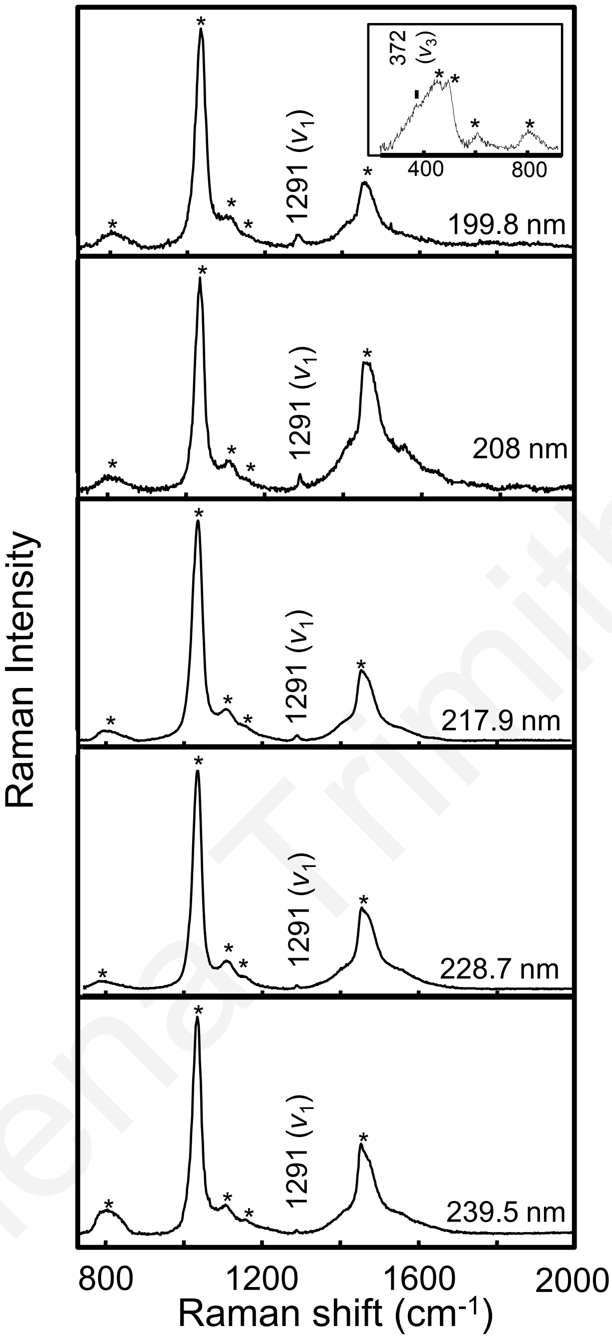

Figure 5.2 Resonance Raman spectra of $ClNO_2$ in methanol with excitation within the D band. A transition corresponding to v_1 is observed at all excitation wavelengths. The inset presents the low frequency region of the spectrum at 199.8 nm demonstrating the presence of v_3. The asterisks denote methanol bands and quartz scattering (451 cm^{-1}, 494 cm^{-1}, 610 cm^{-1} and 800 cm^{-1}).[9,10]

Table 5.3 Fundamental vibrational modes for $ClNO_2$

Transition	Vibrational mode[1] (symmetry)	ω (cm^{-1})[a] gas phase	ω (cm^{-1})[a] solid state	ω (cm^{-1})[a,b] liquid state	ω (cm^{-1})[c] methanol
v_1	N-O s stretch (A_1)	1267.3	1259 1252	1258.7	1291
v_2	O-N-O s bend (A_1)	793.8	786.2	786.2	-
v_3	N-Cl s stretch (A_1)	369.6	399 379	370	372
v_4	N-O as stretch (B_2)	1684.6	1664 1648	1667	-
v_5	NO_2 rock (B_2)	412	422 428	411	-
v_6	NO_2 op bend (B_1)	651.7	651.5[b]	652	-

[1] s: symmetric, as: asymmetric, op: out-of-plane
[a] Ref. [11]
[b] Ref. [12]
[c] this study

N-O symmetric bend. The v_2 fundamental expected at ~786 cm^{-1} is not observed, possibly due to overlap with scattering from the material of the spinning cell (suprasil) at 800 cm^{-1}, or due to small structural evolution along this coordinate.

N-Cl symmetric stretch. A very low intensity band corresponding to the N-Cl stretch fundamental transition (v_3), is evident only in the RR spectra at 199.8 nm, probably due to the higher extinction coefficient at this wavelength. This transition is observed at 372 cm^{-1} similar to the frequencies observed in the gas phase and pure liquid phase[11], while shifted to lower frequencies compared to the solid state (Table 5.3). However, the large background in this region deters a more detailed analysis.

The RR results presented here demonstrate that excited state structural evolution is dominated by evolution along the N-O symmetric stretch. Therefore, absolute RR cross sections were measured only for v_1 and are reported in Table 5.4. It is obvious that there is a good agreement between the experimental and calculated values of the RR cross sections except from the 239. 5 nm where a quite big disagreement is observed. A possible reason for this deviation is the very low intensity of the normal mode at this wavelength which makes difficult the calculation of the integrated area.

Understanding the dynamics and photochemistry that occurs following photoexcitation within the $ClNO_2$ D band entails a thorough understanding of the nature of the electronic states involved in the transition and their coupling to any nearby states. The number of states that participate in the scattering process can be determined through the measurement of RR depolarization ratios. A value of $\rho = 1/3$ indicates that the contribution to the scattering is due to a single dipole-allowed transition, while values lower than 0.33 are consistent with the contribution of more than one electronic states. Depolarization ratios of nitryl chloride at the excitation wavelengths employed in this study are presented in Table 5.4 and depicted in Fig. 5.3, where it is clear that the ratios are significantly below 1/3 suggesting that more than one excited state contributes to the D band. As we move towards the lower energy edge of the D band, ρ is approaching 1/3.

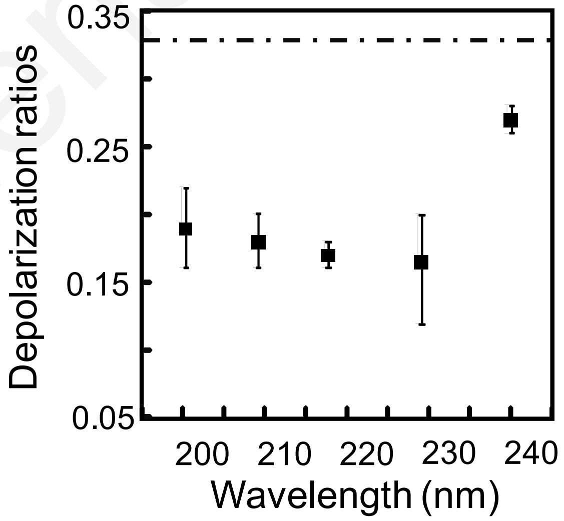

Figure 5.3 Depolarization ratios for the N-O symmetric stretch (v_1) as a function of excitation wavelength.

Table 5.4 Depolarization ratios and absolute RR cross sections for the $ClNO_2$ ν_1 mode.

λ (nm)	$\rho_{\nu 1}$	$\sigma_{\nu 1}$ ($\times 10^9$ Å^2) experimental	$\sigma_{\nu 1}$ ($\times 10^9$ Å^2) calculated
199.76	0.19 ± 0.03	2.34 ± 0.3	2.56
208.8	0.18 ± 0.03	2.21 ± 0.5	2.29
217.85	0.17 ± 0.01	1.43 ± 0.3	1.21
228.7	0.16 ± 0.04	0.513 ± 0.03	0.30
239.5	0.27 ± 0.01	0.202 ± 0.02	0.06

5.2.4 Modeling of the D band

The excited state potential energy surface parameters were determined by simultaneously modeling the absorption and absolute RR cross sections. A model based on a single-dipole allowed transition was not considered, as it failed to reproduce both the absorption spectrum and the Raman excitation profile (REP). In addition, the depolarization ratios obtained in this study are below 1/3 for all the excitation wavelengths used. Therefore, a model based on transition to two dipole-allowed electronic excited states with harmonic ground and excited state potentials was employed using the time-dependent formalism for absorption and Resonance Raman scattering. [13] In this calculation, both homogeneous (Γ) and inhomogeneous broadening was included. The inhomogeneous distributions for both transitions were assumed to be equivalent, such that the absorption cross sections for either transition are convolved with identical Gaussian functions. This assumption leads to the approximation that the energy shifts for both transitions are correlated. Figure 5.4a presents the comparison between the experimental and calculated absorption spectrum, along with the individual absorption spectra for each transition. Quite good agreement is observed; however, inspection of Fig. 5.5 demonstrates that this model is unable to reproduce the REP for the ν_1 mode, especially for the excitation wavelengths at the maximum of the absorption band, where the RR cross sections are overestimated, even for large values of the homogeneous linewidth and the inclusion of inhomogeneous broadening. The experimental data were reproduced well by the two-excited-state model when both excited state potentials were considered linearly dissociative along the Cl-N coordinate with a negative slope β of 2900 cm^{-1} (Figures 5.4b and 5.5). The latter assumption was made based on previous theoretical studies[15] and our previous ab initio calculation (see Chapter 4) which predicted that the excited states contribute to the RR scattering of nitryl chloride on resonance with D band are dissociative along N-Cl bond in the Frank – Condon region. The parameters employed in the calculation for the second model are listed in Table 5.4 Specifically, evolution was only considered along the NO symmetric stretch coordinate with a moderate dimensionless displacement (Δ_1), slightly different for each excited state (2.5 vs. 3.0). The ground state frequency of this mode was taken from the experimental spectra, while the ground state frequencies for the other five modes were taken from liquid phase Raman spectra in the literature. [11] The latter frequencies were retained in the description of the excited-state potentials; however, it was necessary to reduce the ν_1 frequency to 570 cm^{-1} in order to obtain a better fit. Large values of Γ (Γ_1=750 cm^{-1} and Γ_2=700 cm^{-1}) were necessary for each excited state in order to reproduce the ν_1 absolute RR cross sections, in combination with the steep slope of the linear potential along the Cl-N coordinate. The inclusion of inhomogeneous broadening was necessary for broadening the absorption spectrum and constraining the homogeneous linewidth.

Even though the Cl-N stretch only appears at the 199.8 nm RR spectra with very weak intensity, its contribution to the Raman intensity of the ν_1 band is significant and can be quantitated in the time-dependent formalism for absorption and Raman intensities. An unobserved mode with a dissociative excited state potential surface can be accounted for in combination with other excited state parameters. [14] Even though a potential surface may be directly dissociative along some coordinate, that mode will not necessarily show up with much intensity in the RR spectrum if there are also other coordinates that have large geometric changes (although bound) and high frequencies. Qualitatively, the reasonably large displacement in the high-frequency NO_2 stretch could be quite effective (along with a large dephasing rate, here seen as a large Γ) in damping out the Raman intensity in a dissociative but slowly evolving Cl-N stretch. The main effect in the calculation of adding a dissociative mode is the damping of Raman and absorption time-dependent overlaps ($\langle i|i(t)\rangle$ and $\langle f|i(t)\rangle$), broadening of the REP and the absorption spectrum and reduction of the Raman cross sections in the harmonic modes. [13,14] The large value of the slope used in this calculation along with the inhomogeneous linewidth constrained the value for the homogeneous line width, even though a high value of Γ was still necessary to reduce the ν_1

cross sections and fit well with the experimental results. However, the inhomogeneous broadening does not reduce the overall Raman cross section but only broadens the electronic spectra.

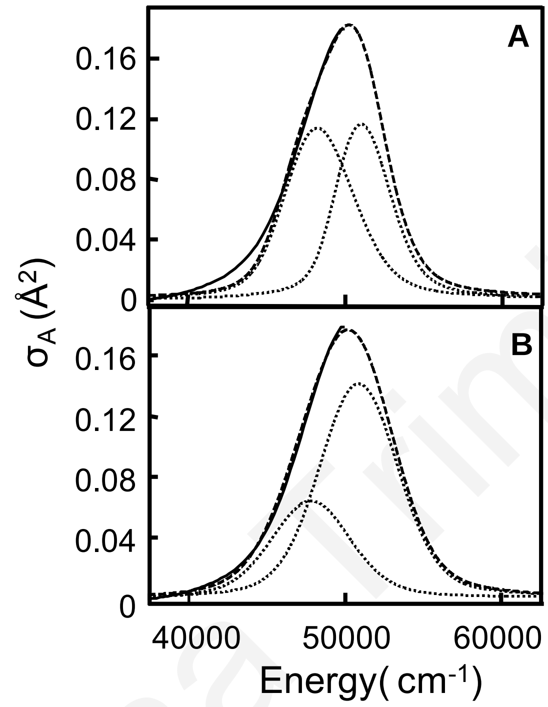

Figure 5.4 Experimental (solid) and calculated (dashed lines) electronic absorption spectra for $ClNO_2$ in methanol using a two-state model (A) and a two-state-model dissociative along the Cl-N coordinate (B). The parameters employed in the calculation for (B) are presented in Table 5.5.

The parameters used for the excited state modeling are consistent with the N-O symmetric stretch and the N-Cl symmetric stretch coordinates dominating the excited-state structural evolution that occurs upon photoexcitation. Correspondingly, the unassignable intensity of the O-N-O symmetric bend is indicative of limited excited-state structural evolution along this coordinate.

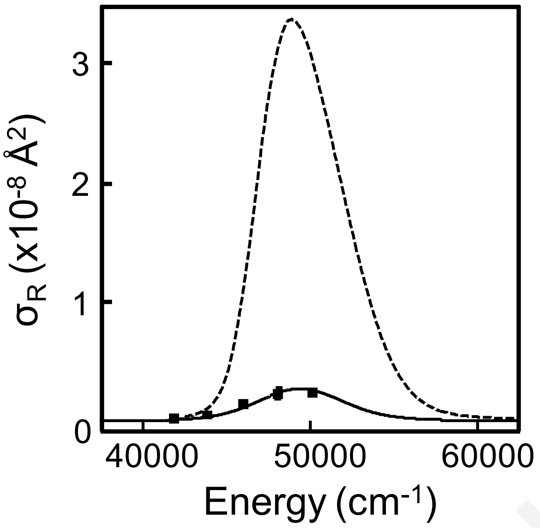

Figure 5.5 Raman excitation profile for the N-O stretch. Points represent the experimental data, while the dashed and solid lines represent the calculation of the REP using two harmonic electronic excited states (dashed line) and two harmonic electronic excited states which are dissociative along the Cl-N coordinate (solid lines).

Table 5.5. Excited state potential energy surface parameters for $ClNO_2$ in methanol[a]

Transition	ω_g (cm^{-1})[b]	ω_e (cm^{-1})[b]	Δ[c]	β (cm^{-1})[d]
		State 1		
v_1	1291	570	2.5	2900
v_2	792	792	0.0	
v_3	369	369	0.0	
v_4	1648	1648	0.0	
v_5	408	408	0.0	
v_6	652	652	0.0	
		State 2		
v_1	1291	570	3.0	2900
v_2	792	792	0.0	
v_3	369	369	0.0	
v_4	1648	1648	0.0	
v_5	408	408	0.0	
v_6	652	652	0.0	

[a] Calculation performed with a Lorentzian line width. Best fit to the experimental values of cross sections yielded for *state 1* $\Gamma_1 = 750$ cm^{-1}, $M_1 = 0.36$ Å^2, $E_{00} = 47000$ cm^{-1} and for *state 2*, $\Gamma_2 = 700$ cm^{-1}, $M_2 = 0.52$ Å^2, $E_{00} = 49700$ cm^{-1}. The standard deviation of inhomogeneous linewidth was $\Theta = 450$cm^{-1} for both states. The refractive index for both states was 1.328.

[b] ω_g and ω_e are the ground- and excited-state harmonic frequencies, respectively.

[c] Δ is the dimensionless displacement of the excited state potential energy surface minimum relative to the ground state along a specific coordinate.

[d] β is the slope of the dissociative excited state potential

5. 3 Discussion

The present study is an initial investigation of nitryl chloride in solution. The results presented here demonstrate that the solvent environment affects both state energetics and molecular structure. The changes in the electronic excited states of nitryl chloride in solution are reflected in the shifted and broadened absorption spectrum while the significant up-shifting of the vibrational frequency of the N-O symmetric stretch in the RR spectrum indicates the dependence of its ground state structure on solvent polarity. We will now discuss the main key points derived from this study; the $ClNO_2$ absorption spectrum in methanol, the effect of the solvent in the molecule's structure, the nature of the absorption D band, the RR scattering in the short limit and the reasons that lead to the consideration of large values of homogeneous broadening.

5.3.1 $ClNO_2$ Absorption spectrum

Theoretical calculation of the low lying excited states of gaseous $ClNO_2$ with the use of multi-reference configuration interaction (MRD-CI) methods was performed by Lesar *et al.*[15] Their study demonstrated that the dominant transition corresponds to the D band in the absorption spectrum which is attributed to the $X^1A_1 \rightarrow 3^1A_1$ transition with a σ(Cl-N) bonding to σ^*(Cl-N) anti-bonding character (7.04 eV, 176 nm, f = 0.6). A second transition with somewhat weaker oscillator strength (f = 0.3), $X^1A_1 \rightarrow 3^1B_2$, with $\pi^*(O_2)$ to $\pi^*(NO_2)$ anti-bonding character (7.25 eV, 171 nm) is closely nearby. The prediction that more than one electronic excited state contributes to the strongest absorption band strengthens our conclusion that the D band involves transitions to two excited states based on depolarization ratios. The increase in the breadth of the D band in solution can be attributed to weakening of the N-Cl bond upon accessing a state with anti-bonding character. The C band at 215 nm is assigned to the $X^1A_1 \rightarrow 2^1A_1$ transition and is described as a charge transfer from *n*(Cl) to $\pi^*(NO_2)$ (5.77 eV).[15] The charge-transfer character of this transition justifies the large red shift (54 nm) of the C band in solution. The structured B band (220-280 nm) was not specifically described in the work by Lesar et al, however, Furlan *et al* suggested that the absorption at 248 nm is due to a partial charge transfer excitation involving the promotion of a non-bonding electron of Cl into a $\pi^*(NO_2)$ orbital.[1] Such a transition is, however, assigned to the C band as described above. A transition with a small oscillator strength around 5 eV (245 nm) can be seen in the calculations, which can either be described as a σ(Cl-N) to a π^*(NO_2) transition (f = 0.0001) ($X^1A_1 \rightarrow 1^1B_1$), or n(Cl) to σ*(Cl-N) (($X^1A_1 \rightarrow 2^1B_1$, f = 0.001). In both cases, a partial charge transfer is observed, which explains the significant red shift observed for this band in solution (310-390 nm). It is interesting to note here that the spacing of the vibronic progression in gaseous nitryl chloride is an average 427 cm^{-1}, while in solution this is calculated as 1036 cm^{-1} along with an anharmonicity constant x_e of 0.017cm^{-1}. Based on analogies to the isovalent $HONO_2$ this progression in the gas phase was attributed to the O-N-O symmetric bend in the excited state. [1] An assignment is difficult to make at this stage in solution, as no Resonance Raman studies have been performed within this very weak band in order to determine the coordinate along which there is such significant structural evolution. However, it could be possible that this high frequency progression observed in solution is due to the N-O symmetric stretch, which would provide a different excited state evolution and a different reaction channel than in the gas phase. On the other hand, if this progression is due to the O-N-O bend as suggested in the gas phase it would obviously suggest a significant change in the excited state geometry in solution with a larger O-N-O angle and/or a shorter N-O bond.

5.3.2 Effect of Solvent on Structure

The solvent environment was shown above to play a key role in $ClNO_2$ state energetics. Considering the RR spectrum in methanol in comparison to the molecule in the gas, solid and liquid phase, we observe a ~24 cm^{-1} up-shift of the N-O symmetric stretch frequency, suggesting a solvent-induced structural change in the ground state. This N-O bond strengthening reflects an increase in the ground state potential curvature and a shift of the equilibrium position along the N-O coordinate. A similar vibrational shift is not observed in the neat $ClNO_2$ liquid,[11] which can be attributed to the different intermolecular interactions operant between two weakly dipolar solute molecules (0.44 – 0.52 D), which must be mainly of the form of induced dipole – induced dipole (van der Waals), versus the interactions of the solute with a protic polar solvent. In the thorough work of Reid and coworkers on ClNO, another dissociative molecule along the Cl-N coordinate, a very strong dependence of the N-O stretch frequency on the polarity of the solvent was clearly demonstrated.[16-18] Particularly, the frequency increased with increased polarity of the solvent. This was attributed to a long Cl-N bond (1.973 Å) that leads to poor overlap between the p orbital of Cl and the 2π anti-bonding orbital of NO and consequently to a partial charge transfer from NO to the more electronegative Cl, comprising thus NO ionic-like with a stronger bond that further decreases in length with increasing polarity of the solvent.

In the case of $ClNO_2$, the Cl-N bond in the gas phase structure is long (1.837 Å) and the N-O bond length is 1.202 Å. However, $ClNO_2$ has a significantly smaller dipole moment (0.44 – 0.52 D) compared to ClNO (2.49 D), as the ground state charge distribution mainly rests on the NO_2 moiety with only about 2.5% positive charge on the Cl.[19] We believe that two types of solute-solvent interactions may occur in the $ClNO_2$/MeOH system; the orientation of positively charged chloride towards the negatively charged oxygen of the methanol hydroxyl group; and the hydrogen bond between the negatively charged nitryl chloride oxygen and the hydrogen of the methanol hydroxyl group. Both interactions may induce lengthening of the N-Cl bond in the excited state. In the next Chapter we will go into more details extracted from a Molecular Dynamics Simulation (MD) study.

Elongation of the N-Cl bond in methanol should be reflected in the RR spectrum, but the small intensity observed for this mode and experimental uncertainties in this region deter unequivocal analysis. However, the red shift observed for the D band in the absorption spectrum can be another indication for elongation of this bond, as transitions in this region involve the σ(Cl-N) and σ*(Cl-N) orbitals.

5.3.3 The Nature of the D band

The results derived from the analysis presented here establish that the D band is composed of more than one electronic transition. The depolarization ratios across the absorption D band are below 1/3, which is the single-state value. The inclusion of transitions to two excited states that are dissociative along the N-Cl coordinate in the expressions of absorption and absolute resonance Raman cross sections reproduce well both the breadth and intensity of both observables. The calculated absorption spectra for these two states demonstrate maxima at 209 and 197 nm. As discussed above, theoretical calculations of isolated $ClNO_2$ [15] predict two closely-spaced excited states in the spectral region of the D band in the gas phase, with vertical transitions calculated at 171 and 176 nm. The 12 nm spacing between the two calculated spectra in our study is relatively close to this 5 nm difference, considering any calculation error. Additionally, a REMPI–TOF photodissociation dynamics study of isovalent nitric acid at 193 nm showed that different reaction channels with different translational energy distributions create OH and NO_2.[20] These studies suggest that more than one electronic state is accessed following D band photoexcitation. More details on the multi-transition composition of the D band can be extracted from the calculation of depolarization dispersion curves. This study is currently underway.

5.3.4 Short time dynamics

The RRIA study performed here indicates that nitryl chloride in methanol scatters at the short time limit. This can be borne out of the combination of the steep potential along the Cl-N symmetric stretch and a large homogeneous linewidth that approximates the frequency of the ν_1 mode[13], which is the only mode with observable intensity in the RR spectra. The effect of the low-frequency Cl-N stretching mode on the observed intensity of the ν_1 band can be understood within the time-dependent formalism of Raman scattering. Fig. 5.6 shows the single-mode Raman overlap, $\langle \mathrm{f} | \mathrm{i(t)} \rangle$, for the fundamental transition of the N-O symmetric stretch (ν_1) (long dashed) and the autocorrelation $\langle i | i(t) \rangle$ overlap for the Cl-N stretch in the linear dissociative potential (short dashed). The single mode Raman time correlator is zero at t=0 and demonstrates recurrences corresponding to the return of the propagating wavepacket to the Frank Condon region along the N-O symmetric stretch after 30 fs. The time correlator reaches its first maximum by 8 fs, while the autocorrelation overlap for the dissociative surface undergoes a rapid and irreversible decay by 10 fs. In the limit that all vibrational coordinates are considered separable, which is the assumption in this study, the multimode Raman correlation function for ν_1 is computed by taking the product of $\langle f | i(t) \rangle$ corresponding to this mode and the $\langle i | i(t) \rangle$ overlaps for the O-N-O symmetric bend, Cl-N symmetric stretch, N-O asymmetric stretch, NO_2 rock and NO_2 out-of-plane bend, respectively. This product is also depicted in Fig.5.6 (dot dashed). As the potentials for all the modes except ν_3 are modeled as harmonic, the only autocorrelator with a significant effect on the ν_1 Raman correlator amplitude is this rapidly decaying Cl-N overlap, which truncates $\langle f | i(t) \rangle$ before enough time is allowed for overlap to develop along the N-O coordinate, and consequently results in reducing the corresponding RR cross section and broadening the REP.

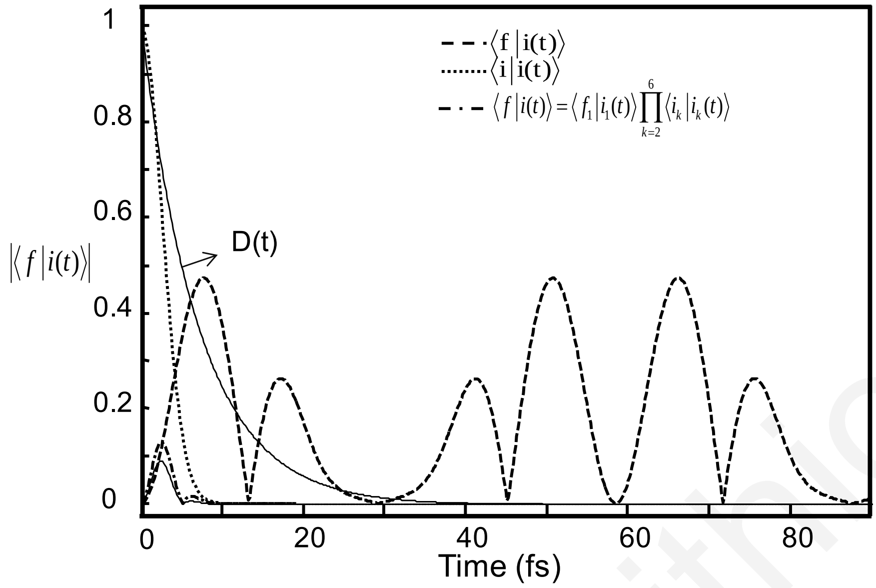

Figure 5.6 Absolute values of the calculated time-dependent single mode Raman overlap $\langle f|i(t)\rangle$ corresponding to the N-O symmetric stretch (dashed) and autocorrelation overlap $\langle i|i(t)\rangle$ for the N-Cl symmetric stretch (dotted). The product of $\langle f|i(t)\rangle$ with the single mode $\langle i|i(t)\rangle$ overlaps corresponding to the O-N-O symmetric bend, Cl-N symmetric stretch, N-O asymmetric stretch, N-O rock and out-of-plane bend, respectively, is shown as a dot dashed line, and the multimode Raman correlator for the first state multiplied by the damping function $D(t)=e^{-\Gamma_1 t}$ (Γ_1=750 cm^{-1}) as a solid line. The latter function for both excited states included in the modeling is indicated in the plot.

However, even with the inclusion of a steep dissociative potential in the calculation, $\sigma_R(v_1)$ is still too high. Thus the calculation of the RR cross section requires the inclusion of a rapidly decaying function, $e^{-\Gamma t/\hbar}$, in order for $\sigma_R(v_1)$ to fit the experimental values. The effect of a large homogeneous linewidth is also shown in Fig.5.6 (solid line). The large value of Γ does not affect the propagation time but results in further reducing the amplitude of the multimode $\langle f|i(t)\rangle$ and ensures the permanence of its decay. Therefore, we can conclude that only the early time buildup of the Raman time correlator is important in determining Raman intensity.

5.3.5 Homogeneous Broadening

The next question that arises here is what the origin of the large homogeneous linewidth is (~700 cm^{-1}). Theoretically, the homogeneous linewidth is composed of two parts: the lifetime of the excited state and the solvent-induced pure dephasing (Eq.5.2):

$$\Gamma = \frac{1}{T_2} = \frac{1}{2T_1} + \frac{1}{T_2^*} \tag{5.2}$$

In the above equation, T_2 is the total dephasing time, T_1 is the excited state lifetime and T_2^* is the time scale for pure dephasing. For a better understanding and a fuller investigation of the contributions of T_1 and T_2^* to the value of Γ, time-resolved experiments and fluorescence cross-section measurements are required.[21,22] These experiments can accurately establish the excited state lifetime T_1 due to population decay, and can disentangle the contribution of lifetime and pure dephasing to Γ. These experiments are under consideration. Notwithstanding, a likely source for the large Γ is the large polarity of the solvent. This is consistent with the RRIA study on ClNO dissolved in cyclohexane and acetonitrile,[23] which has shown that the value of Γ was solvent-dependent, and particularly increased as the solvent changed from non-polar (cyclohexane (200 cm^{-1})) to polar (acetonitrile (1200 cm^{-1})). A later time-resolved IR absorption study in the same system demonstrated that the vibrational bandwidth increased with the solvent polarity.[17] Based on these observations, the authors concluded that the excited state energetics modified by the solvent can affect the coupling with other states and thus non-adiabatic relaxation dynamics, as well as excited state vibrational relaxation. Red shifts in the absorption bands of $\mathrm{ClNO_2}$ in methanol were observed here as well with respect to the gas phase, while hydrogen bonding has been documented to influence vibrational relaxation rates.[24] More insights on the effect of solvent and solvation dynamics can be garnered from theoretical calculations, which will be shown in the next chapter.

References

(1) Furlan, A.; Haeberli, M. A.; Huber, J. R. *Journal of Phyisical Chemistry A* **2000**, *104*, 10392.

(2) Nelson, H. H.; Johnston, H. S. *Journal of Physical Chemistry* **1981**, *85*, 3891.

(3) Carter, R. T.; Hallou, A.; Huber, J. R. *Chemical Physics Letters* **1999**, *310*, 166.

(4) Plenge, J.; Flesch, R.; Schurmann, M. C.; Ruhl, E. *Journal of Physical Chemistry* **2001**, *105*, 4844.

(5) Eiserich, J. P.; Cross, C. E.; Jones, A. D.; Halliwell, B.; vanderVliet, A. *Journal of Biological Chemistry* **1996**, *271*, 19199.

(6) Collis, M. J.; Gintz, F. P.; Goddard, D. R.; Hebdon, E. A.; Minkoff, G. J. *Journal of the Chemical Society (Resumed)* **1958**, 438.

(7) Ghosh, B.; Papanastasiou, D. K.; Talukdar, R. K.; Roberts, J. M.; Burkholder, J. B. *Journal of Physical Chemistry A* **2011**, *116*, 5796.

(8) Dudik, J. M.; Johnson, C. R.; Asher, S. A. *Journal of Chemical Physics* **1985**, *82*, 1732.

(9) Dracinsky, M.; Benda, L.; Bour, P. *Chemical Physics Letters* **2011**, *512*, 54.

(10) Duan, Y. B.; Yuan, S. P.; Wang, R. B.; Mukhopadhyay, I. *Chemical Physics* **2006**, *330*, 9.

(11) Durig, J. R.; Kim, Y. H.; Guirgis, G. A.; McDonald, J. K. *Spectrochimica Acta A* **1994**, *50*, 463.

(12) Christe, K. O.; Schack, C. J.; Wilson, R. D. *Inorganic Chemistry* **1974**, *13*, 2811.

(13) Myers, A. B.; Mathies, R. A. In *Biological Applications of Raman Spectroscopy*; Spiro, T. G., Ed.; John WIley &Sons, Inc.: New York, 1987; Vol. 2, p 1.

(14) Myers, A. B.; Harris, R. A.; Mathies, R. A. *Journal of Chemical Physics* **1983**, *79*, 603.

(15) Lesar, A.; Hdoscek, M.; Muhlhauser, M.; Peyerimhoff, S. D. *Chemical Physics Letters* **2004**, *383*, 84.

(16) Barham, B. P.; Reid, P. J. *Chemical Physics Letters* **2002**, *361*, 49.

(17) Bixby, T. J.; Patterson, J. D.; Reid, P. J. *Journal of Physical Chemistry A* **2009**, *113*, 3886.

(18) Patterson, J. D.; Reid, P. J. *The Journal of Physical Chemistry B* **2012**, *116*, 10437.

(19) Non shown data from theoretical calculations in collaboration with C. Jouvet.

(20) Li, Q.; Robert Huber, J. *Chemical Physics Letters* **2001**, *345*, 415.

(21) Foster, C. E.; Barham, B. P.; Reid, P. J. *Journal of Chemical Physics* **2001**, *114*, 8492.

(22) Hayes, S. C.; Cooksey, C. C.; Wallace, P. M.; Reid, P. J. *Journal of Physical Chemistry A* **2001**, *105*, 9819.

(23) Nyholm, B. P.; Reid, P. J. *Journal of Physical Chemistry B* **2004**, *108*, 8716.

(24) Stratt, R. M.; Maroncelli, M. *Journal of Physical Chemistry* **1996**, *100*, 12981.

CHAPTER 6

ANALYSIS OF DEPOLARIZATION RATIOS OF $ClNO_2$ DISSOLVED IN METHANOL

6.1 Introduction

In Chapter 5 it was clearly demonstrated that the solvent environment plays a key role in $ClNO_2$ state energetics and excited structural evolution along fundamental coordinates. Moreover, it was suggested that two excited states participate in the D band transition.

In an attempt to produce a physically acceptable description of the excited states contributing to the electronic absorption spectrum in the D band region and to provide insights on solute-solvent interactions operating in this molecular system we performed the study we describe in this Chapter. To explore these issues we analyze $ClNO_2$ RR Depolarization Ratios Dispersion curves (DPR’s) in combination with theoretical calculations such as ab initio and linear response studies and Molecular Dynamics (MD) Simulations.

The depolarization ratios (DPR’s) measured at excitation energies on resonance with an electronic absorption can be used to model the theoretical depolarization ratio dispersion curve simultaneously with the REP and absorption cross sections.[1-8] Jerneshoj *et al.* have shown that by using several different combinations of excited state parameters one can obtain a good fit of the REP, but only one set of these parameters can simultaneously describe the depolarization ratios.[3] The sensitivity of Raman excitation profiles, when two electronic excited states contribute to the scattering, to various physical quantities such as the energy separation of the two states, the homogeneous linewidth (Γ), the displacements of the PES minima and the transition dipole moments of states have been examined in detail by Shin et *al*.[9] The general trend derived from these calculations is that the electronic excited state with the largest transition dipole moment dominates the Raman excitation profile. It was also shown that the shape of the REP is very sensitive to the displacements and Γ. Furthermore, the effect of homogenous and inhomogeneous broadening (Θ) on the REP, absorption spectrum and DPR has been demonstrated effectively through a number of separate calculations.[10] RRIA on other halooxides in solution such as chlorine dioxide[1] revealed that including depolarization ratios in the modeling is necessary for the determination of the phase-dependent reactivity in the solvent environment.

The theoretical methods implemented here complement the experimental work and give primary evidence on the mechanistic details that govern the phase dependent reactivity of $ClNO_2$.

The experimental methods and the theoretical details for the RRIA are described in Chapter 3. In Chapter 2 there is an extensive theoretical approach for the DPR's. In the next subchapter we deal with the theoretical background for the computational methods.

6.2 Ab initio, molecular dynamics and linear response calculations

The electronic structure calculations were performed with the Quantum Espresso program,[11] utilizing a converged plane wave basis and a pseudopotential representation of core electrons. In particular, the norm-conserving pseudopotential generated within the Perdew-Burke-Ernzerhof (PBE)[12,13] generalized gradient approximation (GGA) was used. The valence electrons were described using the hybrid PBE0 functional. The size of the plane wave basis was chosen to satisfy the 40 Ry energy cutoff. All calculations were performed at a single k-point (gamma-point).

To analyze the nature of the electronic excited states and the effect of the environment on it, we computed the projected density of states (pDOS) of the $ClNO_2$ molecule in the gas-phase (isolated) and in solution (solvated by methanol). For the isolated molecule the geometry of $ClNO_2$ was optimized with the computational setup described above. The simulation cell was chosen to be cubic with the cell parameter 15 Å that provides sufficient vacuum region to minimize interaction of the system with its periodic replica. For the solvated molecule the geometry was taken randomly from the MD trajectories. In this case the simulation cell contained additional 59 methanol molecules and the cell parameters varied. A snapshot of the system with the solvent at a random MD step is shown in Figure 6.1

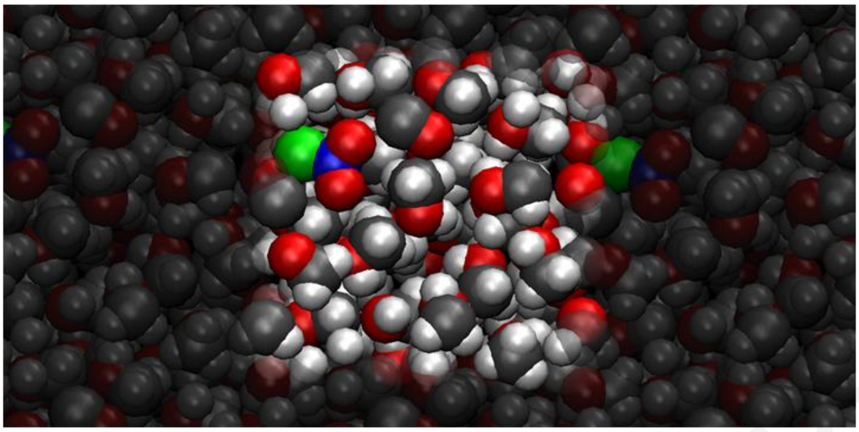

Figure 6.1. A snapshot of the $ClNO_2$/MeOH system along an MD trajectory.

To compute the pure dephasing times in a solvated $ClNO_2$ molecule we employed the linear response formalism[14-16] previously used by Reid and Prezhdo.[17] Namely, the classical molecular dynamics simulations for the system of interest were performed, giving the energy of the ground state as a function of time $E_0(t)$. The energy of the excited state $E_1(t)$ was then computed for each MD trajectory point by modifying the partial charges of the atoms – the effect associated with the electron density redistribution upon photoexcitation. By such a construction we focus only on the electrostatic origins of the dephasing. In principle, one can also include effects of the changed covalent bonding and dispersion, but the electrostatic contribution is expected to be dominant due to its long-range nature.

The quantities $E_0(t)$ and $E_1(t)$ are used to compute the dephasing function, defined as:

$$D_{01}(t) \equiv \exp\left(-\Gamma_{01}^2 t^2\right) = \int_0^t dt' \int_0^{t'} dt'' C_{01}(t''), \qquad (6.1)$$

where

$$C_{01}(t) = \left\langle \delta E_{01}(t') \delta E_{01}(t-t') \right\rangle_{t'}, \qquad (6.2)$$

is the autocorrelation function of the fluctuation $\delta E_{01}(t)$ of the energy difference $\Delta E_{01}(t)$ between the ground and excited states:

$$\delta E_{01}(t) = \Delta E_{01}(t) - \left\langle \Delta E_{01}(t) \right\rangle. \qquad (6.3)$$

The energy difference is defined by:

$$E_{01}(t) = E_0(t) - E_1(t). \tag{6.4}$$

One can note that the (practically) constant energy difference between the ground and excited state energy levels that arises from electronic structure calculations (band gap) does not affect the dephasing time calculations. Therefore, in our calculations it is enough to compute only the classical electrostatic contributions to the energy levels. The homogeneous fluorescence linewidth, Γ_{01}, computed from Eq. (6.1), is related to the pure dephasing (decoherence) time τ_{01}:

$$\Gamma_{ij} = \frac{\hbar}{\tau_{ij}} \tag{6.5}$$

In addition to the pure dephasing rate calculations, the half-Fourier transform of the autocorrelation function, Eq. (6.2), represents the influence spectrum. The latter contains the information about the ro-vibrational modes driving the electronic dephasing and relaxation processes (fluorescence in particular).

The molecular dynamics simulations of the solvated $ClNO_2$ molecule are performed in the NPT ensemble under external pressure of p = 1 atm. and temperature of T = 278 K. The temperature is controlled by the Nose-Hoover thermostat,[18-22] and the pressure is controlled by the Parrinello-Rahman barostat.[21-23] The atomic positions are propagated by the velocity Verlet integration scheme.[24] The equations of motion are solved for 1 ns with the time step of 1 fs and the energies $E_0(t)$ and $E_1(t)$ printed every 100 fs.

The bonded and dispersion interactions in the simulated system are described using the Universal Force Field (UFF).[25] The non-bonded van der Waals (vdW) interactions are smoothly switched off in the radius between 10 and 12 Angstrom. To describe the electrostatic interactions we employed Ewald summation method[26,27] that is crucial in achieving good accuracy and high performance in computing the long-range interactions. The partial charges on atoms of the solvent and solute molecules are obtained from Mulliken [28] population analysis of the gas-phase electronic structure calculations of these species (Fig. 6.2). The calculations are performed at the CCSD/aug-cc-pvdz level of theory as implemented in the Gaussian program package.[29]

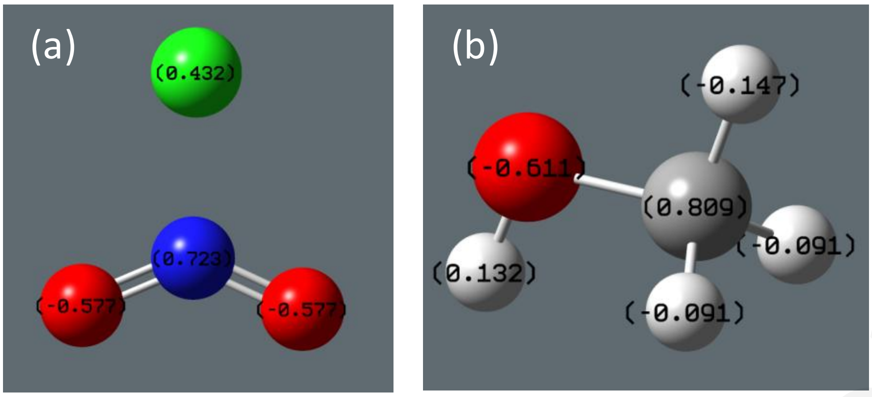

Figure 6.2. Mulliken atomic charges computed at CCSD/aug-cc-pvdz level of theory for (a) $ClNO_2$ and (b) MeOH.

Since the Mulliken charges are not intended to accurately reproduce the electrostatic potential, we rescaled them by different scaling parameters. The latter were found by comparing the experimental density and the evaporation enthalpy for liquid methanol with those obtained from the MD simulations using a particular scaling factor for the partial charges. We found that reasonable agreement is found for the scaling factors in the range 1.6 – 1.75, in agreement with typical scaling found for other systems.[30] Such a parameter can also be thought of as a measure of the solvent polarity, so in our calculations we used the limiting values (1.6 and 1.75) to elucidate the role of the solvent polarity on the dephasing rates.

To model the electrostatic potential in the excited state of $ClNO_2$, the negative charge -0.625e was removed from the Cl atom and evenly redistributed among the atoms of NO_2 fragment. Keeping in mind the scaling factors for partial charges, this corresponds to a photoexcitation of a single electron from one of the occupied orbitals to the empty levels. Similarly to the scaling factors for the partial charges, we varied the amount of charge being redistributed across the orbitals, to understand the role of this factor in linewidth broadening.

6.3 Results and Discussion

6.3.1 Experimental results

The polarization-dependent RR spectra of nitryl chloride dissolved in methanol were obtained at 199.75, 208.8, 217.9, 228.8 and 239.5 nm. Figure 6.3A and 6.3B demonstrate the parallel and perpendicular spectra at 217.9 nm, respectively. The spectra are dominated by intensity corresponding to methanol vibrational modes. The band observed at 1291 cm^{-1} was assigned to the N-O symmetric stretch (v_1) after comparison to the solvent spectrum and the mode frequencies observed in the gas and liquid phase for this molecule.[31-33]

Figure 6.4 presents a portion of the electronic absorption spectrum of $ClNO_2$ in methanol where the D band is observed at 200 nm. The points represent the Raman depolarization ratios for v_1 corresponding to excitation wavelengths resonant within the D band (see Table 6.1). The absorption spectrum of $ClNO_2$ in methanol has been discussed in detail in Chapter 5.[31] The dominant transitions corresponding to the D band in the absorption spectrum, according to Lesar and coworkers were attributed to the $X^1A_1 \rightarrow 3^1A_1$ transition at 176 nm and $X^1A_1 \rightarrow 3^1B_2$ at 171 nm.[34] In contrast to the work of Lesar *et al*, our symmetry considerations (the z axis oriented along the C_2 axis of molecule and the x axis perpendicular to the plane of the molecule) define A_1 and B_1 as the symmetries of the two optically-accessible excited states.

Figure 6.4 shows that the DPR's are significantly below 1/3 and as we move towards the lower energy edge of the D band, ρ approaches 1/3. This suggests that transitions to more than one excited states contribute to the D band, with more than one non-zero matrix elements in the polarizabilty tensor.[35] Rotation of the molecule during the Raman scattering process is another possible explanation for the deviation of ρ from the single excited state value. However, the effect of rotation in a transition is to elevate the depolarization ratio.[1,36] Generally, rotational motion affects the depolarization ratios when $\exp\left[-2\Gamma t\right]\left|\langle f \,|\, i(t)\rangle\right|^2$ is significantly different from zero and depending on the system, either of the two factors (homogeneous broadening or FC overlap) could dominate.[36] In the case of $ClNO_2$, a dissociative molecule that places the scattering in the short time limit, we do not consider slow rotational dynamics in solution, especially in a polar solvent such as methanol.

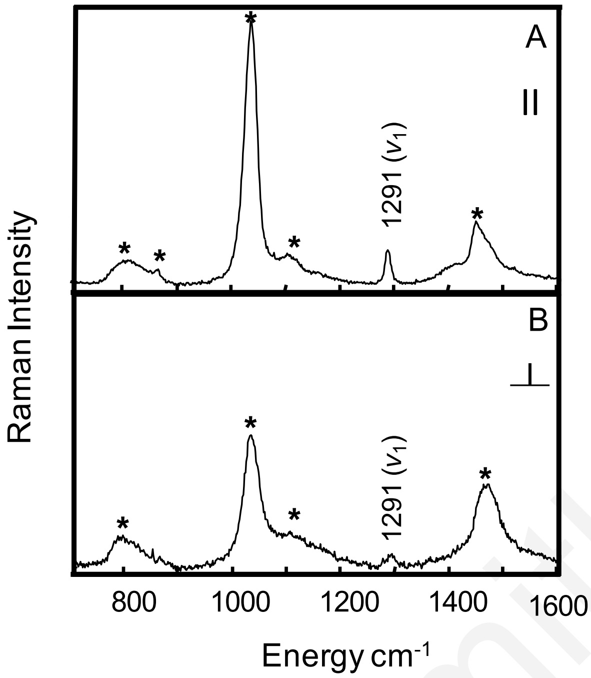

Figure 6.3. RR spectrum of $ClNO_2$ dissolved in methanol at 217.9 nm with the polarization parallel (A) and perpendicular (B) to that of the incident light. The fundamental transition at 1291 cm^{-1} corresponds to the NO symmetric stretch. The asterisks denote methanol bands [37] and quartz scattering (451 cm^{-1}, 494 cm^{-1}, 610 cm^{-1}, 800 cm^{-1} and 865 cm^{-1}).[38,39]

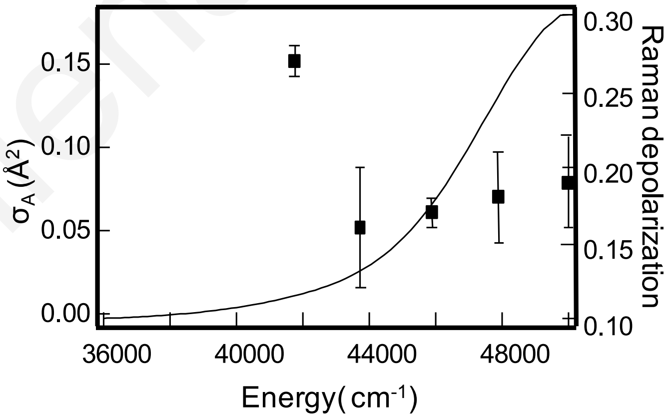

Figure 6.4. Absorption spectrum of nitryl chloride in methanol (solid line) and the Raman depolarization ratios for the NO symmetric stretch fundamental transition (points) determined at excitation wavelengths spanning the D band. The values of the experimental depolarization ratios for the N-O symmetric stretch were calculated in Chapter 5 and reproduced here in Table 6.1

Table 6.1. Depolarization ratios of the N-O symmetric stretch fundamental transition of nitryl chloride dissolved in methanol. [31]

λ (nm)	$\rho_{\nu 1}$
199.76	0.19 ± 0.03
208.8	0.18 ± 0.03
217.85	0.17 ± 0.01
228.7	0.16 ± 0.04
239.5	0.27 ± 0.01

The analysis described below demonstrates the sensitivity of the depolarization ratio dispersion curves to various parameters of each excited state and reveals which excited state transition is more prominent.

6.3.2 Modeling of the D band and broadening effects

In solution, the interaction between molecule and solvent causes stochastic fluctuations to the molecular states. These fluctuations are responsible for decoherence of the resonant emission by the generation of a new population that radiates with a rate defined as the dephasing rate and given by $\Gamma = 1/T_2$, where T_2 is the total dephasing time.[10,40,41] This process occurs when the molecule is excited to a bound excited state. Thus, the magnitude of the RR cross section is constrained by the vibrational dephasing time. There is a direct dependence of the REP on Γ (see Eq.3.3): as Γ decreases the Raman cross sections increases. However, if the excitation occurs to a dissociative excited state, the molecule is not trapped any more in the Frank Condon (FC) region where the overlap with the ground state is non-zero, which results in a shorter time limit for the wavepacket propagation in the FC region. If the excited state potential energy surface is steep enough, the constraining parameter for the intensity of the REP is no longer the dephasing time ($1/\Gamma$) , but rather it is the slope of the linear excited state that becomes a major limiting factor.[10] The loss of overlap caused by a dissociative normal mode in the excited state resembles the reduction caused by the homogeneous linewidth.[42] However, as the homogeneous broadening imposed on the absorption cross section consists of both effects (slope and Γ), the differentiation of the two damping factors in the absorption spectrum is difficult, as the integrated absorption is unaffected by any of them. The polarizability tensor and, consequently, the depolarization ratio, are also unaffected, in contrast to the RR cross section. Therefore, in RRIA, the value of the slope must be constrained in order to reach realistic values of Γ that reproduce the REP.

Usually, in a solvent environment, homogeneous broadening does not account for all the broadening observed in the REP and absorption cross section, and inhomogeneous broadening (Θ) must also be considered. However, the average Resonance Raman intensities and the depolarization dispersion curve (DPR) are relatively unaffected because the inhomogeneous broadening acts at the level of the cross section and not the polarizability. Therefore, the different dependence of the absorption and Raman cross sections and DPR's on the homogeneous linewidth (Equations 10 and 12) helps to distinguish the role of homogeneous and inhomogeneous broadening, thus providing a more accurate measure of the excited state lifetime and better understanding of the factors affecting the excited state dynamics.

The above discussion calls for a systematic approach for the separation of the broadening mechanisms to obtain a physically appropriate description of the contributing excited states and the experimental observables. There are various ways to disentangle the different contributions to the homogeneous linewidth. Time-resolved fluorescence and stimulated emission measurements can provide a measure for the excited state lifetime, from the intensity decay curves fit to an exponential. In addition, theoretical calculations of electronic excited state potential energy surfaces can offer insights on the slope along the dissociative coordinates. In the case of $ClNO_2$, time-resolved measurements have not yet been performed, so we used Lesar and coworkers' calculated surfaces for the gaseous molecule to constrain the slope of the dissociative surface along the Cl-N coordinate. The 3^1A_1 (2^1A_1 here) potential energy surface along the Cl-N coordinate in the Frank Condon region was reproduced and depicted in Figure 6.5 using dimensionless coordinates. The Cartesian coordinates were converted to dimensionless displacements via Equation 16, for a direct comparison to the results of RRIA.[43]

$$q = \left(\frac{\mu\,\omega}{\hbar} \right)^{1/2} (x - x_0) \qquad (6.6)$$

Here, q is the dimensionless displacement, μ is the reduced mass, ω is the frequency of the corresponding mode in cm^{-1}, and x_0 and $(x- x_0)$ are the minimum of the ground state potential energy surface and the displacement of the potential energy surface minimum of the excited state relative to the ground state in Å, respectively. The calculated slope β was found equal to 2980 cm^{-1}, very close to the slope reported in a previous chapter and provides thus an upper limit for the excited state slope we must consider. This is exemplified in the RRIA study of ClNO in solution (another dissociative molecule) by Nyholm *et al.* where it was shown that excited state structural evolution following excitation is dominated by evolution along the dissociative N-Cl stretch, with a solvent-dependent slope.[2] This slope was shown to decrease with the polarity of the solvent as a result of the weakening of the N-Cl bond length, with a corresponding shift of the ground state potential energy surface along this coordinate.

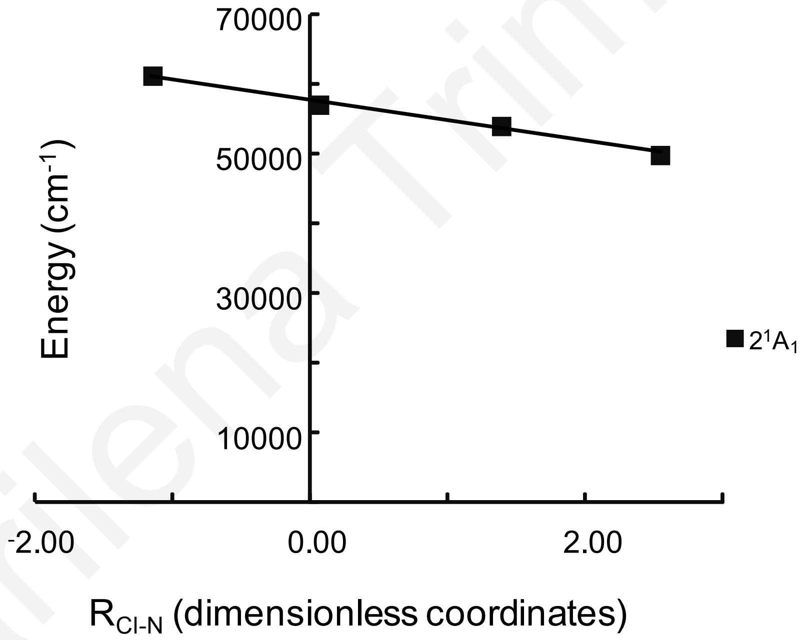

Figure 6.5. Potential energy surface of the 2^1A_1 excited state along the Cl-N bond.[34] The energy curve is linearly dissociative with slope β = 2980 cm^{-1} in the Frank Condon region. The displacement is given in dimensionless coordinates.

As a consequence of the broad absorption spectrum of $ClNO_2$, there are several parameter sets (Γ, Θ, Δ, M and excited state frequency for the NO symmetric stretch, ω_e) that can give an almost equally good fit to the absorption spectrum and the REP. The following sections examine the key parameters that provide the most physically realistic model for the D band, enabled by additionally considering depolarization dispersion curves.

6.3.2.1 Modeling of D band by considering all broadening as homogeneous

In the first case, we applied a simplification of the source of broadening, where we treated the broadening as *phenomenological* [9] or *effective* [44] due to the diffuse line shape of the absorption spectrum in methanol. There are a few cases in the literature for molecules in solution where this assumption was made,[2,9,44,45] including the study of ClNO in solution, where, as in $ClNO_2$, two electronic excited states contributed to the Raman scattering.[2] In the latter case, inhomogeneous broadening was not included to avoid the assumption of correlation of the two states, which resulted in the use of large values of homogeneous broadening. However, in that case the model used to simulate the absorption spectrum and excitation profile was able to reproduce the depolarization ratios for the Raman fundamental modes. In the effective homogeneous broadening used here, both inhomogeneous broadening and the contribution of normal modes with low frequency are included.[9,44] Calculated influence spectra of the $ClNO_2$/methanol system (see below) indicate, indeed, that the low frequency modes of $ClNO_2$ are the main mechanism of energy dissipation via fluorescence.

Best fit to the absorption and REP was accomplished with a moderate dimensionless displacement (Δ_1) for the v_1 coordinate, slightly different for each excited state (2.8 vs. 2.3), while the transition moment lengths for the two excited states were taken to be very close to each other ($M_1 = 0.429$ Å and $M_2 = 0.464$ Å). The inclusion of large values of homogeneous line width (Γ_1, $\Gamma_2 = 1000$ cm^{-1}) was necessary to reproduce the Raman cross sections, along with a reduced frequency of v_1 (650 cm^{-1}) in both excited states. Figures 6.6A and 6.6B demonstrate the simulation of the absorption and REP. The parameters employed in the model are reported in Table 6.2. Figures 6.7A and 6.7B present the real and imaginary parts of the tensor elements that correspond to the two excited states (α_{xx} and α_{zz}), while 6.7C shows the values of the rotational invariants Σ^0 and Σ^2. Both excited states affect the Raman scattering and their contribution to the Raman depolarization curves is similar due to the similar values of the transition dipole moment.[9] The equal amplitudes and the same sign of the real and imaginary parts of the polarizabilty tensors for the two states throughout the 35000 cm^{-1} – 65000 cm^{-1} energy range resulted in a larger contribution of the isotropic part (Σ^0) of the scattering tensor than the symmetric anisotropy (Σ^2), and consequently in a DPR dispersion curve of 1/8 (value for two perpendicular transitions). We find that even though this approach results in a DPR dispersion curve that deviates from 1/3, the dispersion curve is underestimated by this set of parameters (Fig.6.7D).

The results of this initial analysis show that a different approximation must be taken into account in order to simulate not only the absorption and REP but the DPR’s as well. The next section will show that the inclusion of inhomogeneous broadening permits the consideration of more reasonable values of homogeneous linewidth and of new combinations of excited states parameters that cause insignificant differences in the absorption and REP but reproduce well the DPR experimental values.

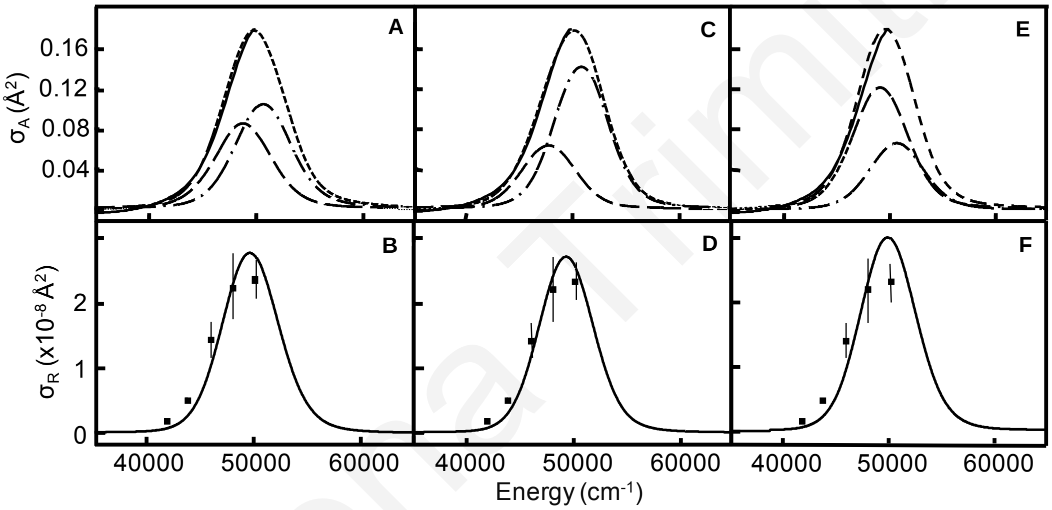

Figure 6.6. Experimental (solid) and calculated (dashed lines) electronic absorption spectra for $ClNO_2$ in methanol where (A) the broadening is considered all homogeneous, (C) both homogenous and inhomogeneous broadening were included with $M_1 < M_2$, and (E) same as (C) but with $M_1 > M_2$. The calculated excited states are also shown (dotted lines). (B), (D) and (F) Corresponding Raman excitation profiles for the N-O stretch for the three cases. Points represent the experimental data, solid line represents the calculation of the REP. The parameters employed in the calculation are presented in Table 6.2.

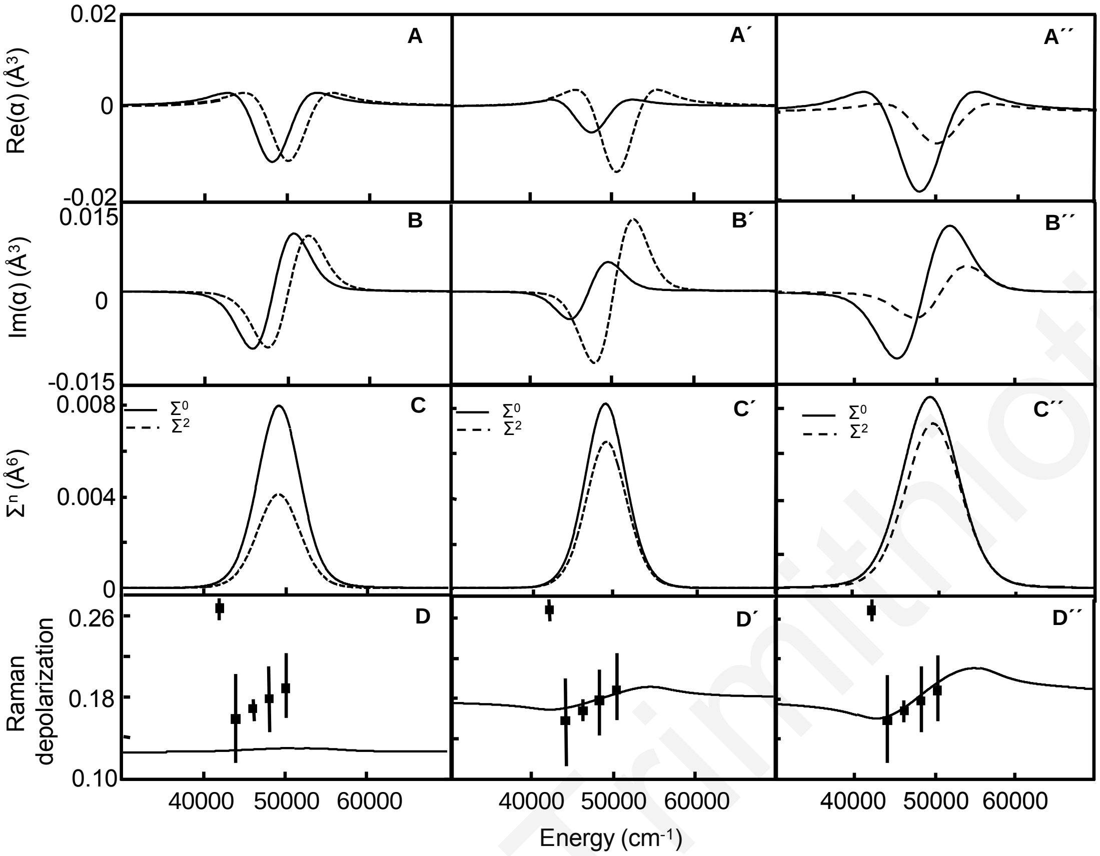

Figure 6.7. Calculation of the Raman depolarization ratio dispersion considering two harmonic electronic excited states that are dissociative along the Cl-N coordinate. Three cases are considered: (A, B, C) The broadening includes only Γ, (A′, B, C′′) includes Γ and Θ with $M_1 < M_2$ and (A′′, B′′, C′′) includes Γ and Θ with $M_1 > M_2$. (A, A′, A′′) Real parts of the polarizabilty tensor elements of state 1 (solid line) and state 2 (dashed line). (B, B′, B′′) Imaginary part of the polarizabilty tensor elements of state 1 (solid line) and state 2 (dashed line). (C, C′, C′′) The rotational invariants used in this calculation (Σ^0: solid line and Σ^2: dashed line. (D, D′, D′′) The Raman depolarization ratio dispersion curve (solid line). The square points represent the experimental depolarization ratios measured previously at excitation wavelengths spanning the absorption band.[31] The parameters employed in this calculation are presented in Table 6.2.

Table 6.2. Excited state potential energy surface parameters for $ClNO_2$ in methanol[a]

Transition	**ω_g (cm^1)^b**	**ω_e (cm^1)^b**	**Δ^c**	***β*** **(cm^1)^d**
		state 1		
v_1	1291	650^{i}	2.8^{i}	
		570^{ii}	2.5^{ii}	
		560^{iii}	3.8^{iii}	
v_2	792	792	0.0	
v_3	369	369	0.0	2900
v_4	1648	1648	0.0	
v_5	408	408	0.0	
v_6	652	652	0.0	
		state 2		
v_1	1291	650^{i}	2.3^{i}	
		570^{ii}	3.0^{ii}	
		560^{iii}	2.8^{iii}	
v_2	792	792	0.0	
v_3	369	369	0.0	2900
v_4	1648	1648	0.0	
v_5	408	408	0.0	
v_6	652	652	0.0	

[a] Calculation performed with a Lorentzian homogeneous linewidth. The refractive index was 1.328.

[b] ω_g and ω_e are the ground- and excited-state harmonic frequencies, respectively.

[c] Δ is the dimensionless displacement of the excited state potential energy surface minimum relative to the ground state along a specific coordinate.

[d] *β* is the slope of the dissociative excited state potential.

[i] excited states parameters employed resulting in Fig. 6A-B & **7**(A-D).

Other parameters for state 1: Γ_1 = 1000 cm^{-1}, M_1 = 0.429 Å, E_{00} = 47400 cm^{-1} and, Γ_2 = 1000 cm^{-1} and for state 2: M_2 = 0.464 Å, E_{00} = 49700 cm^{-1}.

[ii] excited states parameters employed resulting in Fig.6C-D & 7(A'- D').

Other parameters for state 1: Γ_1 = 750cm^{-1}, M_1 = 0.360 Å, E_{00} = 47000 cm^{-1} and for state 2*:* Γ_2 = 700 cm^{-1}, M_2 = 0.520 Å, E_{00} = 49700 cm^{-1}. The standard deviation of inhomogeneous linewidth was Θ = 450 cm^{-1} for both states.

[iii] excited state parameters employed resulting in Fig.6E-F & 7(A''- D'').

Other parameters for state 1: Γ_1 = 800cm^{-1}, M_1 = 0.50 Å, E_{00} = 47300 cm^{-1} and for state 2: Γ_2 = 800 cm^{-1}, M_2 = 0.36 Å^2, E_{00} = 49700 cm^{-1}. Θ = 450 cm^{-1} for both states.

6.3.2.2 Modeling of D band by considering both homogeneous and inhomogeneous broadening

A number of studies in the condensed phase have focused on the fundamental source of broadening in the absorption spectrum and the REP (Γ, vs. Θ or both).[40,44,46-49] In RRIA cases where methanol was the solvent,[50-54] the contribution of inhomogeneous broadening in combination with homogeneous broadening was necessary for the description of the absorption spectrum and absolute RR cross sections. In the RRIA study of benzamide[50] the dramatic increase in the inhomogeneous broadening observed in methanol compared to acetonitrile was attributed to hydrogen bonding between methanol and the molecule. In the case of p-nitroalanine in these two solvents, this increase was suggested to originate from the slower time for solvation in methanol, with the part of the reorganization that is slow on the ground state vibrational time scale appearing as inhomogeneous broadening.[52] In a later study of Moran *et al.,* in which the solvent effects in the ground and excited state of a push-pull chromophore were examined, it was concluded that the model in methanol requires larger values of Θ compared to other solvents due to the involvement of torsional modes in this solvent,[53] which are usually at low frequencies. Fairly large values of Θ were also necessary in the case of charge transfer complexes in methanol.[54]

As it follows from the analysis of the Mulliken charges (Fig. 6.2), the electrostatic interactions between solute and solvent may be quite significant. One can distinguish two main types of such interactions that occur in the $ClNO_2$/MeOH system: a) the orientation of positively charged chloride towards the negatively charged oxygen of the methanol hydroxyl group (e.g. see Figure 6.1); and b) the hydrogen bond between the negatively charged nitryl chloride oxygen and the hydrogen of the methanol hydroxyl group. As we will discuss below such specific interactions can break the symmetry of the electronic wavefunction of the solute and induce notable changes in its electronic structure. Experimentally, this is seen as the additional broadening, arising because of distinct response of different electronic states on the complex changes of the collective coordinate of the solvent (inhomogeneous broadening). Because the effect of the polar solvent on the electronic structure of the solute is quite strong, the inhomogeneous broadening must be taken into account in order to accurately reproduce the experimentally measured spectra with our models.

For all these reasons we believe that it is necessary to adopt a significantly different set of parameters that includes both homogenous and inhomogeneous broadening. The poor fit to the DPR in the previous section may be due to the neglect of the Θ parameter. A value of Θ = 450 cm^{-1}, a reduced amount of Γ (Γ_1=750 cm^{-1} and Γ_2=700 cm^{-1}) and always considering a steep potential along the N-Cl (β = 2900 cm^{-1}) led to an overestimation of the RR cross sections, therefore a further reduction of the N-O symmetric stretch frequency (ν_1=570 cm^{-1} for both states) was required to depress the absolute Raman cross sections. This latter adjustment caused down shifting of the absorption spectrum. However, the DPR curve showed minimal sensitivity to this change. Therefore, the displacements and the transition dipole moments for both states were iteratively varied to obtain a good fit to the absorption bandwidth and the pattern of the RR intensities and DPR's. Best fit was achieved with Δ_1 = 2.5 and M_1 = 0.360 Å for state 1 and Δ_2 = 3.0 and M_2 = 0.520 Å for state 2. In comparison to the initial simulation, larger displacements along the N-O coordinate in the excited state were required, along with larger values of M_1 and M_2 and particularly, a greater transition dipole moment for excited state 2 than state 1. The calculated fits to the absorption spectrum and REP are given in Figures 6.6C and 6.6D and for DPR in Figure 6.7D΄. The parameters employed in the calculation for the second model are presented in Table 6.2.

Figures 6.7A΄-D΄ illustrate the dependence of the depolarization ratio on the amplitude of the polarizability tensor elements and the contribution of each excited state in the DPR for this set of parameters. The DPR curve never reaches the single excited state value 1/3 due to the fact that both states contribute to the scattering but greater values than 1/8 are obtained due to the different amplitudes in the real and imaginary parts of the polarizability. State 2 has a stronger contribution to the depolarization ratio dispersion curve than state 1 in the energy range from 40000 cm^{-1} to 60000 cm^{-1} due to its larger transition moment length ($M_1 < M_2$). The Raman intensity is proportional to the fourth power of M [40] and thus the REP is more strongly affected by the excited state with the larger transition dipole moment (state 2).[9] However, in our case the two excited states are close in energy (ΔE_{00}= 2700 cm^{-1}) and the transition dipole moments are within the same order of magnitude. Thus, although the contribution of excited state 1 is smaller, it cannot be ignored. Consequently, this analysis demonstrated that best fit to the experimental depolarization ratio dispersion curve is not achieved by the variation of the homogeneous and inhomogeneous broadening but these parameters permit the variation of M, Δ andv_1 excited state frequency, which act at the level of the polarizability and affect not only the REP and absorption cross sections, but also the DPR's.

A third possibility to explore is the case where transition to state 1 is stronger than transition to state 2 ($M_1 > M_2$), We examine this by alternating the transition dipole moments which required $\Delta_1 > \Delta_2$ to reproduce the observed overall width of the absorption spectrum and the increasing trend of the DPR with increasing excitation energies. We chose to vary the displacements and not readjusting Θ to reproduce the experimental electronic absorption spectrum, because changes in the displacements affect both the absorption spectrum and DPR in contrast to Θ, which affects only the absorption spectrum. Furthermore, a small reduction of the excited state frequency along the N-O stretch, and a small increase of the homogeneous linewidth was necessary. The excited state parameters were varied iteratively to obtain the best fit to all the observables, which are depicted in Figures 6E, 6F and $7D''$, respectively. The behavior of the real and imaginary parts of the polarizability tensors α_{zz} and α_{xx} are depicted in Fig. $6.7A''$ and $6.7B''$, respectively. As in the previous example, both states contribute to the scattering with the difference that here excited state 1 has a stronger contribution to the depolarization ratio dispersion curve than excited state 2 in the energy range from 40000 cm^{-1} to 60000 cm^{-1} due to its larger transition dipole moment. The imaginary parts of both excited states exhibit a maximum after ~50000 cm^{-1} in contrast to the previous case when only state 2 reaches a maximum after this energy value, leading to overestimation of the Raman cross section at 50600 cm^{-1}. In addition, the shift of the maximum of state 1 after 50000 cm^{-1} is due to the relatively large value of Δ_1 ($\Delta_1 = 3.8$).

The rotational invariants derived from this analysis are shown in Fig. $6.7\ C''$, and reveal that compared to Figures 6.7C and $6.7C'$, Σ^0 and Σ^2 are not centered at the same value of energy, with Σ^2 slightly blue shifted. This is a likely reason that a better fit of the experimental depolarization ratios was obtained.

The set of parameters employed in this case led to a less good fit of the red edge of the electronic absorption spectrum in contrast to the previous set of parameters. This observation for the experimentally well-defined edge of the spectrum puts a limit on the magnitude of the homogeneous broadening. In the first example, the red edge of the spectrum was also well reproduced due to the large value of the homogeneous broadening. In the two latter sets of calculations the standard deviation of the inhomogeneous broadening, Θ, was kept the same and the homogeneous broadening was varied. Consequently, an upper limit for the homogeneous broadening emerged with $\Gamma = 750\ cm^{-1}$ for state 1 and $\Gamma = 700\ cm^{-1}$ for state 2.

6.3.3 Insights from the atomistic modeling

6.3.3.1 Molecular dynamics and linear response calculations (mechanism of the homogeneous broadening)

The homogeneous linewidth used in the modeling of the depolarization and absorption spectra has been considered as an adjustable parameter so far. In order to get an estimate of it from the atomistic point of view and to get further insight into the physical origin of this effect we performed MD simulations and linear response calculations of a $ClNO_2$/MeOH system as described in Section 6.2.

The effect of solvent polarity is accounted for by considering two scaling factors that convert the Mulliken charges of the atoms to charges utilized for the electrostatic potential calculation. As has been noted in Section 6.2 these two values represent the range of scaling factors that are capable of reproducing evaporation enthalpy and the density of methanol. Thus, they are correct in the sense of the order of magnitude, yet, they may not be precise. However, these values serve the main purpose of elucidating the role of polarity, rather than providing an exact answer. For each value of the scaling factor we systematically varied the amount of charge density being redistributed across the solute molecule (from Cl to NO_2 group). This type of variation helps elucidate the role of solute polarizability in determining the fluorescence linewidth broadening. The results of these calculations are presented in Table 6.3.

From Table 6.3 one can observe that the increased polarizability of the solute reduces the pure dephasing time and, equivalently, increases the linewidth for fluorescence. Such dependence predicts that excitations with the largest transition dipole moment lead to a larger broadening. In the case of multiple electronic states involved in the photodynamics, the most important contribution is associated with the transition that has the largest oscillator strength.

Table 6.3. Fluorescence line widths (cm^{-1}) and decoherence times (given in parentheses, fs) for the $ClNO_2$/MeOH system as a function of its polarity and polarization of the solute.

scaling factor (polarity)	1.6	1.75
Charge redistribution (polarizability)	linewidth, cm^{-1} (dephasing time, fs)	linewidth, cm^{-1} (dephasing time, fs)
0.625	843 (6.3)	792 (6.7)
1.0	1292 (4.1)	1223 (4.3)
1.6	1940 (2.7)	1811 (2.9)

For gas-phase $ClNO_2$ such a transition is σ→σ*(Cl-N). Thus, the factors affecting this transition will have the most significant impact on the experimentally measured spectra. In the next section we shall discuss how this transition is affected by a solvent and what this implies.

The other factor affecting the homogeneous broadening is the polarity. In contrast to the polarizability it has an opposite effect - it slows down the dephasing in more polar solvents. This observation has a clear physical interpretation. In general, as the solvent polarity increases, its reorganization requires more energy. Therefore, it becomes more difficult for the solute molecule to change its local environment than in less polar or non-polar solvent. The cage effects become more pronounced, effectively keeping the system in a local energy minimum similar for both ground and excited states. Because of such a similarity in the slopes of the PES the wavepackets evolving on the ground and excited state PES decohere more slowly than on the PES with different slopes. As mentioned earlier, the excited state PES of the gas-phase $ClNO_2$ has an unbound character providing a natural reason for fast dephasing. However, in the solvent environment the excited state PES may have a local minimum and a barrier for dissociation along the N-Cl coordinate. This barrier can increase in highly polar solvents, leading to longer dephasing times and narrower fluorescence bands by the mechanisms discussed above.

Among different polarity/polarizability parameter sets used in Table 6.3 the one corresponding to transfer of 0.625e (Mulliken) charge and the scaling factor of 1.75 predicts the homogeneous linewidth broadening parameter $\Gamma = 792\ cm^{-1}$ – the value close to the one used in the modeling described in Section 6.3.2.2 (Γ_1 and $\Gamma_2 = 800\ cm^{-1}$). Thus, our atomistic simulations ensure that the homogeneous broadening effects should be described with the value of Γ taken in a relatively narrow range. This re-emphasizes the role of inhomogeneous broadening as the next important factor contributing to the overall broadening.

In addition to the luminescence linewidth calculations we computed the influence spectra for the $ClNO_2$/MeOH system with different polarity (given by the scaling factors) of the solvent (Fig. 6.8). It shows that the electronic transitions are driven by the low-frequency modes spanning a range from 84 to 210 cm^{-1}. They correspond to collective "lattice" vibrations of the solute and solvent molecule. In addition, the low-frequency modes can also be associated with the motion of the heavy atoms, such as chlorine. In this case, the mode may even include stretching or bending of intramolecular bonds and angles.

As the solvent polarity increases, the higher-frequency modes at ~460 cm^{-1} start playing more significant role. One may associate such type of motions with the specific electrostatic interactions, such as hydrogen bonding or "salt-bridge"-like electrostatic interactions. As it follows from the analysis of the partial charges the hydrogen bonds are more likely to be formed between O atoms in NO_2 group and the H atom of the MeOH hydroxyl. As the charge on both H and O atoms increases, the interaction strength increases, opening an effective pathway for energy dissipation from $ClNO_2$ into the solvent bath.

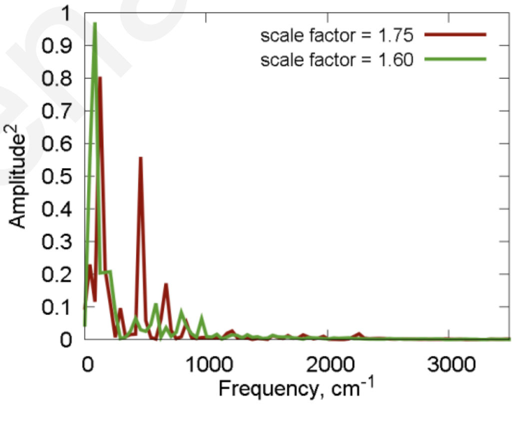

Figure 6.8. Influence spectra for the $ClNO_2$/MeOH system showing the vibrational modes important for energy dissipation via fluorescence.

6.3.3.2 Electronic structure calculations (mechanism of the inhomogeneous broadening)

As it has been shown in previous sections, the contribution of the inhomogeneous broadening to the linewidth is relatively small, but it cannot be neglected if a consistent and accurate description of the RR DPR's and the electronic absorption spectra are to be obtained. One can expect that the inhomogeneous broadening effects are due to specific solvent-solute interactions that differently affect the electronic energy levels involved in the photodynamics. To uncover the effects associated with the solvent, we computed the pDOS for the gas-phase $ClNO_2$ molecule (Fig. 6.9A) and for $ClNO_2$ solvated by methanol (Fig. 6.9B-D).

A detailed analysis of the frontier orbitals of the gas-phase system is presented in Table 6.4. On the basis of the dominant contributions of the atomic orbitals to the KS MOs one can deduce the symmetry and the bonding character of the states. The resulting assignment is in good agreement with previous calculations[34] with a few minor variations. The transitions that can be deduced from Table 6.4 are also in reasonable agreement with those calculations: $\sigma \rightarrow \sigma^*$(Cl-N), $\Delta E = 6.9$ eV (Lesar's value: 7.04 eV); $\pi(O_2) \rightarrow \pi^*(NO_2)$, $\Delta E = 8.09$ eV (Lesar's value: 7.25); n(Cl) $\rightarrow \pi^*(NO_2)$, $\Delta E = 6.67$ eV (Lesar's value: 5.77 eV). Thus, the computational method (PBE0 functional with the pseudopotentials) is sufficiently accurate for description of the electronic structure and transitions in the system of interest and, therefore, is expected to be accurate for the extended solvent-solute system.

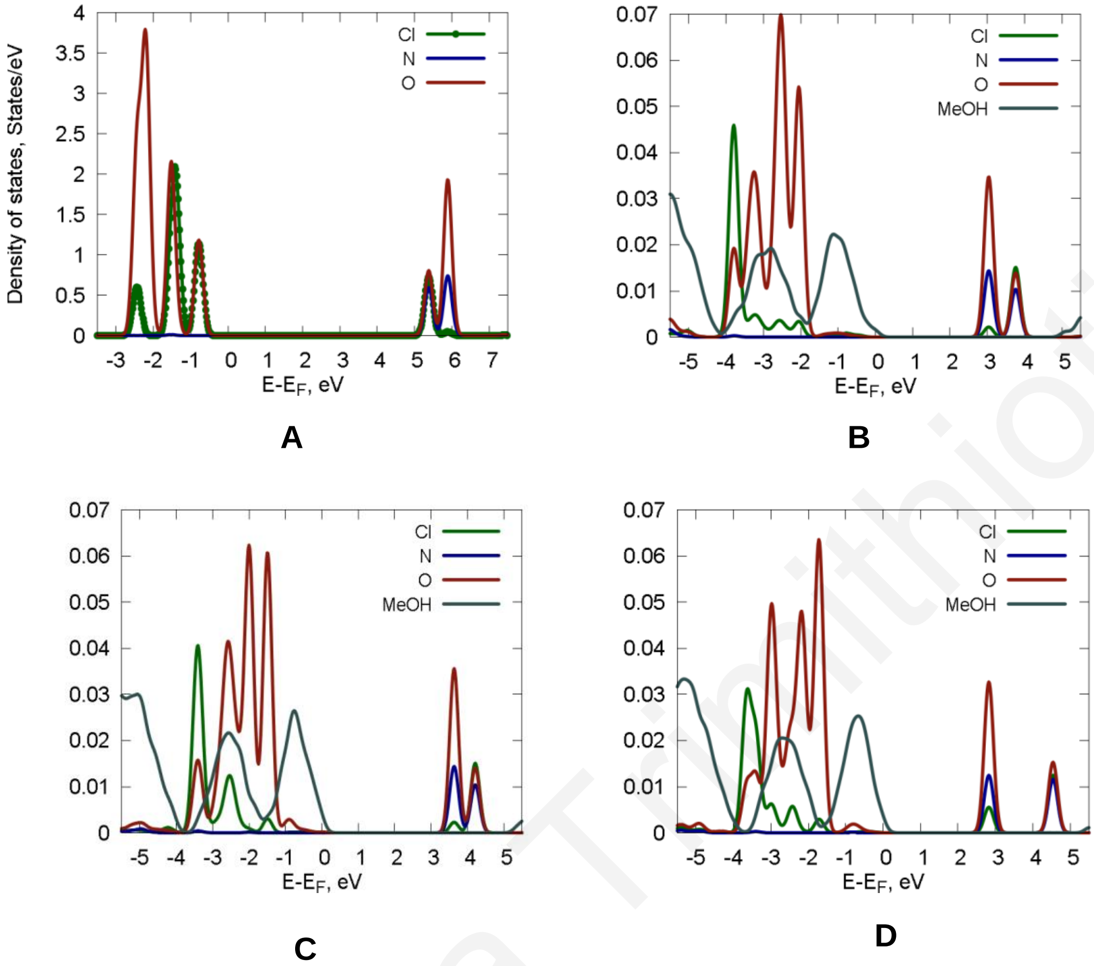

A

B

C

D

Figure. 6.9. Partial density of states of the $ClNO_2$ molecule, computed with the hybrid PBE0 functional: (A) isolated molecule, note that HOMO-1 and HOMO-2 are almost degenerate; (B)-(D) in MeOH solvent, representative configuration. The dot-and-line representation is used to show the density of Cl states in the isolated molecule more clearly, because it strongly overlaps with the density of O states. E_F indicates the Fermi energy of the system.

The computed pDOSs for the extended system (Fig. 6.9, panels B-D) clearly indicates that the solvent has a significant impact on the electronic structure of the $ClNO_2$ molecule. In the gas-phase system the Cl (2p) states have notable weight in HOMO, HOMO-1 and LUMO orbitals and a smaller weight in the HOMO-4. The LUMO+1 state is composed primarily of the O and N 2p orbitals. On the contrary, in the solvated $ClNO_2$ molecule the HOMO, HOMO-1 and HOMO-2 of the solute are all composed primarily of the O 2p states. A notable contribution of Cl (2p) states is found only in HOMO-3 orbital.

Table 6.4. Characterization of the frontier orbitals of gas-phase $ClNO_2$. The orbital labels in parentheses denote the orbital symmetries

Label	**Energy, eV**	**Dominant contribution to the KS wavefunctions**
HOMO-4 (n(Cl) + n(O))	-10.64	0.336 (Cl, $2p_y$)+ 0.202 (O2, $2p_z$) + 0.202 (O1, $2p_z$)+ 0.124 (O1, $2p_y$) + 0.123 (O2, $2p_y$)
HOMO-3 ($\pi(O_2)$)	-10.39	0.494 (O1, $2p_x$) + 0.494 (O2, $2p_x$)
HOMO-2 (σ(Cl-N))	-9.72	0.421 (Cl, $2p_z$) + 0.278 (O1, $2p_z$) + 0.278 (O2, $2p_z$)
HOMO-1 (n(Cl))	-9.58	0.958 (Cl, $2p_x$)
HOMO (n(Cl) + n(O))	-8.97	0.656 (Cl, $2p_y$) + 0.132 (O1, $2p_z$) + 0.131 (O2, $2p_z$)
LUMO (σ*(Cl-N))	-2.82	0.366 (Cl, $2p_z$) + 0.165(N, $2p_z$)
LUMO+1 ($\pi^*(NO_2)$)	-2.30	0.399 (N, $2p_x$)+0.260 (O1, $2p_x$)+0.260 (O2, $2p_x$)

The bonding character of these orbitals is presented in Table 6.5 and, in general, follows that of the gas-phase system, with only n(Cl) orbitals shifted to the lower energy levels. In addition, due to the asymmetry of the $ClNO_2$ environment, the character of some orbitals is mixed. For example, the HOMO is best represented as a mix of σ(Cl-N) and n(O) bonding types. This is because only one of the O atoms hybridizes its $2p_z$ orbital with the $2p_z$ orbital of the Cl atom. The other O contains only $2p_y$ orbital, that is left alone (lone pair) and is not involved in σ-bonding. Note, that because in the solvated system there are many more states than in the gas-phase system, each orbital label corresponds to a set (usually one or two for $ClNO_2$-projected states) of nearly-degenerate KS orbitals with similar composition (see Table 6.5).

Table 6.5. Orbital assignment for panel 6.9B

Label	Energy, eV	Dominant contributions
HOMO-3	-6.15	0.487 (Cl, $2p_z$) + 0.131 (Cl, $2p_y$)
n(Cl)	-6.11	0.520 (Cl, $2p_x$)
HOMO-2 (n(Cl)+n(O))	-5.61	0.082(O2, $2p_y$)+0.033 (O1, $2p_z$) +0.031(O1, $2p_y$)+ 0.029(Cl, $2p_y$)
	-5.51	0.041 (O2, $2p_y$) + 0.035 (O1, $2p_z$) + 0.032(O1, $2p_y$)
HOMO-1 (π(O_2))	-4.90	0.045 (O1, $2p_x$) + 0.030 (O2, $2p_x$)
	-4.84	0.291 (O2, $2p_x$)+0.234 (O1, $2p_x$)
HOMO σ(Cl-N)+n(O)	-4.38	0.366 (O2, $2p_y$)+0.301 (O1, $2p_z$) + 0.061 (Cl, $2p_z$)
LUMO (π*(NO_2))	0.71	0.357 (N, $2p_x$) + 0.223 (O2, $2p_x$) + 0.212 (O1, $2p_x$)
LUMO+1 n*(Cl)	1.43	0.276 (Cl, $2p_y$) + 0.183 (N, 2s) + 0.105 (Cl, $2p_z$) + 0.077 (O2, $2p_z$) + 0.069 (O1, $2p_y$)

The composition of the LUMO and LUMO+1 is reversed with respect to those of the gas-phase molecule – the LUMO is now composed of the N and O 2p orbitals, and has a π*(NO_2) bonding character, as the LUMO+1 in the gas-phase molecule. The LUMO+1 contains a notable contribution of the Cl 2p states (lone pairs) and N 2s states, thus it is best characterized as n*(Cl) rather than expected σ*(Cl-N). This suggests, that the σ→σ*(Cl-N) transition, dominant in gas-phase system, is now substituted with n→n*(Cl). Such transition corresponds to excitation from the HOMO-3 to the LUMO+1. The energy for such transition is 7.58 eV. Naturally, the π(O_2) →π*(NO_2) and n(Cl) →π*(NO_2) transition are still preserved in the solvent, but the corresponding energies change – 5.61 eV and 6.86 eV, respectively.

So far we have given the description of the static pDOS. In reality, thermal motion of nuclei causes structural reorganization of the solvent-solute system and consequently affects the electronic structure. This leads to additional effects, represented in Fig. 6.9, panels (C) and (D). One of them is a possibility of the solute HOMO-2 orbital to show notable localization of the charge density on Cl atom (Fig. 6.9C). This means that the n→n*(Cl) transition may also be described by promotion of the electron from HOMO-2 to LUMO+1 with the energy E = 7.04 eV. This causes the excitation energy to fluctuate by ~0.5 eV.

The other effect is a notable splitting of the LUMO and LUMO+1 levels by as much as ~1.5 eV (Fig. 6.9D). The total value of this splitting is composed of ~0.5 eV increase of the LUMO+1 and ~1.0 eV decrease of the LUMO energy levels. These values determine the magnitude of the excitation energy fluctuation for n→n*(Cl) and $\pi(O_2)$ $\rightarrow\pi^*(NO_2)$ transitions, respectively.

One should note that the effects just discussed arise only because of the polar interactions with the solvent. Such interactions favor some instantaneous charge density distributions and they influence the orbital energies. Although the fluctuations of the energy levels are quite notable and are on the order of ~0.5 eV, in order to get the numerical estimate for the inhomogeneous broadening one needs to average such fluctuations over a sufficiently long time period of the molecular evolution. Because of high computational demands of the PBE0 functional and because of the relatively large system size used in this study such a dynamics cannot be currently computed. Still, the qualitative analysis described above elucidates possible mechanisms for the inhomogeneous line broadening of the electronic absorption spectra of $ClNO_2$ molecule in polar solvents, such as methanol.

6.3.4. Assignment of electronic transitions

Considering the experimental results and computational analysis presented here, there is no doubt that two separate transitions contribute to the scattering. However, the excited-state parameters obtained from RRIA do not allow us to directly distinguish which excited state is 2^1A_1 and which one is 3^1B_1. From the literature[34] it is known that the vertical excitation energy to 3^1B_1 is higher (7.25 eV) than the vertical excitation energy to 2^1A_1 (7.04 eV) for the gas phase. The theoretical calculations for the electronic structure performed here also predict higher vertical excitation energy to the 3^1B_1 than to 2^1A_1 (8.09 eV vs 7.04 eV). Lesar *et al.*[34] have calculated the oscillator strengths for transitions to all singlet states, with the transition to 2^1A_1 found stronger than transition to 3^1B_1 ($f = 0.66$ vs $f = 0.28$).

Although the transition assignment for the gas-phase system is clear, there is no such assurance regarding the dominant transition in solution. The RR intensity analysis described above leads to the adoption of the second set of excited states parameters as the best combination for $ClNO_2$ dissolved in methanol due to the better agreement between experimental and calculated results. This model presupposes that a lower energy state (state 1) has also a lower value of oscillator strength than a higher-lying excited state (state 2) ($M_1 < M_2$). Thus, considering the theoretical results for the gas phase one may attribute state 1 to 3^1B_1 ($\pi(O_2)\rightarrow\pi^*(NO_2)$ transition) and state 2 to 2^1A_1 ($\sigma\rightarrow\sigma^*$(Cl-N) transition). However, the vertical excitation energies derived from our RR study (maxima of the calculated absorption bands for the two states) are reversed compared to theoretical results for the gas phase. The energy maximum for state 1 is 5.94 eV and the corresponding value for state 2 is 6.33 eV.

Both absorption spectrum and pDOS calculations of $ClNO_2$ in MeOH demonstrate that the solvent influences the excited state energies. Specifically, in the section above it was shown that in solution the ordering of the two transitions involved in the D band is reversed because of the notably different effect of the solvent on the orbitals involved in these transitions. In both cases the energies for the transition $\pi(O_2)\rightarrow\pi^*(NO_2)$ and $\sigma\rightarrow\sigma^*$(Cl-N) shift to lower values - from 8.09 eV to 5.83 eV for the former and from 6.9 eV to 6.79 and 6.65 eV for the latter. Because the $\pi(O_2)\rightarrow\pi^*(NO_2)$ transition is affected to a larger extent – shift by 2.26 eV– than the $\sigma\rightarrow\sigma^*$(Cl-N) transition for which the shift is only 0.11 – 0.25 eV, the overall effect of the solvent is seen as the reversal of the character of the excited states.

In addition to the energy shift of the electronic levels, the solvent splits the $\sigma\rightarrow\sigma^*$(Cl-N) transition into two energetically close states, resulting in two closely-spaced peaks at 6.79 and 6.65 eV, as has been noted in the previous section. The energy difference of 0.14 eV is comparable with the one calculated from RRIA (0.39 eV). On the contrary, the energy difference between 2^1A_1 and 3^1B_1 states is somewhat larger – 0.96-1.07. Keeping in mind that these values correspond to instantaneous nuclear configurations one can expect that the ensemble-averaged values can provide better agreement with the values deduced from the RRIA measurements.

Thus, the most important factors leading to deviation of the depolarization ratios of $ClNO_2$ in methanol from 1/3 are: a) involvement of both 2^1A_1 and 3^1B_1 states in the excited state dynamics, and b) additional splitting of the levels of originally degenerate excited state 2^1A_1 due to solvent-solute interactions.

References

(1) Reid, P. J.; Esposito, A. P.; Foster, C. E.; Beckman, R. A. *J. Chem. Phys.* **1997**, *107*, 8262.

(2) Nyholm, B. P.; Reid, P. J. *Journal of Physical Chemistry B* **2004**, *108*, 8716.

(3) Jernshoj, K. D.; Hassing, S. *Journal of Raman Spectroscopy* **2010**, *41*, 727.

(4) Zgierski, M. Z. *Journal of Raman Spectroscopy* **1988**, *19*, 23.

(5) Li, B.; Myers, A. B. *The Journal of Chemical Physics* **1988**, *89*, 6658.

(6) Kelley, A. M. *The Journal of Chemical Physics* **2003**, *119*, 3320.

(7) Schweitzer-Stenner, R.; Dreybrodt, W. *Journal of Raman Spectroscopy* **1985**, *16*, 111.

(8) Huang, Q.; Szigeti, K.; Fidy, J.; Schweitzer-Stenner, R. *The Journal of Physical Chemistry B* **2003**, *107*, 2822.

(9) Shin, K. S. K.; Zink, J. I. *Journal of the American Chemical Society* **1990**, *112*, 7148.

(10) Sension, R. J.; Kobayashi, T.; Strauss, H. L. *Journal of Chemical Physics* **1987**, *87*, 6221.

(11) Giannozzi, P.; Baroni, S.; Bonini, N.; Calandra, M.; Car, R.; Cavazzoni, C.; Ceresoli, D.; Chiarotti, G. L.; Cococcioni, M.; Dabo, I.; Dal Corso, A.; de Gironcoli, S.; Fabris, S.; Fratesi, G.; Gebauer, R.; Gerstmann, U.; Gougoussis, C.; Kokalj, A.; Lazzeri, M.; Martin-Samos, L.; Marzari, N.; Mauri, F.; Mazzarello, R.; Paolini, S.; Pasquarello, A.; Paulatto, L.; Sbraccia, C.; Scandolo, S.; Sclauzero, G.; Seitsonen, A. P.; Smogunov, A.; Umari, P.; Wentzcovitch, R. M. *Journal of Physics-Condensed Matter* **2009**, *21*.

(12) Perdew, J. P.; Burke, K.; Ernzerhof, M. *Physical Review Letters* **1996**, *77*, 3865.

(13) Perdew, J. P.; Burke, K.; Ernzerhof, M. *Physical Review Letters* **1997**, *78*, 1396.

(14) Madrid, A. B.; Hyeon-Deuk, K.; Habenicht, B. F.; Prezhdo, O. V. *Acs Nano* **2009**, *3*, 2487.

(15) Prezhdo, O. V.; Rossky, P. J. *Physical Review Letters* **1998**, *81*, 5294.

(16) Prezhdo, O. V.; Rossky, P. J. *Journal of Chemical Physics* **1997**, *107*, 5863.

(17) Brooksby, C.; Prezhdo, O. V.; Reid, P. J. *Journal of Chemical Physics* **2003**, *118*, 4563.

(18) Nose, S. *Journal of Chemical Physics* **1984**, *81*, 511.

(19) Nose, S. *Journal of the Physical Society of Japan* **2001**, *70*, 75.

(20) Kleinerman, D. S.; Czaplewski, C.; Liwo, A.; Scheraga, H. A. *Journal of Chemical Physics* **2008**, *128*.

(21) Nose, S.; Klein, M. L. *Physical Review B* **1986**, *33*, 339.

(22) Kamberaj, H.; Low, R. J.; Neal, M. P. *Journal of Chemical Physics* **2005**, *122*.

(23) Ciccotti, G.; Martyna, G. J.; Melchionna, S.; Tuckerman, M. E. *Journal of Physical Chemistry B* **2001**, *105*, 6710.

(24) Verlet, L. *Physical Review* **1967**, *159*, 98.

(25) Rappe, A. K.; Casewit, C. J.; Colwell, K. S.; Goddard, W. A.; Skiff, W. M. *Journal of the American Chemical Society* **1992**, *114*, 10024.

(26) Karasawa, N.; Goddard, W. A. *Journal of Physical Chemistry* **1989**, *93*, 7320.

(27) Aguado, A.; Madden, P. A. *Journal of Chemical Physics* **2003**, *119*, 7471.

(28) Mulliken, R. S. *The Journal of Chemical Physics* **1955**, *23*, 1833.

(29) *Gaussian 03, Revision D.01*, M. J. Frisch, G. W. T., H. B. Schlegel, G. E. Scuseria, M. A. Robb, J. R. Cheeseman, J. A. Montgomery, Jr., T. Vreven, K. N. Kudin, J. C. Burant, J. M. Millam, S. S. Iyengar, J. Tomasi, V. Barone, B. Mennucci, M. Cossi, G. Scalmani, N. Rega, G. A. Petersson, H. Nakatsuji, M. Hada, M. Ehara, K. Toyota, R. Fukuda, J. Hasegawa, M. Ishida, T. Nakajima, Y. Honda, O. Kitao, H. Nakai, M. Klene, X. Li, J. E. Knox, H. P. Hratchian, J. B. Cross, V. Bakken, C. Adamo, J. Jaramillo, R. Gomperts, R. E. Stratmann, O. Yazyev, A. J. Austin, R. Cammi, C. Pomelli, J. W. Ochterski, P. Y. Ayala, K. Morokuma, G. A. Voth, P. Salvador, J. J. Dannenberg, V. G. Zakrzewski, S. Dapprich, A. D. Daniels, M. C. Strain, O. Farkas, D. K. Malick, A. D. Rabuck, K. Raghavachari, J. B. Foresman, J. V. Ortiz, Q. Cui, A. G. Baboul, S. Clifford, J. Cioslowski, B. B. Stefanov, G. Liu, A. Liashenko, P. Piskorz, I. Komaromi, R. L. Martin, D. J. Fox, T. Keith, M. A. Al-Laham, C. Y. Peng, A. Nanayakkara, M. Challacombe, P. M. W. Gill, B. Johnson, W. Chen, M. W. Wong, C. Gonzalez, and J. A. Pople; Gaussian, Inc., Wallingford CT, 2004.

(30) Cox, S. R.; Williams, D. E. *Journal of Computational Chemistry* **1981**, *2*, 304.

(31) Trimithioti, M.; Hayes, S. C. *Journal of Physical Chemistry A* **2013**, *117*, 300.

(32) Durig, J. R.; Kim, Y. H.; Guirgis, G. A.; McDonald, J. K. *Spectrochim. Acta A* **1994**, ***50***, 463.

(33) Christe, K. O.; Schack, C. J.; Wilson, R. D. *Inorganic Chemistry* **1974**, *13*, 2811.

(34) Lesar, A.; Hdoscek, M.; Muhlhauser, M.; Peyerimhoff, S. D. *Chem.Phys.Lett.* **2004**, ***383***, 84.

(35) Mortensen, O. S.; Hassing, S. In *Advances In Infrared and Raman Spectroscopy*; Hester, R. J. H. C. a. R. E., Ed.; Wiley: London, 1980; Vol. 6.

(36) Myers, A. B.; Hochstrasser, R. M. *Journal of Chemical Physics* **1987**, *87*, 2116.

(37) Duan, Y. B.; Yuan, S. P.; Wang, R. B.; Mukhopadhyay, I. *Chemical Physics* **2006**, *330*, 9.

(38) Dracinsky, M.; Benda, L.; Bour, P. *Chemical Physics Letters* **2011**, *512*, 54.

(39) Aguiar, H.; Serra, J.; González, P.; León, B. *Journal of Non-Crystalline Solids* **2009**, *355*, 475.

(40) Myers, A. B.; Mathies, R. A. In *Biological Applications of Raman Spectroscopy*; Spiro, T. G., Ed.; John WIley &Sons, Inc.: New York, 1987; Vol. 2, p 1.

(41) Myers, A. B. *Journal of the Optical Society of America B-Optical Physics* **1990**, *7*, 1665.

(42) Myers, A. B.; Harris, R. A.; Mathies, R. A. *Journal of Chemical Physics* **1983**, *79*, 603.

(43) Myers, A. M.; Rizzo, T. R. In *In Laser Techniques in Chemistry*; John WIley &Sons, Inc.: New York, 1995; Vol. 23, p 325.

(44) Myers, A. B.; Trulson, M. O.; Pardoen, J. A.; Heeremans, C.; Lugtenburg, J.; Mathies, R. A. *Journal of Chemical Physics* **1986**, *84*, 633.

(45) Myers, A. B.; Mathies, R. A. *Journal of Chemical Physics* **1984**, *81*, 1552.

(46) Myers Kelley, A. *The Journal of Physical Chemistry A* **2008**, *112*, 11975.

(47) Mukamel, S.; Sue, J. *Journal of Chemical Physics* **1985**, *82*, 5291.

(48) Siebrand, W.; Zgierski, M. Z. *Journal of Physical Chemistry* **1982**, *86*, 4718.

(49) Myers, A. B.; Trulson, M. O.; Mathies, R. A. *Journal of Chemical Physics* **1985**, *83*, 5000.

(50) Pei, K. M.; Ma, Y. F.; Zheng, X. M. *Journal of Chemical Physics* **2008**, *128*.

(51) Stuart, C. M.; Tauber, M. J.; Mathies, R. A. *Journal of Physical Chemistry A* **2007**, *111*, 8390.

(52) Moran, A. M.; Kelley, A. M. *Journal of Chemical Physics* **2001**, *115*, 912.

(53) Moran, A. M.; Delbecque, C.; Kelley, A. M. *Journal of Physical Chemistry A* **2001**, *105*, 10208.

(54) Kelley, A. M. *The Journal of Physical Chemistry A* **1999**, *103*, 6891.

CONCLUSIONS

In this doctoral dissertation we performed the first RR study of nitryl chloride in solution. This study constitutes the first step for the elucidation of the chemical behavior of nitryl chloride in a solution environment, especially for the determination of solute-environment interactions that can lead to phase-dependent reactivity. In this chapter we summarize the various conclusions that derive from this thesis.

Our initial studies focused on finding a suitable environment, where the molecule would be stable with no signature of reaction products or dissociation. We studied $ClNO_2$ in various solvents using absorption and RR spectroscopy and found that methanol was the most appropriate solvent from a range of non-polar to polar/ionic candidates. *Ab initio* calculations confirmed the stability of the molecule in methanol, therefore the work presented in this dissertation focused on this chemical system.

Our RR investigations focused on understanding the nature of the D absorption band (λ_{max} = 200 nm). We observed structural evolution only along the N-O symmetric stretch, which appears at 1291 cm^{-1}. Resonance Raman depolarization ratios are found to deviate significantly from 1/3, which suggests that the D band is composed of at least two separate electronic transitions. Indeed, RRIA suggested the contribution from transitions to two closely-spaced electronic states in the description of the D band, which are dissociative along the Cl-N coordinate, with a large excited state slope (2900 cm^{-1}). This steep dissociative potential and the large homogeneous linewidth necessary to reproduce the ν_1 experimental RR cross-sections led to the depression of the ν_2 and ν_3 intensities, which were not observed, with the exception of the latter with excitation at the maximum of the absorption band. The role of the low frequency dissociative mode (ν_3) is, however, significant as observed through the analysis of the excited-state early time dynamics within the Frank-Condon region. Using the time-dependent formalism of absorption and Raman, we find that $ClNO_2$ scatters within the short-time limit, where evolution along the Cl-N coordinate terminates by 10 fs and thus truncates any further evolution along the N-O coordinate. The increased frequency of the ν_1 mode in methanol, the red shift of the whole absorption spectrum, and the dissociative excited-state potential in the description of the Cl-N coordinate all indicate the influence of the solvent on molecular structure and excited-state dynamics.

Analysis of DPR curves in combination with computational methods (MD, ab initio and linear response calculations) strengthened our conclusion for the key role of the solute–solvent interactions in this molecular system. This extensive study indicated clearly that inhomogeneous broadening is a limiting factor for the quantification of the spectral broadening in dissociative molecules which scatter in the short time limit. Inclusion of Θ was necessary in order to model all the experimental observables (REP, absorption spectrum and DPR's).

The MD simulations clearly demonstrated that interactions of the solvent with $ClNO_2$ involve both electrostatic interactions of the MeOH oxygen with the Cl and hydrogen bonding between the negatively charged nitryl chloride oxygen and the OH hydrogen. Moreover, combination of pDOS calculations and RRIA revealed a number of solvent-induced changes in the electronic structure of the molecule through the alteration of their energies and their transition dipole moments.

We believe that the main goals of this dissertation which were the determination of the role a polar solvent plays in the molecular system of interest and the definition of the microscopic details that govern that behavior are extensively accomplished. The importance of nitryl chloride in atmospheric chemistry is linked to its abundance and ability to release Cl and NO_2. The PSCs, which are formed from ice or nitric acid and promote the conversion of inert Cl to active nitryl chloride, provide chemistry that is different from what occurs in the gas phase but similar with that in the condensed phase. In this work we have demonstrated that the rupture of the Cl-N bond still occurs in methanol as in the gas phase suggesting that the photodissociation of $ClNO_2$ in solution leads to Cl and NO_2 fragments. However, this thesis cannot form a complete picture of the chemical behavior of nitryl chloride in the atmosphere by itself; additional RRIA studies in other solvents (e.g. acidic, non-polar to polar) are necessary, as well as a variety of other studies mentioned in the next chapter. It is however important to note that the excitation wavelengths used for the investigation of $ClNO_2$ fall within the spectral region where solar photolysis occurs in the stratosphere, and were used here for the first time. Previous studies focused on information provided on resonance with excitation to lower energy bands (A and B band), indicating the relevance of the present work to atmospheric chemistry.

Future research is designed to settle various issues that arose from the present investigation and briefly outlined in the next Chapter.

CHAPTER 8

FUTURE WORK

8.1 Introduction

This doctoral dissertation is the first study of nitryl chloride in solution and has sought out to identify the solute–solvent interactions that govern its behavior in the solution environment. Through RRIA study it was shown that the solvent indeed plays a role in $ClNO_2$ state energetics causing structural changes both in the ground and excited states state, compared to the gas phase. The results generated from the present doctoral dissertation have sparked our interest for further investigations. Our goals for future work are presented below and can be achieved through both experimental and theoretical methods.

Firstly, in order to gain a complete picture of $ClNO_2$ photoreactivity in the condensed phase we need to explore the reaction dynamics of $ClNO_2$ in methanol using time resolved methods such as Transient Absorption (TRA) Spectroscopy in combination with Time-resolved Resonance Raman Spectroscopy (TRRR). Through these ultrafast techniques we will be able to investigate the timescales on which possible processes occur (photodissociation, geminate recombination, vibrational relaxation etc.) and to determine the number of excited states involved in the photochemistry of nitryl chloride in solution. These results in combination with our RRIA will provide an overall understanding of its photochemistry in methanol.

Moreover, through the implementation of classical Molecular Dynamics we can investigate in more depth the solvation dynamics following photoexcitation of $ClNO_2$ dissolved in methanol. Moreover, we suggest that Molecular Dynamics may be implemented for other solvents such as non polar or aprotic solvents in order to clarify to what extent the nature of the solute-solvent interactions affects the time scale of the dephasing process.

8.2 Expected Results from Experimental methods

8.2.1 Time Resolved Absorption Spectroscopy

TRA is a pump-probe technique, where a pump pulse is used to excite a sample in a region where it absorbs, so that photochemistry will be initiated. A second pulse is then used to probe what is occuring in the sample at different time delays after the arrival of the pump pulse, monitoring changes in absorption due to the production or decay of particular species. The wavelength of the second pulse is selected according to what one expects to monitor. If one expects to observe photoproduct generation, then the probe pulse should be in a region where the expected products absorb. If one anticipates geminate recombination, then the probe pulse should be the same as the pump pulse. Probing in the region where fluorescence occurs, as determined from steady state fluorescence measurements, will result in the observation of stimulated emission, extracting thus the excited state lifetime T_1.[1,2] Combination of RR and TRA can thus provide insights on the contribution of pure dephasing (time constant T_2), through the homogeneous linewidth determined based on RRIA, (Eq. 2.15).

In addition, anisotropy studies ($r = (I_P - I_\perp)/(I_P + 2I_\perp)$), where the change in absorption is detected with pump and probe beam polarizations parallel or perpendicular, will provide information on the number of excited states involved in the photochemistry of nitryl chloride in solution. A value of r = 0.4 indicates a single dipole-allowed transition, while values below 0.4 can indicate the existence of more excited electronic states and will complement the depolarization ratio studies mentioned above. Time-dependent anisotropy studies can also provide useful information on the fate of photoproducts at early times.

The ultrafast TRA studies suggested here for $ClNO_2$ in methanol will provide the timescales on which various processes occur in this system (e.g. dissociation, geminate recombination, isomerization, energy transfer etc), as well as kinetic information concerning the appearance or decay of photoproducts. Investigation of the photochemistry of $ClNO_2$ in solution will help elucidate the solute-solvent interactions that lead to different dissociation pathways comparing to the gas phase.

8.2.3 Time Resolved Resonance Raman

TRRR is a useful technique that combines the benefits of vibrational spectroscopy and the ability to follow reaction dynamics. In TRRR a short pump laser pulse (~1 ps) is used to promote a molecule to an excited electronic state or to produce photoproducts, while a probe pulse initiates the spontaneous Raman scattering from the transient species.[3,4] The time evolution of the transient signal is monitored by recording a series of spectra at different delays after photolysis.[3]TRRR studies can therefore monitor directly on ultrafast time scales photoproduct formation and subsequent fate, geminate recombination if it occurs in the particular solvent as well as vibrational relaxation dynamics through the temporal evolution of Raman bands.. Such a method is highly important for the elucidation .[3-5]

The synergistic application of TRA and TRRR, in combination with RRIA will provide profound understanding of the photochemical reactivity of $ClNO_2$ in methanol from the initial excited state evolution to the appearance and relaxation of the ground state photoproducts.

8.3 Molecular Dynamics Simulations

8.3.1 Theory

The solvent response function (C(t)) describes the solvent–induced fluctuations in the energy gap between the ground and excited states of the solute [6,7]

$$C(t) = \frac{\langle \delta U(t)\,\delta U(0)\rangle}{\langle \delta U^2 \rangle} \qquad 8.1$$

where $U(t)$ is the energy gap between ground and excited states and $\delta U(t) = U(t) - \langle U \rangle$ is the fluctuation of energy gap from its equilibrium value.

Besides vibrational relaxation, a non-isolated molecule can change its chemical behavior through a process called *solvation* where the central molecule induces its surrounding molecules to rearrange resulting in stabilization of the system.[7] Due to this process, the electronic energy gap of the solute evolves. The energy gap can be measured experimentally and simulated using Molecular Dynamics and provides an ideal estimate of the solvent response. S*olvation* is given by the Fourier transform of the energy gap autocorrelation function. [5,6]

$$I(\omega)=\left|\frac{1}{\sqrt{2\pi}}\int_{-\infty}^{\infty}dt\,e^{-i\omega t}\left[U(t)-\langle U\rangle\right]\right|^{2} \qquad 8.2$$

The unnormalized solvent response $\langle \delta U(t)\,\delta U(0)\rangle$ is given by equation 8.3 and can be used to calculate the damping function *D*(t) via integration of the unnormalized solvent response and subsequent exponentiation.

$$\langle \delta U(t)\,\delta U(0)\rangle = C(t)\langle \delta U^{2}\rangle \qquad 8.3$$

D(t) is related to the homogeneous line width for an isolated molecule through *D*(t) = exp(-Γt). In interacting systems this relation is converted to D(t) = exp[-g(t)] where

$$g(t)=\int_{0}^{t}d\tau_1\int_{0}^{\tau_1}d\tau_2\,\langle \delta U(\tau_2)\,\delta U(0)\rangle \qquad 8.4$$

The total dephasing time (T_2) is associated with the homogeneous linewidth (Γ) via equation 2.15. Given the values of T_1, from pump-probe measurements as described above, and Γ (from RRIA), T_2* (pure dephasing) can be then calculated.

8.3.2 Expected Results

Through MD simulations the ground state $ClNO_2$ – MeOH radial pair distribution functions g(r) can be obtained. Specifically, the molecular center of mass distribution functions and the pair distribution functions between atoms of $ClNO_2$ and methanol may be calculated. The distances the solvation shells of methanol peaks are indicative of the solute solvent interactions. Of particular interest is the radial distribution function $g_{O\text{-}Cl}(r)$ between the oxygen of the hydroxyl group of methanol with the chloride of $ClNO_2$. If the solvation shell of this pair distribution function peaks at small distances (close to zero) will confirm our suggestion that the Cl atom is oriented toward the O atoms of the nearby methanol molecules (see Chapter 6).

Moreover, we can obtain the normalized response functions (Equation 8.1), which describe the time scales and amplitudes of solvent rearrangement that follow $ClNO_2$ photoexcitation. These figures can demonstrate the time scale where most of the response of the solvent occurs. The unnormalized solvent response function (Equation 8.3) determines the pure dephasing contribution to the homogeneous linewidth.[6] Another consequence of a MD simulation would be the power spectrum of $ClNO_2$ in methanol (Equation 8.2). This spectrum shows the solvent induced fluctuation of the electronic energy gap. Analysis of the structural features present in the power spectrum indicate which motions are affected from the relaxation of the excited state of the solute.

The dephasing function (*D*(t)) may be determined through equation 8.4 Thus a comparison between *D*(t) resulting from RRIA and *D*(t) obtained by Molecular dynamics simulations is possible.

In addition to the MD study on $ClNO_2$/MeOH, we intend to perform such calculations in non-polar solvents (e.g cyclohexane, chloroform). Through this study we may explore the origin of dephasing in each system.

8.4 Conclusions

The solvent dependence of the excited state reaction dynamics of nitryl chloride was examined for the first time through the RRIA we performed here. The subject of the phase-dependent reactivity of nitryl chloride does not end here. On the contrary, our study is a stimulus for further study of the solution phase photochemistry of nitryl chloride. Various issues such as the exact processes that occur in this chemical system as well as in other solvents after photoexcitation, the timescales on which the different process occur , and more importantly the clarification of the nature of the solute-solvent interactions that can cause phase-dependent reactivity are still open and need exploration.

References

(1) Foster, C. E.; Barham, B. P.; Reid, P. J. *Journal of Chemical Physics* **2001**, *114*, 8492.

(2) Hayes, S. C.; Cooksey, C. C.; Wallace, P. M.; Reid, P. J. *Journal of Physical Chemistry A* **2001**, *105*, 9819.

(3) Ferraro, J.R.; Nakamoto, K.; Brown, C. W. *Introductory Raman Spectroscopy,* 2nd Ed., Elsevier: 2002.

(4) Myers Kelley, A. *The Journal of Physical Chemistry A* **2008**, *112*, 11975.

(5) Reid, P. J. *Journal of Physical Chemistry A* **2002**, *106*, 1473.

(6) Brooksby, C.; Prezhdo, O. V.; Reid, P. J. *Journal of Chemical Physics* **2003**, *118*, 4563.

(7) Stratt, R. M.; Maroncelli, M. *Journal of Physical Chemistry* **1996**, *100*, 12981.